Development of sway reduction control for the Jacket Lift System of *Pioneering Spirit*

Martijn A. Kist

Master of Science Thesis

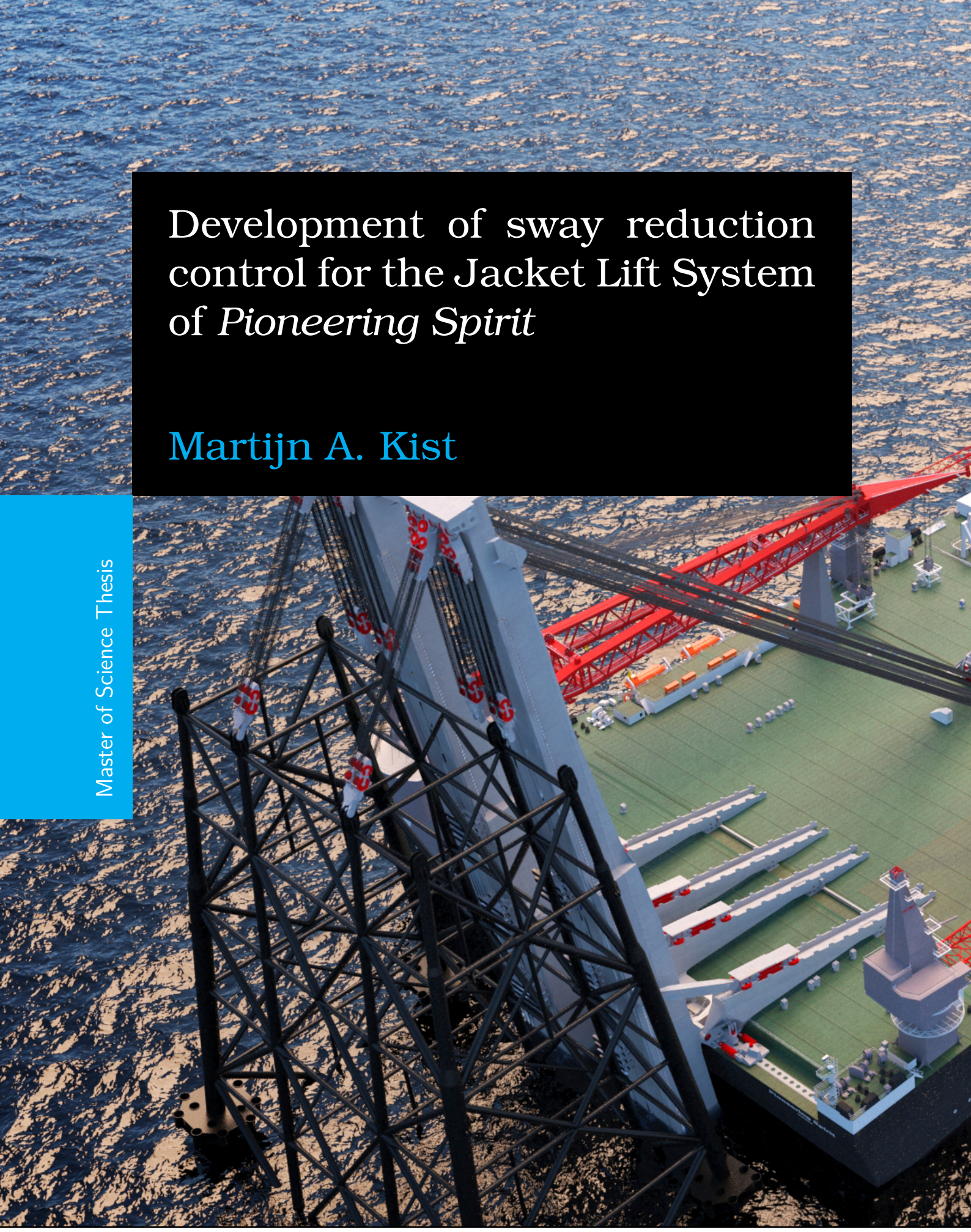

TU Delft Delft University of Technology

Delft Center for Systems and Control

Development of sway reduction control for the Jacket Lift System of *Pioneering Spirit*

Master of Science Thesis

For the degree of Master of Science in Systems and Control at Delft University of Technology

Martijn A. Kist

31st July 2018

Faculty of Mechanical, Maritime and Materials Engineering (3mE) · Delft University of Technology

Copyright © Delft Center for Systems and Control (DCSC)
All rights reserved.

Abstract

Pioneering Spirit, Allseas's largest pipelay vessel, will be outfitted with a novel Jacket Lift System (JLS). A jacket refers to the steel frame which supports the topside of a fixed offshore platform. The Pioneering Spirit was already capable of lifting the topsides of offshore platforms, like the former oil platform Brent Delta, but would have to leave the jacket behind. With the JLS it will also be able to remove and install jackets.
In offshore ship mounted crane applications wave disturbances can create unwanted oscillations in suspended loads. Anti-sway control systems have been developed to aid the crane operator in decreasing these oscillations. But not all crane types have actuators suitable for this compensation. The JLS will be a derrick type crane which will be positioned above a jacket using the dynamic positioning of the ship. The hoist systems of the JLS are then lowered and connected to the jacket. During this lowering process the ship motion induced by wave disturbances create a large oscillation in the hoist system.
In this thesis a controller is developed based on a Proportional Derivative controller found in literature to reduce the sway in the hoist system to make the connection process possible.

Contents

List of Figures

List of Tables

Acknowledgements

First of all I would like to thank Allseas Engineering B.V. for the unique opportunity to do research on the Jacket Lift System of *Pioneering Spirit*. I would like to especially thank Marijn Dijk and Niels Mallon, for all the help and supervision, and Willem Kuipers for his help and tomfoolery.

Secondly I would like to thank my supervisor Jens Kober for his assistance during the writing of this thesis.

I thank all members of the graduation committee:

Prof. Dr. Robert Babuska	TU Delft	Chairman
Dr.ir. Jens Kober	TU Delft	Supervisor
Dr.ir. Milinko Godjevac	TU Delft	External memeber
Dr. ir. Niels Mallon	Allseas Engineering B.V.	Supervisor from company

And lastly many thanks go out to my wife Sarah for her unwavering support during my graduation.

Delft, University of Technology
31st July 2018

Martijn A. Kist

Glossary

List of Acronyms

JLS	Jacket Lift System
PD	Proportional Derivative
LQR	Linear-Quadratic Regulator
LQR-FF	LQR with feedforward gain
LQRi-FF	LQR with integral and feedforward gain
sLQRi-FF	gain scheduled LQR with integral and feedforward gain
MPC	Model Predictive Control

Chapter 1

Introduction

In this MSc Thesis project a sway reduction control method was developed for Allseas's novel Jacket Lift System (JLS). The JLS will be a derrick type crane installed aboard Allseas's largest pipelay vessel *Pioneering Spirit*, shown in Figure 1-1. In the oil and gas industry, jacket refers to a steel frame which supports the deck and topside of a fixed offshore platform. Most oil platforms are installed on a jacket, which can be used up to water depths of 500 metres. After a platform is removed from its jacket the JLS will be able to lift the entire jacket, weighing up to 20.000 tonnes, and tilt it onto its deck for transportation.

Figure 1-1: *Pioneering Spirit*

1-1 Jacket lift procedure

Figure 1-2 illustrates the jacket lift procedure of the JLS. In preparation for the removal of a jacket from the seabed, the beams of the JLS are put upright and are suspended in the derrick hoist cables, as seen in Figures 1-2a and 1-2b. To lift the jacket the JLS will have several hoist systems, consisting of an upper and a lower hoist block. After the JLS beam is put upright, and the ship is in position, the lower hoist blocks have to be connected to the jacket, as seen in Figure 1-2b. Then the jacket is lifted out of the water and the beams are tilted backwards to rest the jacket onto the deck, as seen in Figures 1-2c, d, and e. After the jacket is secured on the deck *Pioneering Spirit* can transport the jacket.

(a) Sail to jacket

(b) Put beams upright and connect the hoist systems

(c) Lift the jacket

(d) Tilt the jacket onto the deck

(e) Sail away

Figure 1-2: Jacket lifting process

1-2 Sway problem

In the connection process of the hoist systems the lower hoist blocks have to be lowered to the top of the jacket, as illustrated by Figure 1-3. It is during this lowering process that the motion of the ship can introduce sway into the hoist system. As the lower block is lowered it will act similar to a mass of a pendulum. The eigenfrequency of a pendulum is dictated by the length of the pendulum, which in this case is the length of cable between the two hoist blocks. As the lower block is lowered the length of cable between the two blocks will reach the value at which the eigenfrequency of the hoist system is the same as the frequency of the ship motion. At this moment the hoist system can develop large oscillations. Cranes usually have low damping, Todd et al. [4] reported a damping of $0.1\% - 0.5\%$ for an offshore boom crane. Thus when the lower hoist block is fully lowered and ready to be connected to the jacket, it will still have a large sway amplitude. To enable the connection process the movement of the lower hoist block relative to the jacket should be small. It could take hours for the sway amplitude to reduce to small enough values to start the connecting process. At high sea states however the sway will never reach a small enough amplitude.

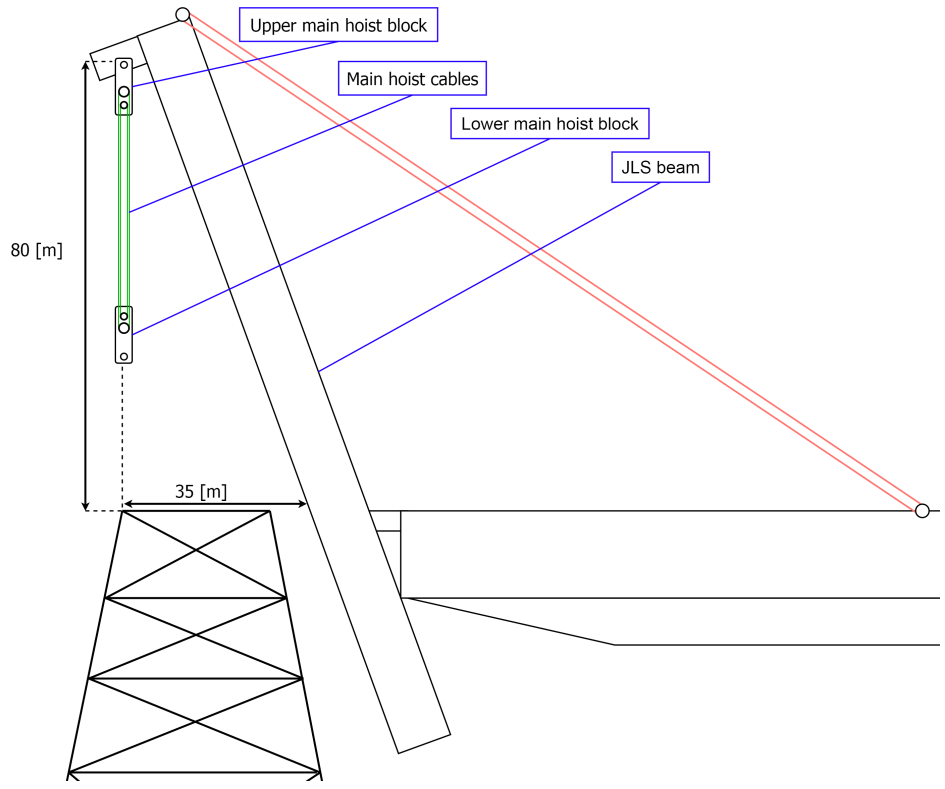

Figure 1-3: Connection process of the Jacket Lift System

1-3 Approach

There are several options to reduce the swaying of the hoist system. In this thesis a solution based on the active control of the lower hoist block position was explored. A control system was developed together with a concept proposal for an actuator and measurement system. The goal of the control system was to reduce the maximum sway amplitude to prevent safety risks, and decrease the final sway amplitude to acceptable levels to start the connection process.

Anti-sway control systems are not a novelty any more, and are full on in development for a large variety of crane types. Most anti-sway control systems are however designed for crane types that control the position of the load using an actuation function of the crane. For a boom crane for instance the boom tip is actuated to control the load. This boom tip actuation can be used for an anti-sway control algorithm, such as Chu et al. [5] developed. Sometimes an auxiliary actuator is used to improve efficiency or performance of the control system as Parker [6] showed with the addition of an actuated tagline. When the position of the load cannot be controlled with the crane, such as the derrick type crane regarded by Ku et al. [3] these advanced anti-sway algorithms are not feasible without the addition of auxiliary actuators. Ku et al. showed that with a tagline actuator controlled by a proportional-derivative control algorithm the sway in the load can still be reduced. Inspired by Ku's results the control algorithm developed in this thesis was also based on proportional-derivative control. To increase the performance and functionality, multiple additions have been made to Ku's basic controller concept.

The development of the control system was made for a two dimensional representation of the JLS as illustrated by Figure 1-3. First a 2D model was created of the hoist system, as discussed in Chapter 2. In Chapter 3 this model was used to analyse the sway problem. In Chapter 2 also a simplified model was derived from the hoist system model, to develop the control algorithm as discussed in Chapter 4. After the control algorithm was completed it was implemented with an observer on the hoist system model as described in Chapter 5. Finally the performance and robustness were evaluated in Chapter 6.

Chapter 2

Modelling

A 2D hoist system model was made in Simulink, in combination with Matlab, to capture the dynamics of the hoist system. This model was used to analyse the sway problem, and to evaluate the performance of the developed control system. A second simple model was also made, based on mathematical pendulums, to develop the control algorithm on.
The hoist system shown in Figure 2-1a consists of three main elements. The upper hoist block, the lower hoist block, and the hoist cable connecting the two. The hoist blocks consist of multiple sheaves. The hoist cable is run along the sheaves and spanned 40 times back and forth between the two hoist blocks, 20 times on the left side, and 20 times on the right side. The hoist blocks were simply modelled as rigid bodies, neglecting sheave dynamics. To model the cable there were multiple options. It was decided to use a lumped-mass model with added variable bending stiffness to capture the cable dynamics. Instead of modelling the 40 cables independently two cables were modelled, each representing 20 cables with accumulative parameters.
First the modelling of the hoist cable will be discussed, secondly the modelling of the hoist blocks, thirdly the assembly of the hoist system model, and lastly the simple pendulum model.

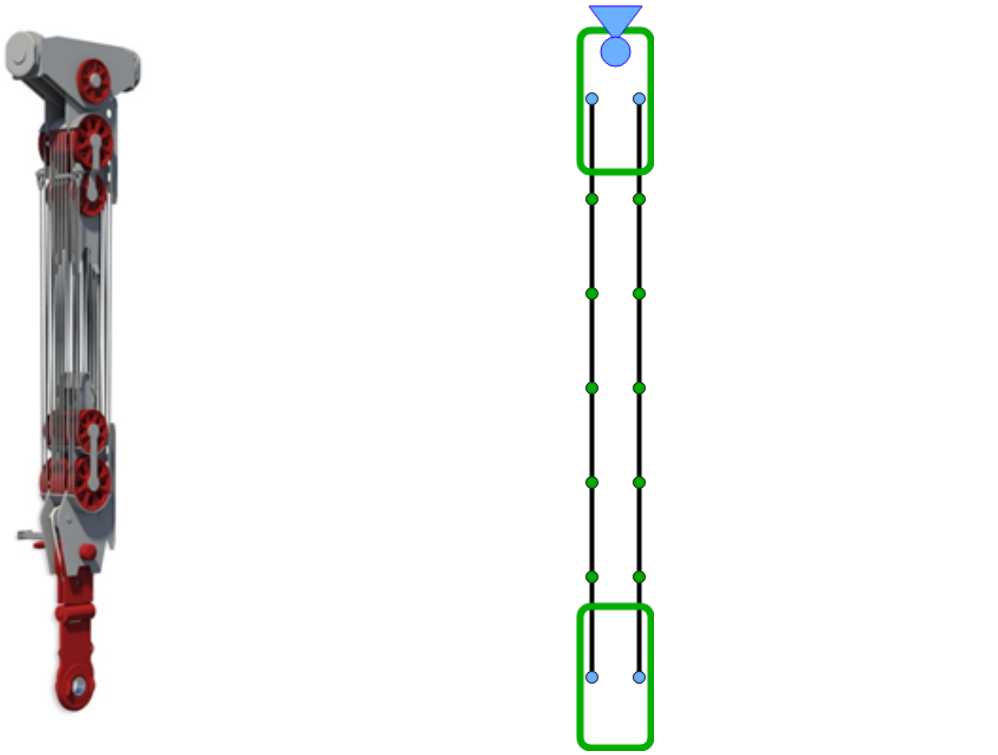

(a) 3D model **(b)** Schematic drawing

Figure 2-1: Hoist system

2-1 Cable model

During development of controllers for crane applications cable dynamics are often neglected. As the hoist system is for a large part made up of cables it can be important to model the dynamics of the cables. Continues models can be very accurate but corresponding PDEs are time consuming to solve as mentioned by Dreyer and Van Vuuren [7]. Therefore a discrete approach is chosen, as advised by them, through the use of the lumped-mass method. The ODEs of the lumped-mass method are solvable using standard numerical integration techniques. By choosing the appropriate number of elements the loss in accuracy can be kept small, while cutting down on computation time.
Figure 2-2 shows a cable model made up of four lumped-mass cable elements. The elements differ from ones found in literature, as apart from the linear viscoelastic element (drawn as a linear spring), a radial viscoelastic element is introduced (drawn as a radial spring). This allows for incorporation of the bending stiffness of cables.
This section will explain the theory behind these lumped-mass cable elements, after which this method will be validated using the theory behind lateral string vibrations and catenary equations.

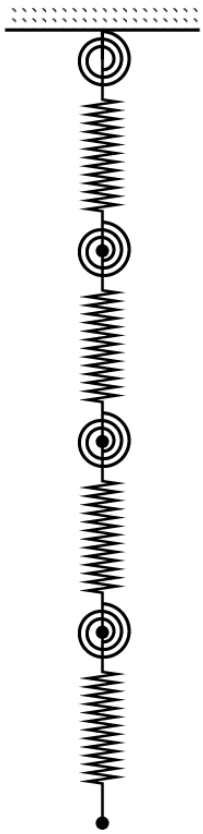

Figure 2-2: Lumped-mass cable model

2-1-1 Lumped-mass cable elements

Mohammadshahi [1] has used the lumped-mass method to model the cables in a cable-actuated system. Using this method the cable is segmented into elements consisting of viscoelastic massless elements composed of springs and dampers, and lumped masses called nodes. Figure 2-3 shows such a lumped-mass cable element. The tension in the spring elements is denoted as T_n, with the spring constant K_n, damping constant C_n^{ID}, and mass m_n.
Using these elements the cable is modeled as a string, without bending stiffness. In the hoist system the 76 mm steel cable is spanned 40 times between the upper and lower hoist block. In this situation the bending stiffness of the cable could alter the dynamics significantly. It was therefore deemed necessary to incorporate bending stiffness in the cable model.

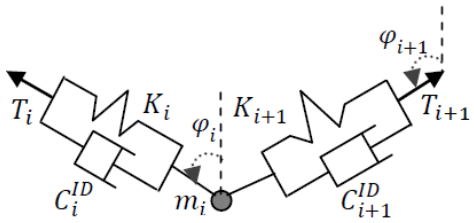

Figure 2-3: Lumped-mass cable element. Reprinted from Mohammadshahi [1]

In Figure 2-3 the angle between the two springs elements K_i and K_{i+1} is determined by ϕ_i and ϕ_{i+1}. In a static situation the angle is determined by the tension in the spring elements, as in a theoretical string. By introducing a moment force relative to the angle between the springs the bending stiffness of the cable can be modelled, making the cable model more akin to beam equations.
Figure 2-4 shows the lumped-mass element adapted with such a moment force created by a radial spring denoted as $K_{r,n}$, and the translational spring is denoted $K_{t,n}$. The damping components are not drawn here. The lengths of the springs are denoted as s_n, and the angles of the springs relative to the world-axis is denoted as ϕ_n.

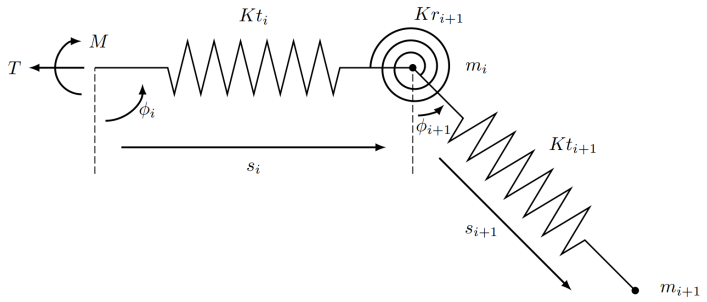

Figure 2-4: Lumped-mass cable element with bending stiffness

The equations of motion for a single mass node in world coordinates (x_n,z_n) are shown by Equation (2-1). The mass node m_n is influenced by gravitational forces, F_g, the forces generated by the translational and radial springs, F_t and F_r respectively, and the linear translational and radial damping terms D_t and D_r, which will be introduced later.

$$\begin{aligned} m_n\ddot{x}_n + F_{t,x,n} + F_{r,x,n} + D_{t,x,n} + D_{r,x,n} = 0 \\ m_n\ddot{z}_n + F_{g,z,n} + F_{t,z,n} + F_{r,z,n} + D_{t,z,n} + D_{r,z,n} = 0 \end{aligned} \tag{2-1}$$

The gravitational forces are simply

$$F_{g,n} = m_n g, \tag{2-2}$$

with g being the gravitational constant.
The n-th mass node is influenced by the translational springs $K_{t,n}$ and $K_{t,n+1}$. Split into x

and z components the forces are

$$F_{t,x,n} = K_{t,n}(s_n - L_{0,n})\sin(\phi_n) - K_{t,n+1}(s_{n+1} - L_{0,n+1})\sin(\phi_{n+1}) \tag{2-3}$$
$$F_{t,z,n} = -K_{t,n}(s_n - L_{0,n})\cos(\phi_n) + K_{t,n+1}(s_{n+1} - L_{0,n+1})\cos(\phi_{n+1}), \tag{2-4}$$

with $L_{0,n}$ the free length of the n-th spring element.
The n-th mass node is influenced by three radial springs $K_{r,n}$, $K_{r,n+1}$, and $K_{r,n+2}$. The moment forces of these springs corresponds to the relative angle between two springs, $\theta_n = \phi_n - \phi_{n-1}$. The Equations (2-5) and (2-6) formulate the forces of the radial springs acting upon the n-th mass node.

$$\begin{aligned} F_{r,x,n} =& M_n(\theta_n, s_n)\frac{1}{s_n}\cos(\phi_n) + M_{n+2}(\theta_{n+2}, s_{n+2})\frac{1}{s_{n+1}}\cos(\phi_{n+1}) \\ &- M_{n+1}(\theta_{n+1}, s_{n+1})\left(\frac{1}{s_n}\cos(\phi_n) + \frac{1}{s_{n+1}}\cos(\phi_{n+1})\right) \end{aligned} \tag{2-5}$$

$$\begin{aligned} F_{r,z,n} =& M_n(\theta_n, s_n)\frac{1}{s_n}sin(\phi_n) + M_{n+2}(\theta_{n+2}, s_{n+2})\frac{1}{s_{n+1}}\sin(\phi_{n+1}) \\ &- M_{n+1}(\theta_{n+1}, s_{n+1})\left(\frac{1}{s_n}\sin(\phi_n) + \frac{1}{s_{n+1}}\sin(\phi_{n+1})\right) \end{aligned} \tag{2-6}$$

The moment force created by the n-th radial spring element Kr_n is denoted as M_n. It is depended on θ_n, and s_n. This moment force is nonlinear as it was decided to use a variable bending stiffness, which will be explained in Section 2-1-2.
The damping behaviour of cables depends on their internal structure and is difficult to model. Therefore the internal dissipation is simply modeled using a viscous damping term, using the damping ratio ζ. These damping components are foremost implemented for the stability of the model as the damping in swinging crane cables is assumed to be very low. Todd et al. [4] report that a ship-mounted boom crane has a damping of 0.1% to 0.5% of the critical damping.

$$D_t = 2\zeta_t\omega_{t,n}\dot{s_n} \tag{2-7}$$
$$D_r = 2\zeta_r\omega_{r,n}s_n\dot{\theta_n} \tag{2-8}$$

The natural frequencies $\omega_{t,n}$ and $\omega_{r,n}$ are computed using the average stiffnesses of the translational $K_{t,avg}$ and radial springs $K_{r,avg}$, and the gravitational constant g, in Equations (2-9) and (2-10).

$$\omega_{t,n} = \sqrt{\frac{K_{t,avg}}{m_n}} \tag{2-9}$$
$$\omega_{r,n} = \sqrt{\frac{K_{r,avg}}{m_n s_n^2} + \frac{g}{s_n}} \tag{2-10}$$

These damping forces are then divided in x and z components.

$$D_{t,x,n} = D_t \sin(\theta_n) \tag{2-11}$$
$$D_{t,z,n} = -D_t \cos(\theta_n) \tag{2-12}$$
$$D_{r,x,n} = D_r \cos(\theta_n) \tag{2-13}$$
$$D_{r,z,n} = D_r \sin(\theta_n) \tag{2-14}$$

2-1-2 Variable bending stiffness

Most cable models use a linear term for bending stiffness. As the lateral motion of the hoist cable is an important factor in the analysis of the hoist system of the JLS, nonlinear bending stiffness will be used in modeling the hoist cable. When bending stiffness is negligible the cable is often modeled as a string, without bending stiffness. When bending stiffness is not negligible the cable is often modeled as a beam. The truth lies somewhere in the middle.

2-1-2-1 Theory

Papailiou [2] developed a comprehensive model for incorporating variable bending stiffness. He modeled the damping of a cable by using a variable bending stiffness due to the frictional contact between wires under bending and tension. Papailiou assumed that the minimum bending stiffness $(EJ)_{min}$ was equal to the summation of the individual bending stiffness of all wires.

$$(EJ)_{min} = E_K \pi \frac{\delta_K^4}{64} + \sum_{d,L} n_L E_{d,L} \pi \frac{\delta_{d,L}^4}{64} \cos(\beta_L), \tag{2-15}$$

with E_K the Young's modulus for the core wire, and $E_{d,L}$ for the wires in the layers around the core. The diameter of the wire is denoted as δ, and β_L is the lay angle of the wires in the layer.
According to Papailiou this minimum stiffness was reached when all the layers around the core of the cable had slipped, which occurred at relatively large curvatures. Figure 2-5 shows the bending moment M of a cable with one layer of wires around its core. The horizontal axis depicts the curvature κ of the cable, which is defined as one divided by the radius of the curve. In Figure 2-5 the curvature at which all the wires have slipped is denoted as κ_e, and it can be seen that after κ_e in 'Region II' of the graph, the bending moment increases with a constant slope, meaning a constant bending stiffness is reached, $(EJ)_{min}$.

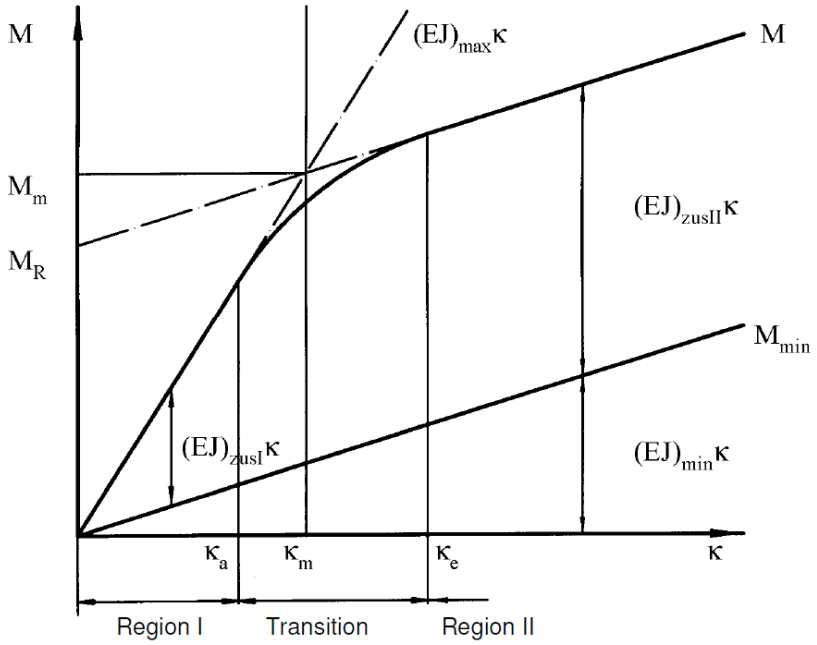

Figure 2-5: Variable bending stiffness w.r.t. curvature of a cable with one layer. Reprinted from Papailiou [2]

Before the layers have slipped the bending stiffness is at its maximum. At this stage the friction between the layers is sufficient to keep the layers from slipping, and the cable bends virtually as a solid cylindrical beam. Papailiou described the maximum bending stiffness added due to the friction between the layers as follows

$$(EJ)_{zus} = \sum_{d,L}(EJ)_{zus,d,L} = \sum_{d,L} \frac{n_L}{2} E_{d,L} A_{d,L} r_L^2 \cos^3(\beta_L). \tag{2-16}$$

By adding this stiffness to the minimum stiffness he obtained the total maximum bending stiffness of the cable:

$$(EJ)_{max} = (EJ)_{min} + (EJ)_{zus}. \tag{2-17}$$

In between the region of maximum bending stiffness, where the layers have not slipped, and the region of minimum bending stiffness, where all the layers have slipped, there are several transition regions. In Figure 2-5 the bending moment of a cable with a core and one layer is shown, thus only one transition region is shown. In Figure 2-6 the bending moment of a cable with multiple layers is shown.

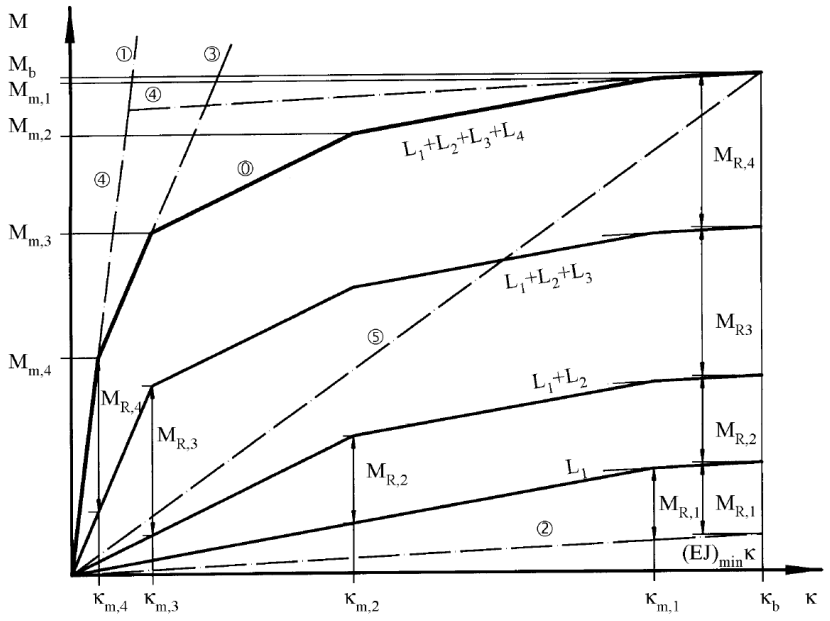

Figure 2-6: Variable bending stiffness w.r.t. curvature of a cable with multiple layer. Reprinted from Papailiou [2]

The slipping of the layer is a non-linear phenomenon, but can be approximated by determining the average transition curvature κ_m and extrapolating the two linear bending moment curves to the point (κ_m, M_m), as illustrated in Figure 2-5. For this purpose Papailiou created an auxiliary parameter M_R.

$$M_R = \sum_d Z_d(e^{\mu \sin(\beta)\phi} - 1)\sin(\phi) r \cos(\beta) = (EJ)_{zus}\kappa, \tag{2-18}$$

with μ being the friction coefficient between the layers, ϕ the wire rotation angle with respect to the bending plane, and Z_d the tensional force in the wire. The radius of the coil made by the wires in the layer is denoted by r_L. By calculating this parameter M_R he could determine the average transition curvature for the individual layers.

$$\kappa_m = \frac{M_R}{(EJ)_{zus}}. \tag{2-19}$$

Papailiou validated his model by measuring the curvature of multiple cables clamped in on both sides with a free length of one metre between. Results for one of the cable measurements is shown in Figure 2-7. It is evident that curve 1, produced by the variable bending stiffness model, has a good fit with the measurement data, depicted by the '+' signs. While curve 2 for maximum bending stiffness, and curve 3 for minimum bending stiffness have a large error.

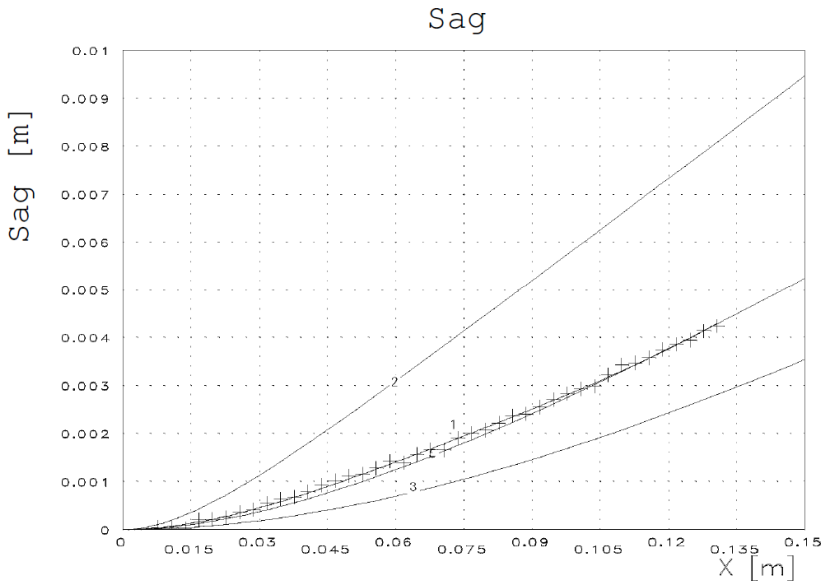

Figure 2-7: Measured and calculated catenary for S32 for S = 280 kN and Vmax = 40 kN; 1: variable stiffness (EJ)(κ);2: minimum (wire) stiffness (EJ)min; 3: maximum (cable) stiffness (EJ) + : measurement. Reprinted from Papailiou [2]

By using this model for bending stiffness a hysteretic effect can be observed when increasing and decreasing the curvature beyond κ_m, as shown in Figure 2-8. The area in between the curves represents the energy dissipated due to the friction between layers. This energy dissipation is a major factor in the damping of cable vibrations.

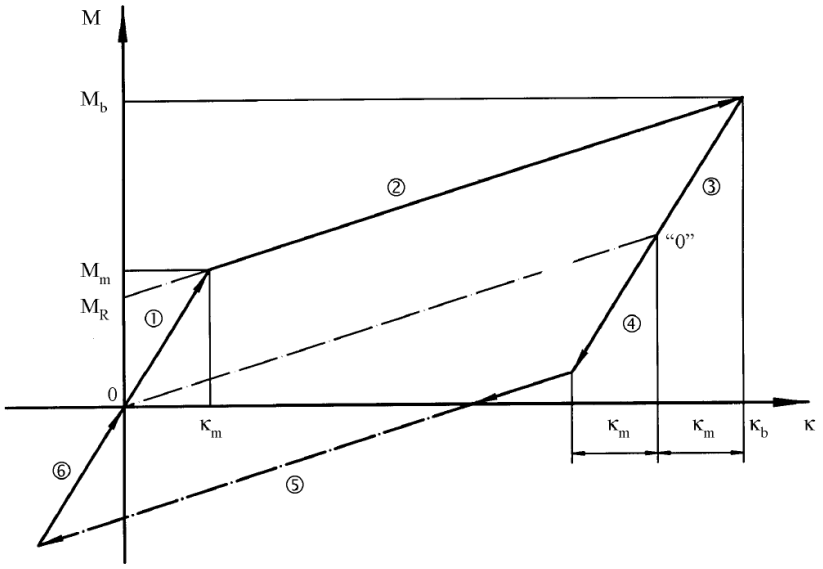

Figure 2-8: Hysteretic variable bending moment. Reprinted from Papailiou [2]

2-1-2-2 Cable parameter calculation

Using the theory of Papailiou [2], parameters of the hoist cable can be determined to implement the variable bending stiffness. First the minimum bending stiffness is determined. This is a summation of the bending stiffness of the individual wires. The bending stiffness of the core wire is equal to

$$(EJ)_k = E_k\left(\frac{\pi\delta_k^4}{64}\right). \tag{2-20}$$

The subscript $(\cdot)_k$ stands for core, thus E_k stands for the Young's modulus of the core wire, etcetera. The bending stiffness of the wires in the layers around the core is

$$(EJ)_L = \sum_d E_L\left(\frac{\pi\delta_{d,L}^4}{64}\right)\cos(\beta_L) = n_L E_L\left(\frac{\pi\delta_{d,L}^4}{64}\right)\cos(\beta_L). \tag{2-21}$$

The subscript $(\cdot)_L$ stands for the layer counted from inside to outside. The bending stiffness of the core wire and the layers around it are summed together to get the minimum bending stiffness

$$(EJ)_{min} = (EJ)_k + \sum_L (EJ)_L. \tag{2-22}$$

When the layer has not slipped yet the bending stiffness due to friction is equal to

$$(EJ)_{fric,L} = \sum_d E_{d,L}\Big(r_L\sin(\phi_{d,L})\Big)^2 A_{d,L}\cos^3(\beta_L) = \left(\frac{n_L}{2}\right)E_{d,L}A_{d,L}r_1^2\cos^3(\beta_L) \tag{2-23}$$

Papailiou called this $(EJ)_{zus,L}$, but this was changed to $(EJ)_{fric,L}$ for better clarity.
The slipping of layers occurs when the tension due to bending in the wires becomes larger than the friction force which keeps them in place. The friction force depends on the tensile force on the wires. When a larger tension force is applied to the cable, the layers will slip at a larger curvature. Therefore the individual wire tension in the layer has to be determined. When multiple layers lay on top of each other the moment of slipping is more complex to determine, as the layers on top also influence the forces on the layers below it. The auxiliary variable $M_{R,L}$ has to be determined for every layer and becomes

$$M_{R,L} = \sum_d \Big(Z_L(\phi_{d,L}) - Z_{d,L}\Big)\sin(\phi_{d,L})r_L\cos(\beta_L). \tag{2-24}$$

The calculation of the tensile stress in an individual wire is simply the total stress divided over all the wires, with each their respective area A, lay angle β, and Young's modulus E.

$$Z_{d,L} = \frac{E_L A_{d,L}\cos^2(\beta_L)}{E_k A_k + \sum_L n_L E_L A_{d,L}\cos^3(\beta_L)}S \tag{2-25}$$

The function $Z_L(\phi)$ can be calculated recursively from the outside layer to the inside. Therefore the outside layer will be regarded as the n-th layer. But first some auxiliary variables

are given.

$$C_{e,n-1} = \mu_{n-1}\sin(\beta_{n-1}) \tag{2-26}$$
$$m_L = \mu_L + \mu_{L-1} \tag{2-27}$$
$$C_{z,n} = 0 \tag{2-28}$$
$$C_{z,n-1} = Z_{d,n} m_n \sin(\beta_n)\frac{l_{n-1}n_n}{l_n n_{n-1}} \tag{2-29}$$
$$C_{z,n-2} = \left[Z_{d,n-1} m_{n-1}\sin(\beta_{n-1}) + C_{z,n-1}\right]\frac{l_{n-2}n_{n-1}}{l_{n-1}n_{n-2}} \tag{2-30}$$

With these auxiliary variables, $Z_L(\phi)$ can be computed for every layer

$$Z_L(\phi_{d,L}) = e^{Ce,L\phi_{d,L}}\left[Z_{d,L} + \frac{C_{z,L}}{C_{e,L}}\right] - \frac{C_{z,L}}{C_{e,L}}. \tag{2-31}$$

When M_R is determined for every layer, the respective averaged slip curvatures κ_m can be determined.

$$M_{R_L} = (EJ)_{fric,L}\cdot\kappa_{m,L} \tag{2-32}$$
$$\kappa_{m_L} = \frac{M_{R_L}}{(EJ)_{fric,L}} \tag{2-33}$$

With the minimum bending stiffness $(EJ)_{min}$, and the array of bending stiffnesses due to friction for every layer $(EJ)_{fric}$, together with the array of averaged slip curvatures κ_m, the variable bending stiffness can be implemented to achieve the nonlinear bending moment.

2-1-2-3 Implementation

To implement the nonlinear bending moment, first the generalized angle θ_n has to be transformed to represent the curvature of the n-th element κ_n. This was achieved by dividing the the angle by the length of the element

$$\kappa_n = \frac{\theta_n}{s_n}. \tag{2-34}$$

With this curvature the linear part of the bending can be computed as $M_{lin} = (EJ)_{min}\kappa_n$. The nonlinear part is a bit more complex as the hysteresis effect shown in Figure 2-8 has to be implemented as well. Therefore the time derivative of the curvature $\dot{\kappa}_n$ is used together with an Integrator Limited block as shown in Figure 2-9.

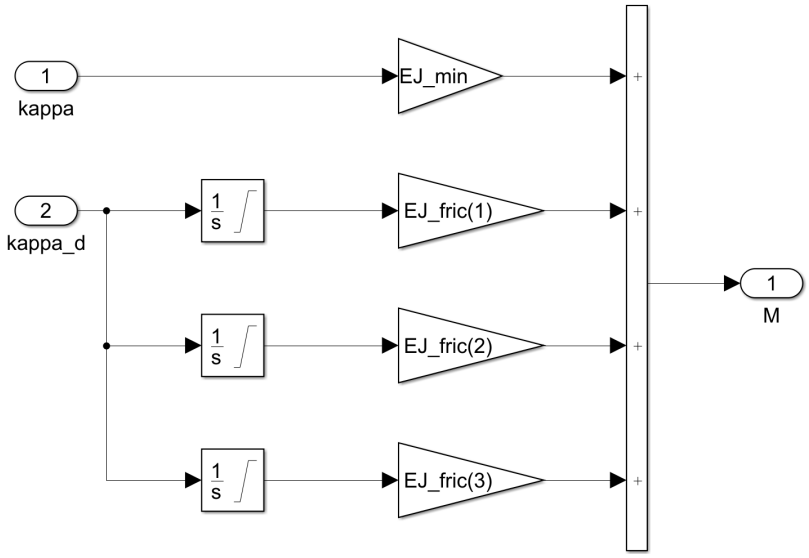

Figure 2-9: Nonlinear bending stiffness implemented in Simulink

This way the hysteresis effect is properly implemented as seen in Figure 2-10, such that the damping due to friction between the layers is incorporated in the lumped-mass cable model together with the variable bending stiffness.

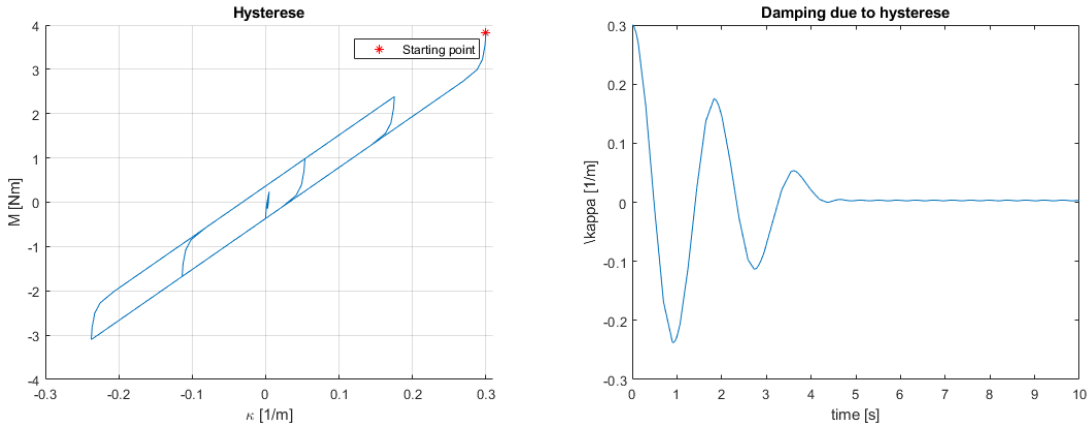

Figure 2-10: Variable bending stiffness hysterese effect in Simulink

Note that a small oscillation is still present, as the damping due to friction only takes effect when the cables are slipping. This is the reason a linear damping term $C_d\dot{\theta}$ is also implemented. Without it the oscillation would never die out.

2-1-3 Validation

The cable modeled with these lumped-mass cable elements is validated for two situations.

2-1-3-1 Transverse vibrations

First, the impulse response of the system in terms of transverse vibrations of the middle node is compared to the theoretical natural frequencies of a string with two fixed ends [8].

$$f_n = \frac{i}{2L}\sqrt{\frac{T}{\rho A}}, \quad i = 1, 2, 3, 4 \tag{2-35}$$

The cable was simulated with a length of $L = 10$ [m], a mass per metre of $\rho A = 2.8$ [kg/m], an axial stiffness of $EA = 50$ [kN] , and a pretension of $T = 1$ [kN]. The first four theoretical natural frequencies according to Equation (2-35) are [0.94 1.89 2.83 3.78] [Hz].

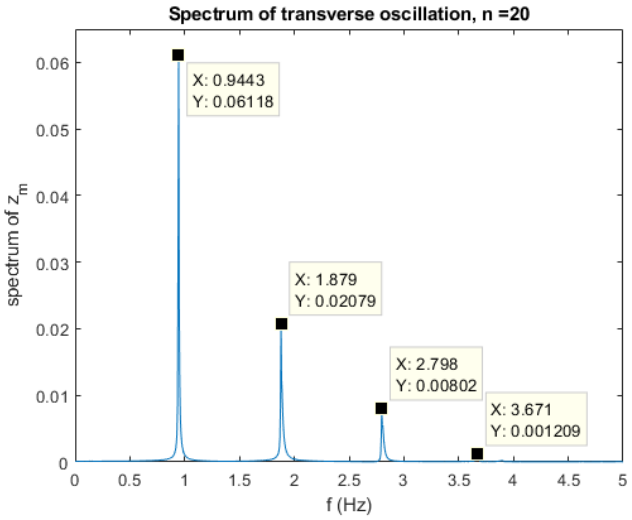

Figure 2-11

Figure 2-11 shows the frequencies present in the impulse response of the cable modeled with twenty elements. Table 2-1 lists the percentage error of the natural frequencies of the lumped-mass cable with eight, twenty, and forty elements, (n). It shows that from twenty elements upwards the lumped-mass cable can accurately represent the natural frequency of a theoretical string, with only a 2.73% error on the fourth natural frequency.

Table 2-1: String vibration test frequency errors

eigenfrequency	n = 8	n = 20	n = 40
1st frequency	0.59%	0.06%	0.06%
2nd frequency	2.46%	0.33%	0.21%
3rd frequency	5.76%	1.13%	0.42%
4th frequency	6.35%	2.73%	1.93%

2-1-3-2 Catenary equation

The second situation in which the lumped-mass cable is compared, is in a static catenary position. Here the incorporated bending stiffness can be tested. Hsu [9] describes the catenary form of a cable without, and **with** bending stiffness. Therefore the incorporation of the bending stiffness can be looked at specifically. The variable bending stiffness can not be compared, as Hsu uses a constant bending stiffness. Therefore the bending stiffness was kept constant at $EJ = 6$ [kN·m^2]. The mass per metre was $\rho A = 6.3$ [kg/m], the axial stiffness was $EA = 145$ [MN], and the length and number of elements were varied over the simulations.

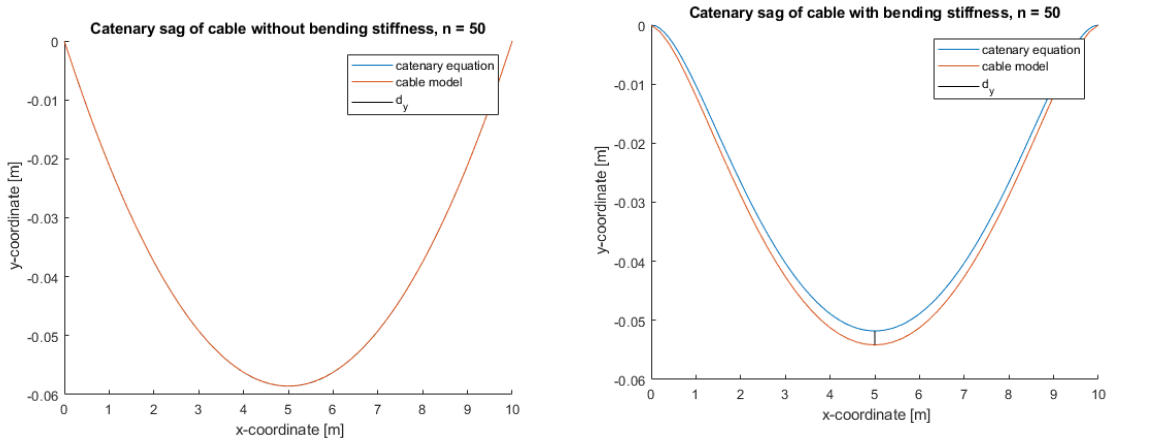

(a) Without bending stiffness

(b) With constant bending stiffness of $EJ = 145$ [KN·m^2]

Figure 2-12: Catenary of lumped-mass cable compared with theoretical cable

Figure 2-12a shows the catenary of the theoretical cable and the lumped-mass cable, without bending stiffness. The bending stiffness of the lumped-mass cable is set to zero. Note that the two curves are almost indistinguishable from each other. Table 2-2 lists that for the lumped-mass cable the error is very small. This error is defined as the vertical difference d_y between the sag of the middle points of the cable ($x = \frac{L}{2}$), divided by the sag of the theoretical cable (y_{sag}), $\varepsilon = \frac{d_y}{y_{sag}}$.

Table 2-2: Catenary sag error, without bending stiffness, $L = 10$

n = 20	n = 50	n = 100
0.004%	0.004%	0.004%

Figure 2-12b shows the catenary of the theoretical cable and the lumped-mass cable, with bending stiffness. The bending stiffness of the lumped-mass cable is set to be constant. Here the difference between the theoretical cable and the lumped-mass cable is more distinct, as the curvature of individual elements is highly dependent on the number of elements. When the lumped-mass cable is simulated with more cable elements, the cable is expected to more accurately represent the theoretical case. In Table 2-3 it is shown that this is indeed the case. It seems that doubling the number of elements used roughly halves the percentage error.

Table 2-3: Catenary sag error, with bending stiffness, $L = 10$ [m]

n = 20	n = 50	n = 100
10.35%	4.58%	2.36%

The cable length was also varied, with the resulting errors shown in Table 2-4. The minimum length of cable between the upper and lower hoist block is ten metres, and it will be paid out to no more than a hundred metres during a connection procedure. With 50 elements the lumped-mass cable shows an error of less then five percent, with a cable length of ten metres. When the length is increased to a hundred metres this value drops significantly, to 0.28%.

Table 2-4: Catenary sag error, with bending stiffness, $n = 50$

L = 10	L = 20	L = 100
4.58%	3.53%	0.28%

The comparison of the lumped-mass cable model with two theoretical situations has validated that the lumped-mass cable model can accurately predict the undamped dynamic and static behaviour of a theoretical cable, when using a number of elements upwards of fifty, in the circumstances presented by the hoist system.

2-2 Hoist blocks

The cables of the hoist system connect the upper and lower hoist block together. The lower hoist block is modeled as a point mass (m_{BL}), with a moment of inertia (I_{BL}), as illustrated by Figure 2-13. The points p_1 and p_2 are the positions where the cable forces interact with the lower hoist block.

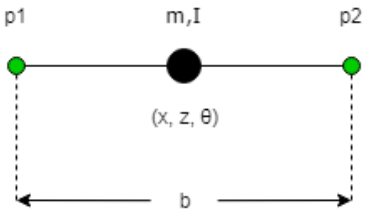

Figure 2-13: Lower hoist block

The equations of motion for the lower hoist block are

$$m_{bl}\ddot{x}_{bl} = F_{1,x} + F_{2,x} \tag{2-36}$$

$$m_{bl}\ddot{z}_{bL} = F_{1,z} + F_{2,z} \tag{2-37}$$

$$I_{bl}\ddot{\theta}_{bl} = F_{1,x}\frac{b}{2}\sin(\theta_{bl}) - F_{2,x}\frac{b}{2}\sin(\theta_{bl}) + F_{1,z}\frac{b}{2}\cos(\theta_{bl}) - F_{2,z}\frac{b}{2}\cos(\theta_{bl}), \tag{2-38}$$

with F_1 the cable force acting on p_1 and F_2 acting on p_2, and the width of the cable attachments b.

The upper hoist block is modelled as a rigid pendulum with a weightless rod and a point mass m_{BU}, as illustrated by Figure 2-14. The upper hoist block has similar cable attachments as the lower block, p_1 and p_2.

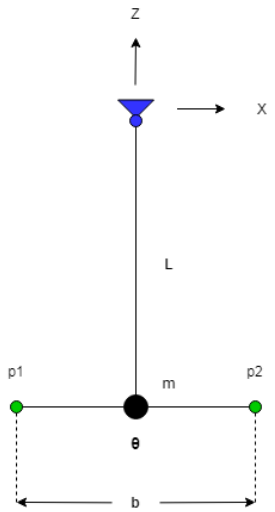

Figure 2-14: Upper hoist block

The equation of motion for the upper hoist block is

$$m_{bu}L^2\ddot{\theta}_{bu} = -m_{bu}gL\sin(\theta_{bu}) - m_{bu}L\cos(\theta_{bu})\ddot{X}(t) - m_{bu}L\sin(\theta_{bu})\ddot{Z}(t) + M_1 + M_2, \quad (2\text{-}39)$$

with L the length of the pendulum, the angle of the pendulum θ_{bu}, the accelerations of the hinge point $(\ddot{X}, \ddot{Z})$ which is part of the JLS beam, and the moment forces exerted by the cable forces M_1 and M_2. The moment forces are given by

$$M_1 = F_{1,x}\left(\frac{b}{2}\sin(\theta_{bu}) + L\cos(\theta_{bu})\right) + F_{1,z}\left(-\frac{b}{2}\cos(\theta_{bu}) + L\sin(\theta_{bu})\right) \quad (2\text{-}40)$$

$$M_2 = F_{2,x}\left(-\frac{b}{2}\sin(\theta_{bu}) + L\cos(\theta_{bu})\right) + F_{2,z}\left(\frac{b}{2}\cos(\theta_{bu}) + L\sin(\theta_{bu})\right). \quad (2\text{-}41)$$

By connecting the hoist blocks with the cable models using the interfacing forces F_1 and F_2, the hoist system model could be assembled, as illustrated by Figure 2-15a. The black nodes are the point masses of the hoist blocks, the green nodes are the lumped masses of the cable model, and the blue nodes are weightless hinge points.
The hoist system model will be used to analyse the dynamics of the hoist system in Chapter 3. In Chapter 6 it will be used to evaluate the performance of the sway reduction controller, which development will be discussed in Chapter 4. For the development of the controller a simple model consisting of mathematical pendulums was developed to reduce complexity, and simulation time during development.

2-3 Pendulum model

For the development of the sway reduction controllers the hoist system was modelled using mathematical pendulums. The two obvious options were the single pendulum, and the double pendulum, illustrated by Figures 2-15b and 2-15c.

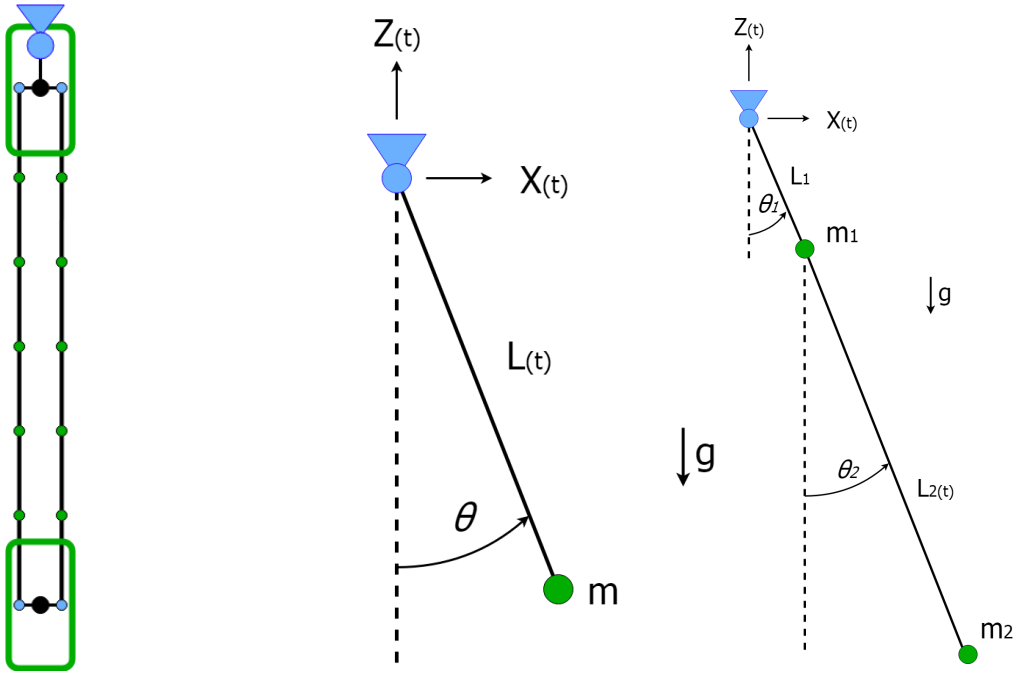

(a) Hoist system model **(b)** Single pendulum **(c)** Double pendulum

Figure 2-15: Hoist system models

The hoist system can be seen as a double pendulum system, as the cables can hinge at the upper hoist block. But as the two cable set-up will create a stiffness against bending, the hoist system will behave as a single pendulum in most situations. To analyse the behaviour the three models were subjected to an impulse in x-direction on the lower mass. For the hoist system model this impulse was applied to the lower hoist block mass, for the single pendulum the impulse was applied to the point mass m, and for the double pendulum the impulse was be applied to the point mass m_2. Figure 2-16 shows the impulse responses of the Single Pendulum, Double Pendulum, and the hoist system model.

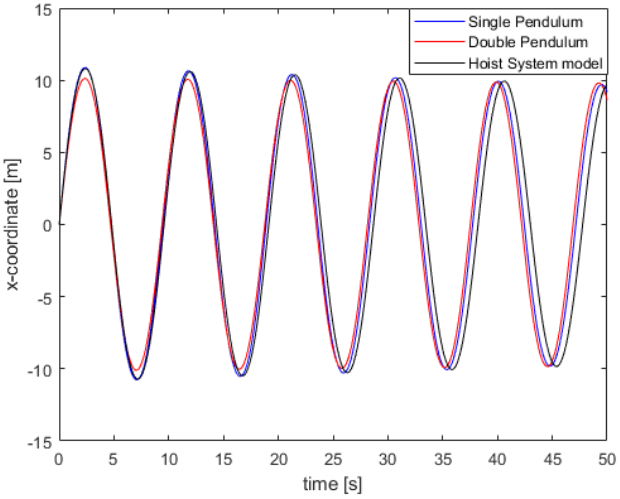

Figure 2-16: Impulse response

The impulse responses of the single and double pendulum models are very similar to that of the hoist system. And when a frequency analysis is performed on the response signals, as illustrated by Figure 2-17, the single and double pendulum models both seem to be able to predict the behaviour of the lower hoist block. But if we look at the movement of the upper hoist block in comparison with the first link of the double pendulum in Figure 2-18 we can see a dissimilarity caused by the aforementioned stiffness to rotation at the hinge points of the upper hoist block. Although the movement of the upper hoist block starts out of phase with the lower hoist block in the first seconds of the impulse response, the phase shift decreases rapidly to zero. While the first link of the double pendulum model clearly has a higher second frequency in its response. Whilst the virtual second link position of the single pendulum shown in Figure 2-18c only has one frequency, although the amplitude is higher due to the lack of damping. The frequency analysis of these responses show this second frequency clearly as illustrated by Figure 2-19. This discrepancy steered the decision towards using the single pendulum model for the development of the sway reduction controller. As the single pendulum better predicts the behaviour of the hoist system model for most situations.
It is also interesting to note that the variable bending stiffness has little influence on the overall dynamics, as the the damping relative to the mass of the lower hoist block is very low. Due to the large linear stiffness, the average curvature is also very small, which further reduces the impact of the variable bending stiffness.

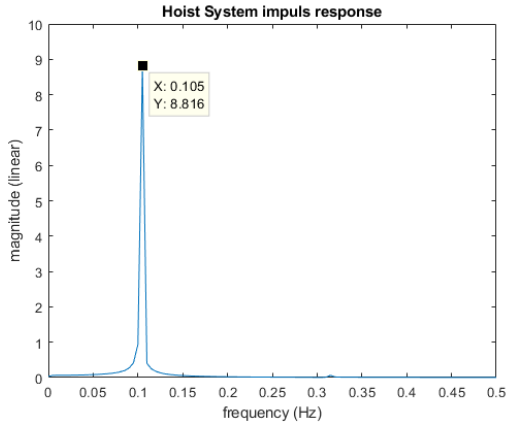

(a) Impulse frequency response Hoist system model

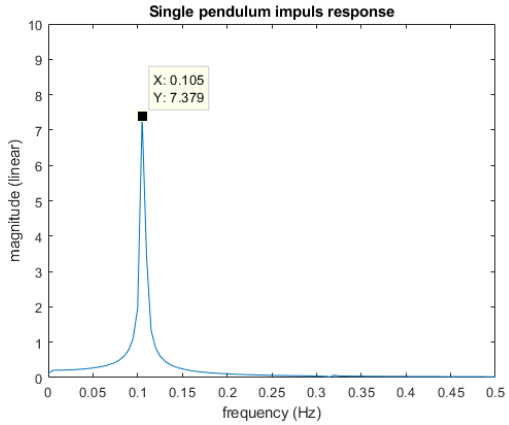

(b) Impulse frequency response Single pendulum

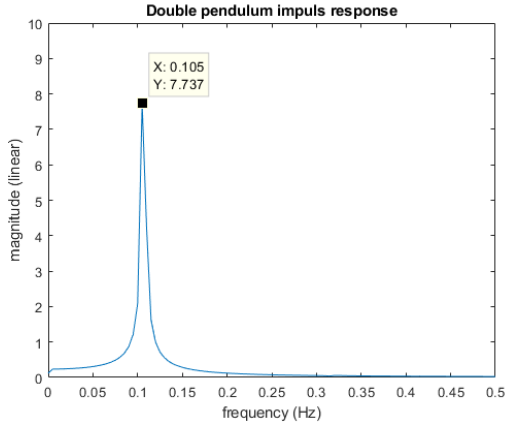

(c) Impulse frequency response Double pendulum

Figure 2-17: Impulse frequency response Hoist system models

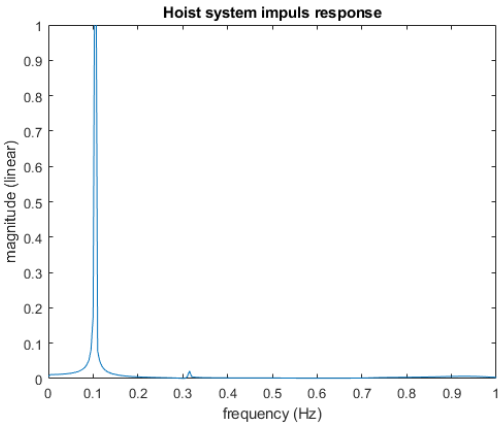

(a) Impulse frequency response upper hoist block

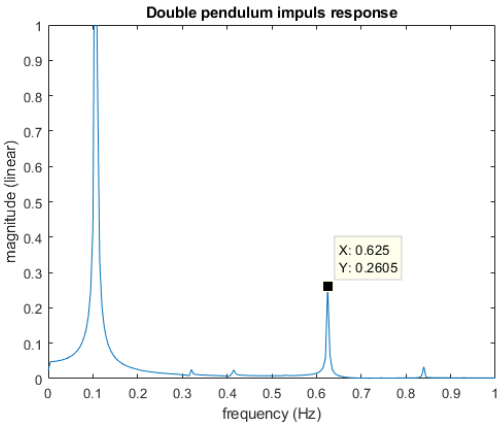

(b) Impulse frequency response first link

Figure 2-19: Impulse frequency response

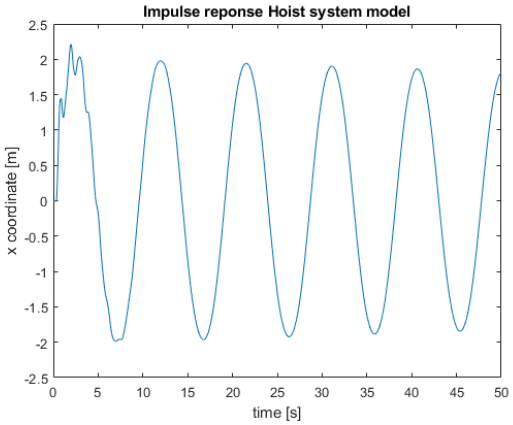

(a) Impulse response upper hoist block

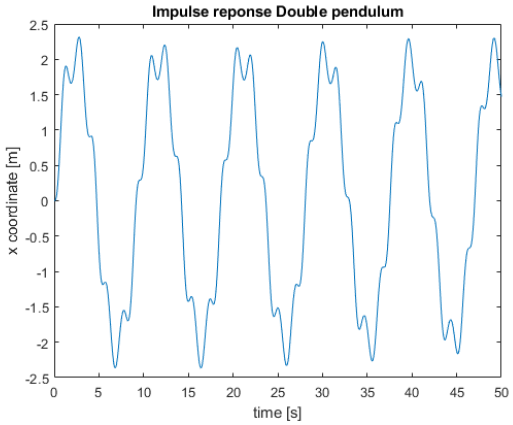

(b) Impulse response first link

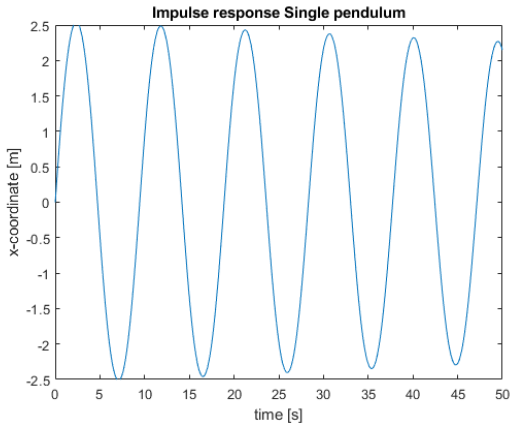

(c) Impulse response virtual first link

Figure 2-18: Impulse response

2-4 Summary

In this chapter it is discussed how the hoist system was modelled. The hoist blocks were modelled as point masses with moment of inertia, neglecting any influence from the sheaves. The hoist cable was modelled using the lumped-mass method with addition of variable bending stiffness. The cable model was validated using the theory behind lateral string vibrations and catenary equations. It was observed that using 50 cable elements created the accuracy necessary to model the cable dynamics with bending stiffness. After which the hoist system model was assembled using the interfacing forces.
The hoist system model was compared with the mathematical single pendulum and double pendulum models, using an impulse response. On the basis of the impulse response and the impulse frequency response it was decided to use the single pendulum as low-detail model. This low-detail model was later used to develop the sway reducing control algorithm.
It was also observed that the variable bending stiffness did not significantly influence the dynamics of the hoist system model.

2-5 Conclusion

As there is no data on the dynamics of the hoist system the assembled model could not be validated using real-life data. This will be a recommendation for future work. The cable model however was validated, which makes up a large part of the hoist system, creating confidence in the accuracy of the model. This hoist system model will be used to evaluate the sway reducing control algorithm after its development.
The dynamics of the hoist system model can be approximated using a mathematical single pendulum. This simplification is very useful for the development of the sway reducing control algorithm, as it reduces simulation time, and makes the process more transparent.
As the variable bending stiffness did not significantly influence the dynamics of the hoist system model, it could have been neglected. But as it is already implemented it will remain in the model.
With the hoist system modelled, the sway problem during the connection process mentioned in Chapter 1 can be analysed.

Chapter 3

Problem analysis

The sway reduction controller will be developed to reduce the sway introduced in the Hoist System during the lowering process. Before clear control objectives can be established, an analysis was first made of the lowering process using the Hoist System model developed in Chapter 2.
First the pre-tension requirement of the hoist system will be discussed, then the three connection cases will be outlined, and finally an analysis will be made on the basis of simulations using the Hoist System model.

3-1 Pre-tension requirement

The engineering team of the JLS has determined that a summed pre-tension of 316 tonnes is needed in the hoist cables at all times to prevent twisting of the cables, which can create damage such as hockling and birdcaging. This pre-tension can be partially or fully generated by the cumulative mass of the lower hoist block and the connection attachment. Because the pre-tension is not fully generated by the mass, two options are being regarded. The first is to add mass to the connection attachment to create the required mass to fulfill the pre-tension requirement. The second option is to use a fibre rope to pull at the lower hoist block to meet the required pre-tension.
Figure 3-1 shows the connection procedure of case 1, with a link-plate attachment, which uses a fibre rope to meet the required pre-tension. The fibre rope is attached with one end to the lower hoist block, and with the other end attached to a 300 tonne winch, which will be used in constant tension modes. To use the fibre rope, first a sheave is installed on the top of the jacket. The fibre rope is slung around the sheave by riggers, and pulled to the required pre-tension. After which the break of the hoist system is released and the hoist cable is paid out.
The drawback of the fibre rope option is the need for extra preparation and time. Before the connection procedure is started multiple sheaves will have to be installed on the jacket. The second drawback is the added risk to safety. During the connection procedure riggers

will have to be present on the jacket to secure the fibre rope around the sheave. The third drawback is the need for a winch of sufficient performance to pull on the fibre rope.
When choosing instead to add mass to the connection attachment, the total lift capacity of the JLS will be decreased. But more important the total mass of the JLS beam is increased, which has to be upended before the lift procedure.
Because every jacket lift procedure has different circumstances, the pros and cons have to be reconsidered every procedure.

3-2 Connection cases

The JLS engineering team is considering three different connection cases. In two of the cases an auxiliary fibre rope is used to pull the required pre-tension into the hoist cables, during the lowering process. The third case, the so called "self-lowering" case, does not use an auxiliary fibre rope, but uses a hook with added mass to provide the required pretension. In all cases the mass of the upper hoist block is 89 tonnes, and the mass of the lower hoist block is 107 tonnes.

3-2-1 Case 1: Link-plate

The first case uses a link-plate attachment to provide the connection between the hoist system and the jacket. The link-plate has a mass of 10 tonnes, which makes the total mass at the lower hoist block 117 tonnes, therefore an auxiliary fibre rope is needed to pull a force of 199 tonnes on the lower hoist block. Figure 3-1 shows the connection procedure of Case 1. For this case a lift point has to be created on the jacket where the link-plate can be attached using a hydraulic pin.

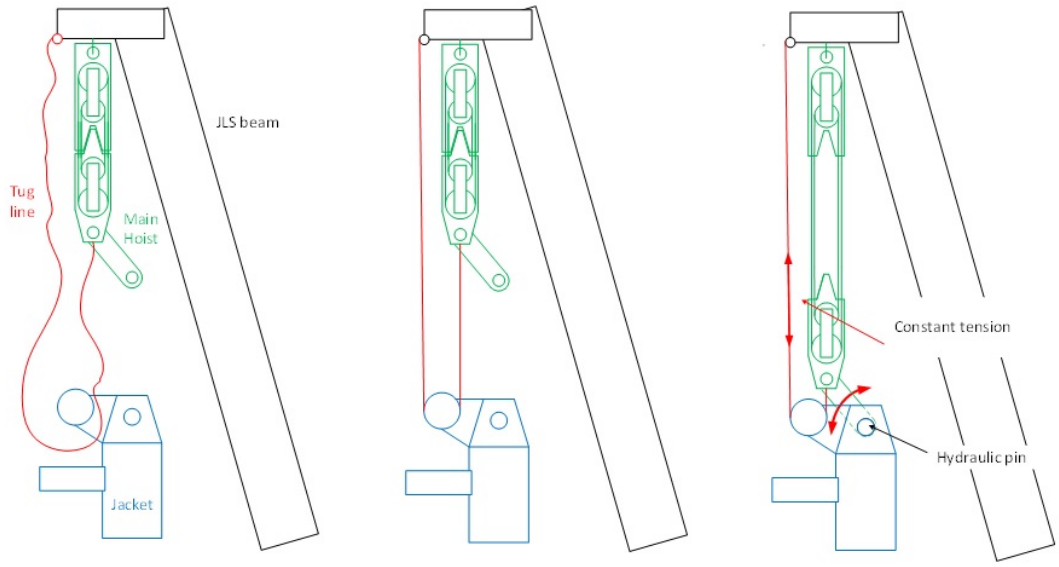

Figure 3-1: Link-plate connection procedure

3-2-2 Case 2: Hook and sling

The second case uses a hook and sling to provide the connection between the hoist system and the jacket. The lowering procedure is identical to the one of Case 1, but instead of connecting a link-plate with a hydraulic pin, the hook is attached to the jacket using slings. The hook adds a mass of 76 tonnes to the lower hoist block, requiring a fibre rope pulling force of 133 tonnes. In future reference the fibre rope force which is implemented is mentioned in the case name: "hook&sling 133".

3-2-3 Case 3: Self-lowering hook

The third case uses the hook and sling method, just like case 2, but instead of using a fibre rope to pull the required pre-tension into the hoist system, extra mass is added to the hook. Thus the hook will have a total mass of 209 tonnes, making the accumulative mass of the lower hoist block and the hook 316 tonnes. This makes the fibre rope method unnecessary.

3-2-4 Simulation cases

To simulate the lowering process of these cases, the masses of the connection attachments will be added to the point mass of the lower hoist block. In the cases where the auxiliary fibre rope is used, a force vector with a constant magnitude is imposed on the point mass of the lower hoist block in the direction of the jacket, (x_{target}, z_{target}). Table 3-1 lists the masses of the hoist blocks, and the magnitude of the pulling force of the fibre rope for the three cases.

Table 3-1: Cases lowering process simulation

Case	Upper block mass [t]	Lower block mass [t]	Fibre rope force [t]
Case 1: link-plate	89	117	199
Case 2: hook&sling133	89	183	133
Case 3: self-lowering	89	316	0

3-3 Lowering process analysis

The lowering process starts when the break of the hoist system is disabled, and the lower hoist block is lowered towards the jacket with a speed of 0.2 [m/s]. The length of the hoist cables start at 10 [m] and are increased to 80 [m] over 350 [s]; with the length of the upper hoist block adding 5 [m] to the total length making it 85 [m]. Figure 3-2a illustrates the length over time of the hoist system. In the simulation the ship motion projected on the hinge of the hoist system, in the tip of the JLS beam, is simplified to an ellipse with an amplitude in x-direction of 0.49 [m] and amplitude in y-direction of 1.26 [m] , with a period of 9.65 [s]. This ellipse, illustrated by Figure 3-2b, is determined on the basis of a 3-hour maximum motion report of *Pioneering Spirit*, which can be found in the appendix in Figure A-1. This ship motion can induce a large sway in the hoist system, therefore the movement in x-direction of the lower hoist block is examined to analyse this problem.

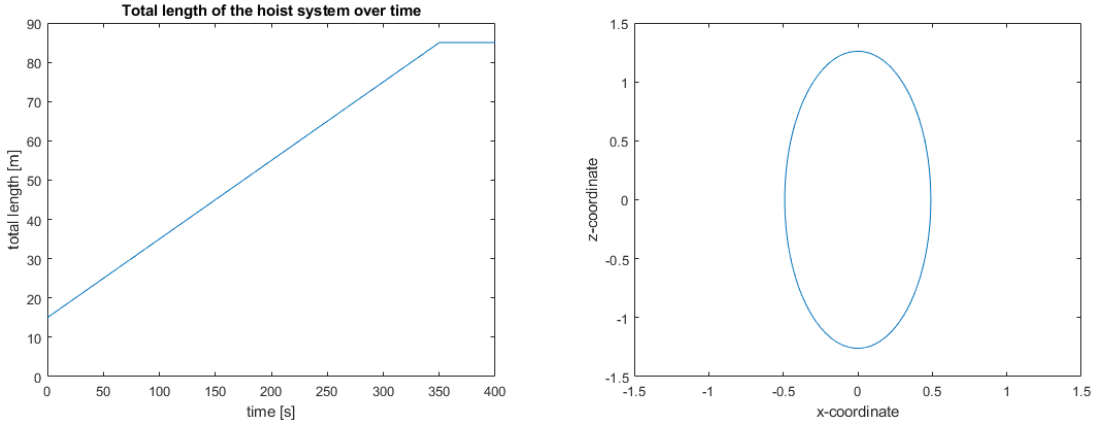

(a) Total length of hoist system over time **(b)** Hinge movement

Figure 3-2: Imposed motion on the hoist system

3-3-1 Case 3: self-lowering

Case 3: self-lowering does not use the fibre rope method, and behaves much like a single pendulum with a moving support, as mentioned in Chapter 2. Figure 3-3a illustrates that the lower hoist block starts to sway due to the movement of the hinge point. Figure 3-3b illustrates the natural period of the hoist system as a function of length. When the length of

the hoist system is increased the natural period will become equal to the period of the hinge motion, as mentioned in Chapter 1; at this point the motion of the hinge point introduces a large amount of energy into the hoist system, resulting in a large sway amplitude. The sway amplitude is limited by the damping in the system. When the length of the hoist cable is further increased the sway amplitude persists, because the damping in the system is very low. The sway amplitude will fall to a minimum within finite time, but this takes hours. The critical length of the hoist cable was observed to be around 18 metres. This makes the length between the hinge point, and the lower hoist block around 23 metres. The natural period T_n of a pendulum with a length L of 23 metres is

$$T_n = \frac{2\pi}{\sqrt{\frac{g}{L}}} \approx 9.65 \quad [s], \tag{3-1}$$

with g the gravitational acceleration. It is also interesting to note that the pay out speed of the hoist cable has influence on the maximum amplitude of the sway. The longer the length of the hoist system is near the critical length the more energy is introduced in the system. Which means a faster pay out speed results in a smaller maximum sway amplitude and vice versa.

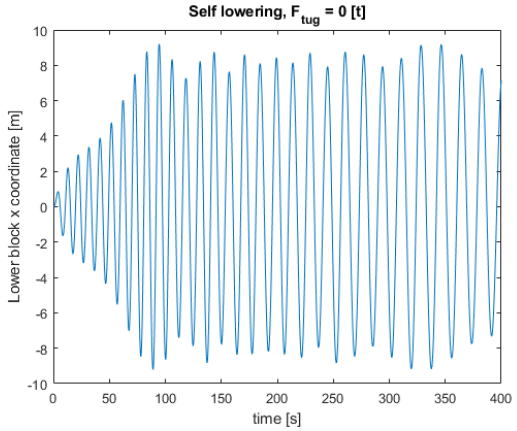

(a) Lowering process analysis Case 3

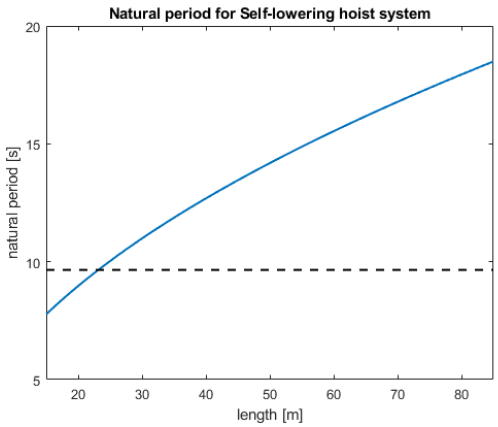

(b) Natural period vs total length of the hoist system

Figure 3-3: Case 3: Self-lowering hook

3-3-2 Case 1: link-plate

Figure 3-5 shows the sway of Case 1: link-plate. In contrast with Case 3: self-lowering, the sway amplitude is small, as the tension of the fibre rope decreases the natural period. The hoist system basically behaves like a weight in between two taut strings. As the natural period does not come close to the period of the hinge motion it can not introduce a large amount of energy into the system. This is an important effect as will be illustrated by Case 2: hook and sling.

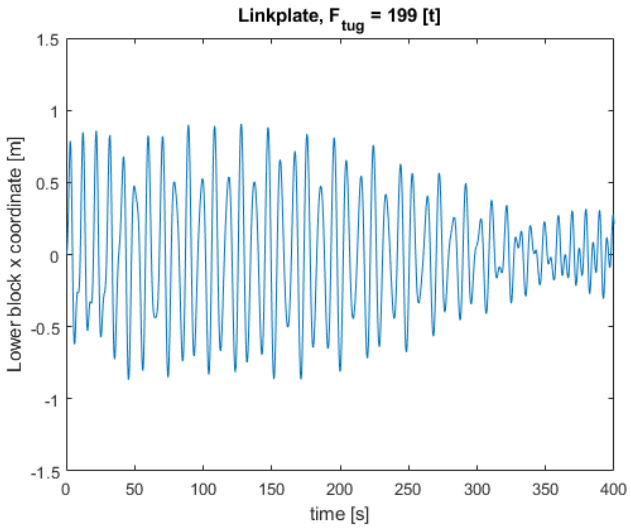

Figure 3-4: Case 1: Link-plate

3-3-3 Case 2: Hook and sling

Figure 3-5 shows the sway of Case 2: hook&sling 133. It is evident that the sway amplitude increases drastically when the length of the hoist cables is paid out to eighty metres. The larger mass at the lower hoist block in combination with a lower tension in the fibre rope results in a natural period close to the hinge motion. On the basis of these results two extra cases were simulated for the hook and sling method. This time the tension in the fibre rope was increased. Table 3-2 lists the parameters for Case 4: hook&sling 199 and Case 5: hook&sling 250.

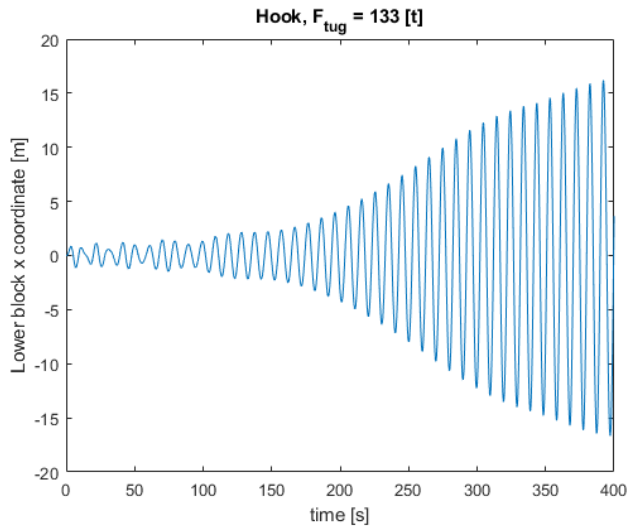

Figure 3-5: Case 2: hook and sling

Table 3-2: Cases lowering process simulation

Case	Upper block mass [t]	Lower block mass [t]	Fibre rope force [t]
Case 4:hook&sling199	89	183	199
Case 5:hook&sling250	89	183	250

Figure 3-6 shows that by increasing the tension in the fibre rope the large sway is eliminated, and the sway amplitude has become similar to that of Case 1.

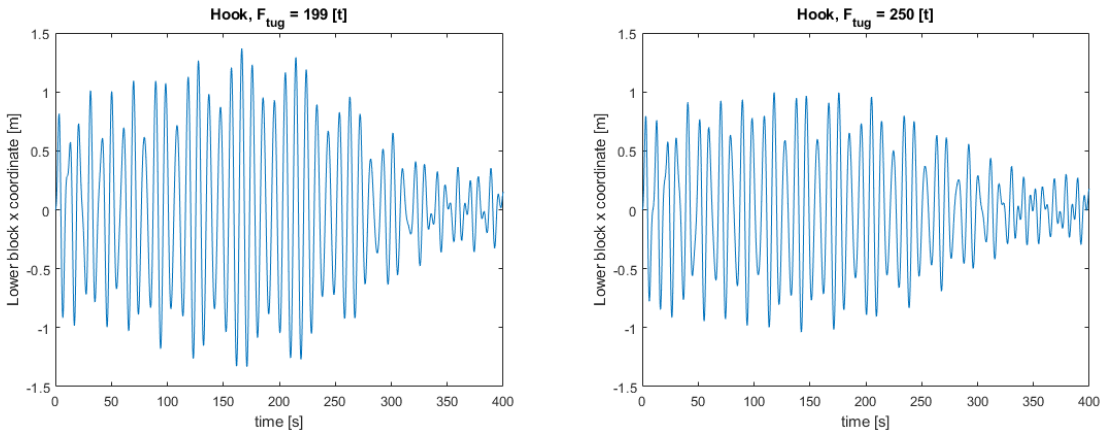

(a) Case 4: Hook and sling 199

(b) Case 5: Hook and sling 250

Figure 3-6: Lowering process analysis 2

To further illustrate this effect multiple simulations were done to map the natural period of the hoist system with hook attachment for different fibre rope tensions. The results are shown in Figure 3-7. When looking at the red line representing Case 2: hook&sling 133, it is clear that the natural period of the hoist system is almost identical to the critical value of 9.65 seconds around the 63 metre length mark. In Figure 3-5 this length is reached around $t = 240$ [s], at this time a large increase in sway amplitude is observed. When using the fibre rope it will be important to make sure the normal period of the hoist system is not near the period of the hinge motion during the lowering process, to prevent large sway amplitudes.

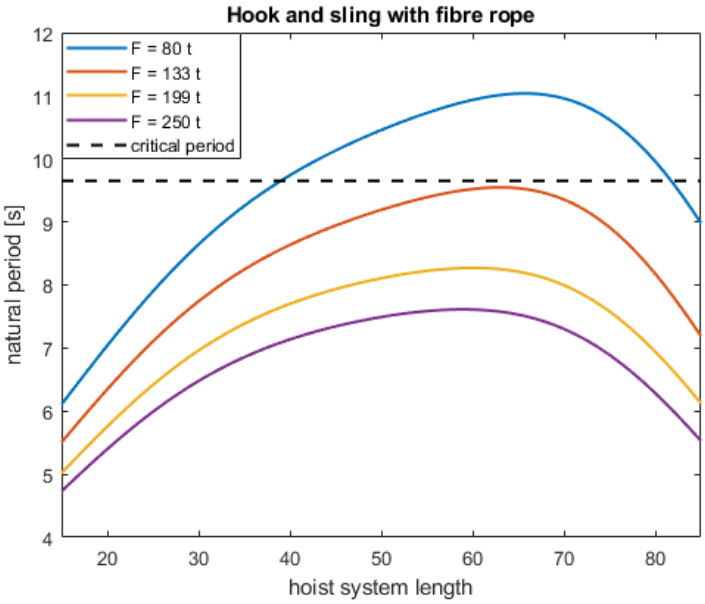

Figure 3-7: Natural period of hoist system with hook and varying fibre rope tension

Increasing the fibre rope tension will have consequences for the needed winch performance. As an example the needed winch power during the lowering process of Case 5: hook&sling 250 is shown in Figure 3-8, which shows a winch of a minimum of 2.5 [MW] would be needed to keep the pre-tension constant during the lowering process. This maximum power need is also influenced by the lowering speed of the hoist system. After the 350 [s] mark the power drops, as a constant length is reached. As discussed in Section 3-3-1 increasing the lowering speed could help decrease the maximum sway amplitude, but this will also result in a higher power need of the winches.

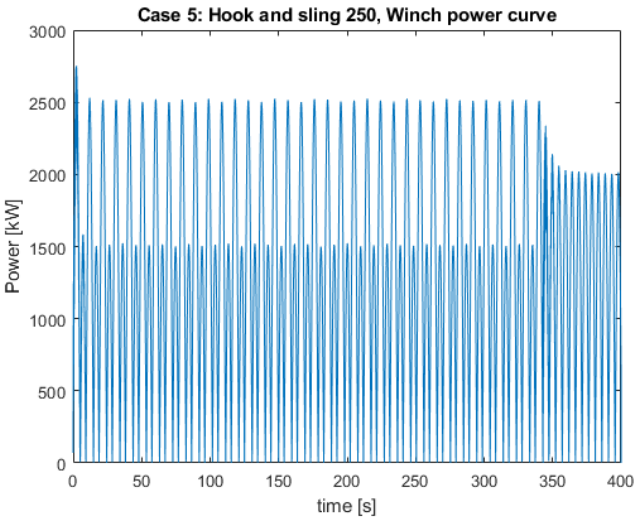

Figure 3-8: Power curve of fibre rope winch with constant tension of 250 t

3-4 Summary

In Case 1: link-plate, the hinge motion does not introduce a large sway into the hoist system, as the fibre rope used to generate the required pre-tension decreases the natural period.
In Case 2: hook&sling133, the hinge motion can induce a large sway into the hoist system if the fibre rope tension is too low relative to the mass of the lower hoist block. In Case 4: hook&sling 199 and Case 5: hook&sling 250 it is shown that by increasing the fibre rope tension the large sway is eliminated, as this decreases the natural period as shown in Figure 3-7.
In Case 3: self-lowering, the natural period is solely influenced by the length of the hoist cable, and the motion of the hinge point will induce a large sway into the system when the total length reaches 23 metres. As no fibre rope is used, and the magnitude of the mass has no influence on the natural frequency, this sway can not be eliminated without additions to the system.

3-5 Conclusion

The simulations of the Hoist System model show that in case an auxiliary fibre rope is used to tension the hoist system during the lowering process, the hinge motion will be prevented of creating a large sway into the system; if the fibre rope tension is large enough relative to the mass at the lower hoist block to keep the natural period away from the critical value.
In case no auxiliary fibre rope is used, there is nothing preventing the hinge motion of creating a large sway into the hoist system. In Case 3: self-lowering adding an actuator in combination with a sway reducing algorithm can prove to be a solution. In Chapter 4 the development of the sway reducing control algorithm for this case will be discussed.

Chapter 4

Controller development

In Chapter 3 the lowering process of Case 3: "Self-lowering" was analysed. It was observed that a large sway resulted from the ship motion. The objective of this thesis is to develop a control system which can reduce this sway to allow the hoist system to be connected to the jacket. Apart from the sway, slow position drift can also occur during the connection process. In this chapter the development of the control algorithm will be discussed. First the control problem will be determined, secondly an actuator will be proposed, and thirdly the control algorithm will be build up step by step, to solve the control problem.

4-1 Control problem

The control problem can be divided into two parts, the avoidance of sway motions and the drift compensation. First clear goals for the sway control problem will be determined, secondly the influence of drift will be discussed.

4-1-1 Sway control problem

For the development of the control algorithm the sway control problem has to be described with clear performance goals. Figure 4-1 illustrates these performance goals. First a maximum amplitude is set at three metres relative to the ship, represented by the dashed black line in Figure 4-1a. A large sway could result in a collision between the hoist system and the JLS beam, or other equipment. By keeping the maximum sway down when the hoist system is short, this risk is reduced. The second goal is to have a final amplitude of half a metre relative to the jacket, to allow the hoist system to be connected to the jacket, as illustrated by Figure 4-1b as a red dashed line. These performance goals have to be met by the control system to be successful. This brings us to the performance indicators. To compare several control algorithms, multiple performance indicators are determined. Two are related to the performance goals. The first is the maximum amplitude, this value should be minimized. The

second is the final amplitude, this one should also be minimized. To put it simple, when the lower hoist block is near the top, the maximum amplitude relative to the ship should remain small. When the lower hoist block is near the bottom, the final amplitude relative to the jacket should be small.

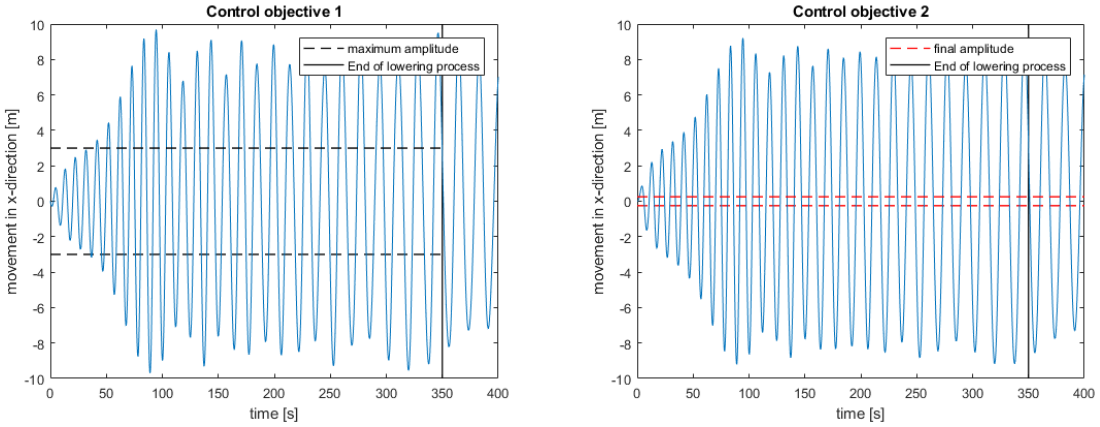

(a) Movement relative to ship **(b)** Movement relative to jacket

Figure 4-1: Control objective

The other performance indicators are related to the efficiency of the control algorithm. Two important parameters of a winch are its rated pulling force, and the motor power. By minimizing the needed force of the actuator and the needed actuator power, a smaller and cheaper winch can be used. The performance goals and indicators are listed below.

Performance Goals

- Maximum amplitude [3 metres], relative to the ship
- Final amplitude [0.25 metres], relative to the jacket

Performance indicators

- Maximum amplitude, relative to the ship [minimize]
- Final amplitude, relative to the jacket [minimize]
- Actuator force [minimize]
- Actuator power [minimize]

4-1-2 Drift control problem

The sway problem is largely caused by fast ship motions, which have a period around 9.65 [s] as seen in Figure 4-2b. Therefore the ship motion was approximated with a sine wave of that period, as seen in Figure 4-2a. However another slower motion can be observed, with a period around 200 [s], as seen in Figure 4-2b. This slow ship motion is caused by the Dynamic Positioning system of *Pioneering Spirit*. This is an oscillatory behaviour, but in short term

the ship seems to drift off. It is clear that the hoist system cannot be connected to the jacket if the position is off set by 1.5 metres. Thus the control algorithm has to be able to compensate for drift of the ship.

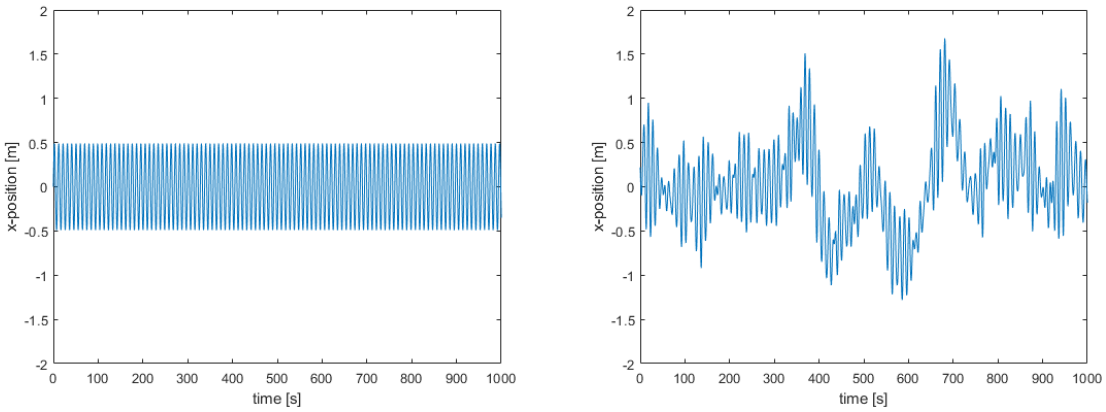

(a) Approximated ship motion in x-direction **(b)** Measured ship motion in x-direction

Figure 4-2: Ship motion approximation

To approximate this slow ship motion, an extra sine wave with a period of 200 [s] is added to the fast sine, as seen in Figure 4-3. This signal will be used as the ship motion for the development of the control algorithm.

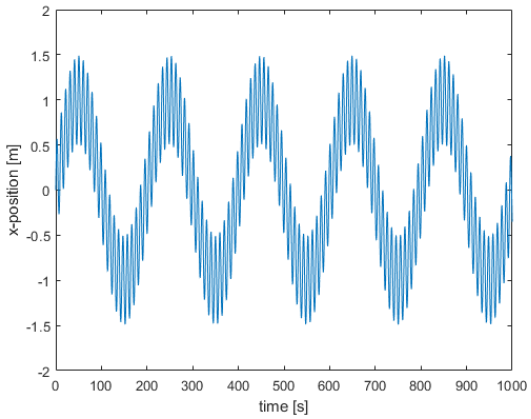

Figure 4-3: Approximation of ship motion in x-direction, with drift

4-2 Actuator

As mentioned in Chapter 3, the hoist system has no suitable actuator for use as an input for a sway reduction controller, therefore an actuator design was proposed in this section. The goal was to propose an actuator that did not require invasive changes in the JLS beam, or the hoist system.

4-2-1 Actuator proposal

The simplest solution to implement an actuator seemed to attach a tagline to the lower hoist block and control the tension with a winch, located on the deck of the ship. As the goal is to create a force in x-direction, the angle between the tension vector and the lower hoist block is important. Therefore the tagline is directed with a sheave on the JLS beam to minimize this angle at the point where the needed force is greatest, as seen in Figure 4-4. The most critical point is when the hoist system is connected to the jacket. Therefore this point is chosen at $z = 85$ metres, measured from the hinge point of the hoist system downwards. In Chapter 6 the advantages and disadvantages of other sheave heights is discussed.
One of the downsides of this actuator is the inability to exert a pushing force. This can be partially compensated by creating an offset from the resting position with a pretension. This way when the tension is lowered, gravity will 'push' on the lower block. This effect is obviously limited by the initial offset, and the gravitational acceleration.

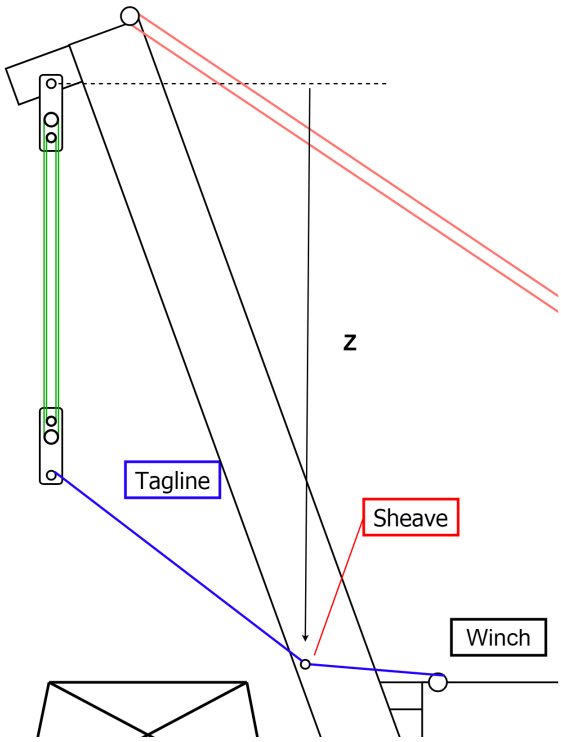

Figure 4-4: Actuator proposal

4-2-2 No control

To explore how the actuator interacts with the hoist system if no control is implemented three cases are discussed. The first case is simulated without any actuator. The second case is simulated such that the actuator has a perfect constant tension on the wire rope. The third case is simulated such that the wire rope has a constant length. In these cases it is assumed that the hoist system is already paid out to 85 metres, ready for connection, and there was no prior sway in the system. The approximated ship motion with, and without drift will be

applied to the hinge point of the hoist system.
First this case is simulated without any actuator. Figure 4-5 shows the output of the hoist system for both the ship motions. Figure 4-5a shows that without drift, the sway induced by the ship motion is twice as large as the objective goal of 0.25 metres; the lower block cannot be connected. With the addition of drift as illustrated by Figure 4-5b final amplitude becomes even larger.

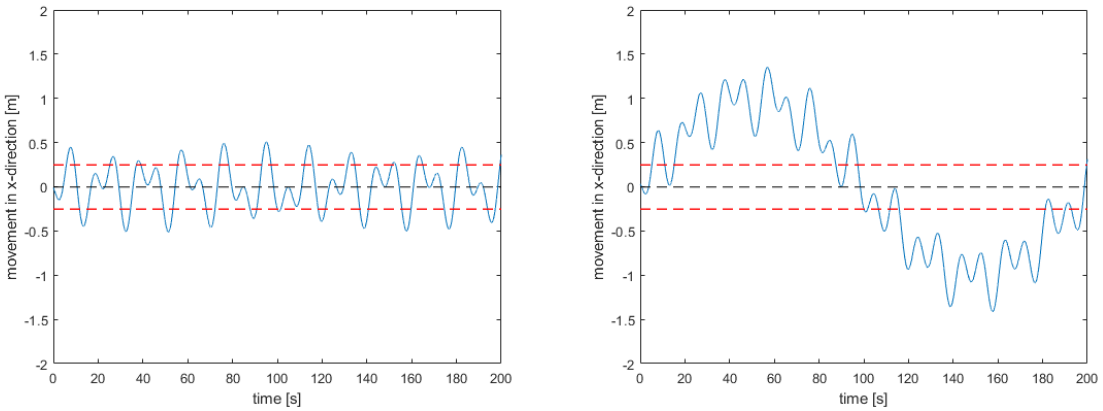

(a) no drift **(b)** with drift

Figure 4-5: No actuation, at 85 metres hoist length.
Motion is relative to jacket.

Second the actuator was simulated with a constant wire rope length, creating a mean strain of $\epsilon = 0.035$ $[m]$ resulting in a mean tension of $T = 50$ $[t]$. By implementing the actuator with a constant wire rope length a spring force is applied to the lower hoist block. This shifts the equilibrium of the lower hoist block, as illustrated by Figure 4-6a. This shift would have to be compensated by the positioning of the ship to still be able to connect the lower hoist block to the jacket. By using a longer constant length this offset can be reduced. But there seems to be no advantage of using a constant length over using no actuator at all. Note however that there is no damping implemented in the wire rope model, which is modelled as a linear spring. It might be possible even to attach a damping device in the wire rope to passively dampen the oscillations. When the ship drifts however, there is no way of compensating, as illustrated by 4-6b.

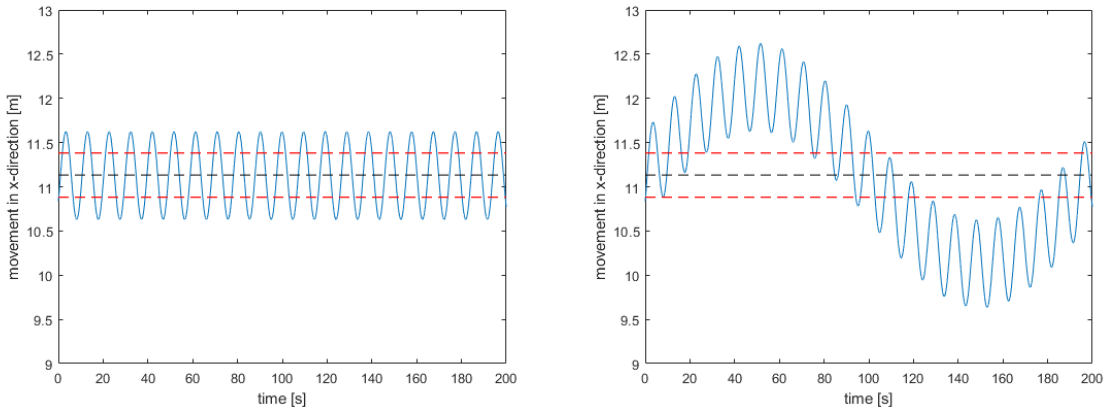

(a) no drift **(b)** with drift

Figure 4-6: Constant length winch, at 85 metres hoist length. Motion is relative to jacket.

Lastly the actuator was simulated with a perfect constant wire rope tension of $T = 50$ $[t]$. The result is similar to the constant length simulation. The sway amplitude is not reduced, and the drift is not compensated, as illustrated by Figure 4-7.

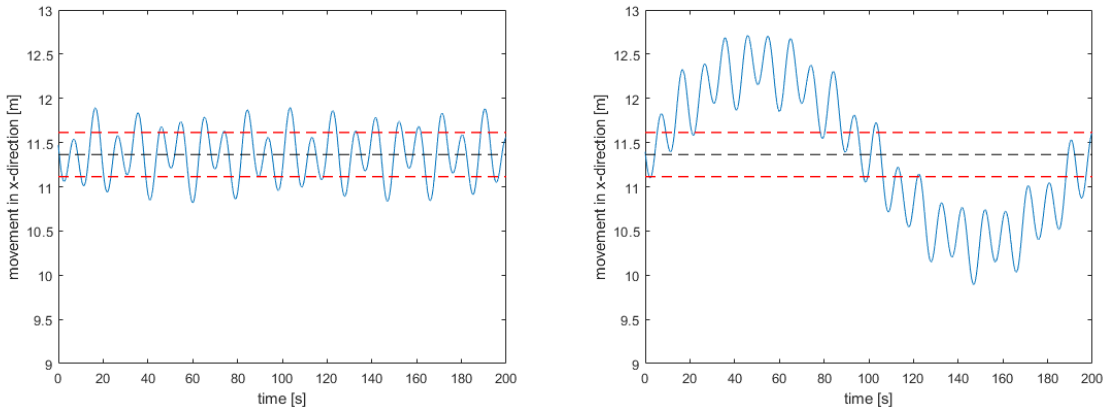

(a) no drift **(b)** with drift

Figure 4-7: Constant force winch, at 85 metres hoist length. Motion is relative to jacket.

In this section it is shown that implementing the actuator with a constant length, or constant force creates no advantages. If the actuator was implemented with an extra damping element this could dampen the oscillations enough to perform the connection procedure, but this would not compensate for the drift of the ship. When the additional sway problem discussed in this chapter is regarded, it is clear a control algorithm has to be developed for the actuator.

4-3 Controller design

In this section the design of the control algorithm will be discussed. The design is split up in three parts. First the controller will be developed assuming there is no drift, secondly the drift compensation will be added, then finally a gain schedule will be introduced for efficiency optimization. During the development the controller was implemented on the single pendulum model discussed in Section 2-3

4-3-1 Sway reducing controller

In this section the sway reducing control algorithm will be discussed. For this purpose it will be assumed that there is no drift. First a controller from literature will be shown, after which the newly developed algorithm based on this controller will be discussed.

4-3-1-1 Proportional Derivative controller

Ku et al. [3] designed a Proportional Derivative (PD) controller for the sway reduction of a derrick type crane on a barge. The controller was implemented using a tagline attached to the load. As the tagline can only pull the load, Ku et al. designated three cases, based on the status of the load. The three possible load statuses are shown in Figure 4-8, where $\theta_{l/A}$ is the load angle, the desired load angle is θ_d, and the error is defined as $e_\theta = \theta_{l/A} - \theta_d$.

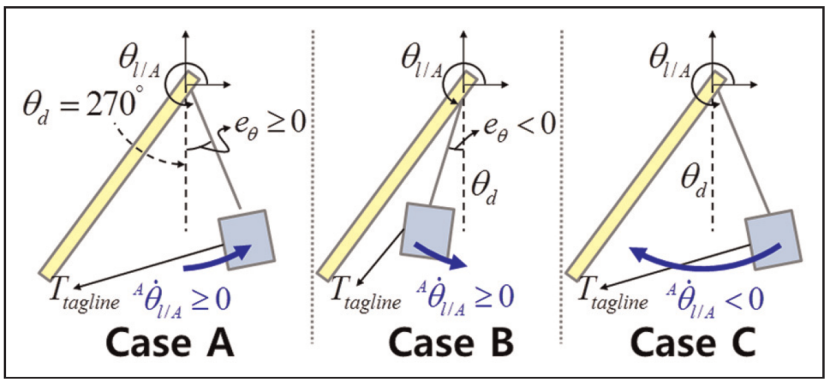

Figure 4-8: Classification of load status. Reprinted from Ku et al. [3].

In case A the load is moving away from the beam with an angle speed larger than zero ($\dot{\theta}_{l/A} \geq 0$). And the angle position is larger than the desired value ($e_\theta \geq 0$). In this case both the proportional and derivative action of the PD controller are used, as seen in Table 4-1, where K_p and K_d are the control parameters.
In case B the load is moving away from the beam towards the desired angle position ($e_\theta < 0$). With an angle speed larger than zero ($\dot{\theta}_{l/A} \geq 0$). In this case only the derivative gain of the PD controller is used, to slow down the load.
In case C the load is moving towards the beam, which means the angular velocity is smaller

than zero ($\dot{\theta}_{l/A} < 0$). In this case the tagline tension is made zero, as it cannot be made negative. The control laws for these three cases are shown in Table 4-1.

Table 4-1: PD control scheme for the three cases

	Case A	Case B	Case C
Control schemes	$T_{tagline} = K_p e_\theta + K_d \dot{e}_\theta$	$T_{tagline} = K_d \dot{e}_\theta$	$T_{tagline} = 0$

4-3-1-2 Linear-Quadratic Regulator

Inspired by the PD controller of Ku [3], a Linear-Quadratic Regulator (LQR) control algorithm was designed for the sway reduction of the hoist system. This section will cover the linearisation of the pendulum model, the switching logic, optimal feedback gain, feedforward gain, and the results.

4-3-1-2-1 Linear model

For the synthesis of the optimal feedback control gain, a linear model has to be derived for the single pendulum model illustrated by Figure 2-15b. For this purpose the movement of the hinge is not included, and the length of the pendulum is assumed to be constant. Which gives us Equation (4-1). By linearising the sine function around $\theta = 0$ to $\sin(\theta) = \theta$ using the small angle rule, Equation (4-2) is derived.

$$\ddot{\theta} + 2\zeta\sqrt{\frac{g}{L}}\dot{\theta} + \frac{g}{L}\sin(\theta) = \frac{1}{mL}u \tag{4-1}$$

$$\ddot{\theta} + 2\zeta\sqrt{\frac{g}{L}}\dot{\theta} + \frac{g}{L}\theta = \frac{1}{mL}u \tag{4-2}$$

With the linear differential Equation (4-2), a state-space representation can be made of the single pendulum around an operating point. For this purpose a new set of coordinates will be introduced $x = [\, x_1 \; x_2 \,]' = [\, \theta \; \dot{\theta} \,]'$. Making the state-space representation

$$\begin{bmatrix} \dot{x}_1 \\ \dot{x}_2 \end{bmatrix} = \begin{bmatrix} 0 & 1 \\ -\frac{g}{L} & -2\zeta\sqrt{\frac{g}{L}} \end{bmatrix} \begin{bmatrix} x_1 \\ x_2 \end{bmatrix} + \begin{bmatrix} 0 \\ \frac{1}{mL} \end{bmatrix} u. \tag{4-3}$$

The state-space representation in Equation (4-3) can be used to calculate the optimal gain for varying hoist system length, L, lower hoist block mass, m, and damping ratio, ζ.

4-3-1-2-2 Optimal feedback gain

If Equation (4-3) is described as

$$\dot{x} = Ax + Bu, \tag{4-4}$$

the optimal feedback gain is

$$K = R^{-1}B^T P, \tag{4-5}$$

with R a tuning variable which puts a weight on the magnitude of the gain, the input matrix B, and the matrix P which is found solving the continuous-time Ricatti differential equation

$$A^T P + PA - PBR^{-1}B^T P + Q = 0, \tag{4-6}$$

with Q the tuning diagonal variable matrix that puts weight on the states

$$Q = \begin{bmatrix} q_1 & 0 \\ 0 & q_2 \end{bmatrix}. \tag{4-7}$$

By solving Equation (4-6) for P the cost function

$$J = \int_0^\infty (x^T Q x + u^T R u) dt, \tag{4-8}$$

is minimized. With P found the optimal feedback gain can be calculated using Equation (4-5) to create the control law

$$u = -Kx. \tag{4-9}$$

One significant difference between Ku's system and the hoist system is that the length of the hoist system changes over time, as illustrated by Figure 3-2a. This means the parameters of the system change over time, and the ideal tuning of the LQR controller does too. As the most important stage of the connection process, is the actual connecting of the lower hoist block to the jacket, which occurs at the final length of the system, in this case 85 [m], the LQR controller is tuned for that case.

4-3-1-2-3 Initial offset: LQR-FF

As mentioned in Section 4-2, to compensate for the lack of 'pushing' ability the hoist system can be off set using a feedforward gain. The ship can then be positioned to compensate for the offset, as illustrated by Figure 4-9. This way the gravitational acceleration can be used to apply a 'pushing' force. Thus the actuator can locally apply a symmetric input, the switching logic Ku et al. [3] used is therefore not needed.

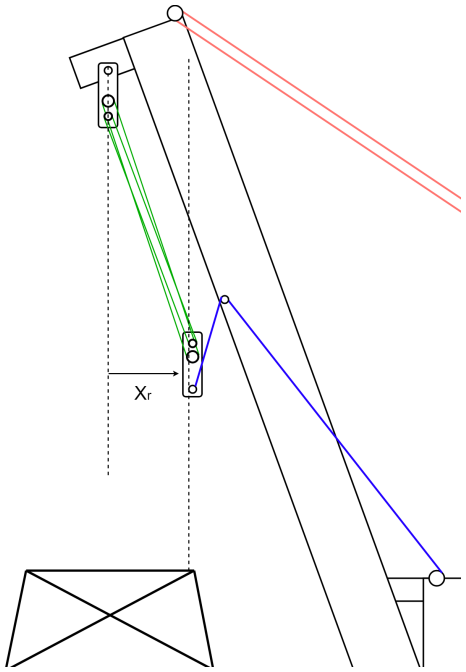

Figure 4-9: Off set hoist system

To offset the lower block the actuator has to apply a feedforward gain such that the x-coordinate of the lower block is equal to a reference signal. This gain should also take into account the angle between the actuator force, and the lower block. This feedforward gain is given by

$$u = mg \sin\left(\tan^{-1}(\frac{r}{L})\right) \frac{1}{\cos\left(\tan^{-1}(\frac{L+dz}{r-dx}) + \tan^{-1}(\frac{r}{L})\right)}, \tag{4-10}$$

where m is the mass of the lower block, the gravitational acceleration is given by g, the reference signal is given by r, the length of the hoist system is given by L, and the position of the guidance sheave on the jacket is given by (dx, dz), relative to the hinge of the hoist system.
The first part of the gain is equal to the force in x-direction needed to pull the lower block to the reference. The second part $[1/\cos(..)]$ is used to compensate for the angle between the fibre rope and the x-axis. The advantage of this initial offset method is discussed in the next section.

4-3-1-2-4 Results

In this section the intermediate results of the controller are discussed. First the results using the PD controller found in the literature will be discussed, secondly the advantage of the LQR with feedforward gain (LQR-FF) will be discussed. The LQR without feedforward is not discussed as its performance is very similar to the PD controller, as both are feedback controllers with a proportional and a derivative gain.

The simulation starts when the break of the hoist system is disabled, and the lower hoist block is lowered towards the jacket with a speed of 0.2 [m/s]. The length of the hoist cables starts at 10 [m] and is increased to 80 [m] over 350 [s] after which it is constant, indicated by the vertical black line; with the length of the upper hoist block adding 5 [m] to the total length making it 85 [m]. The final amplitude goal is represented by the red dashed line. The reference signal is represented by the black dashed line.
Figure 4-10a shows the output of the PD controller. The sway amplitude is significantly reduced, with a maximum amplitude of 1.29 metres relative to the hinge. The final amplitude is also within the goals, as represented by the red dashed lines. Note however that the oscillations of the lower block are off set of the zero position. This is due to the limitations of the actuator. As the fibre rope can only pull on the load, the control algorithm is asymmetric; which means that the control action which slows down the load also pulls it towards the ship. Figure 4-10b shows the output of the system controlled by the LQR-FF controller, with an initial offset of 3 metres. The reference signal slowly pulls the load towards the target of x = 0, as seen by the black dashed line. With this offset implemented, the actuator can locally provide a symmetric control input, which results in a close to symmetric oscillation around the target value. The final amplitude is 0.045 metres, as also shown in Table 4-2.

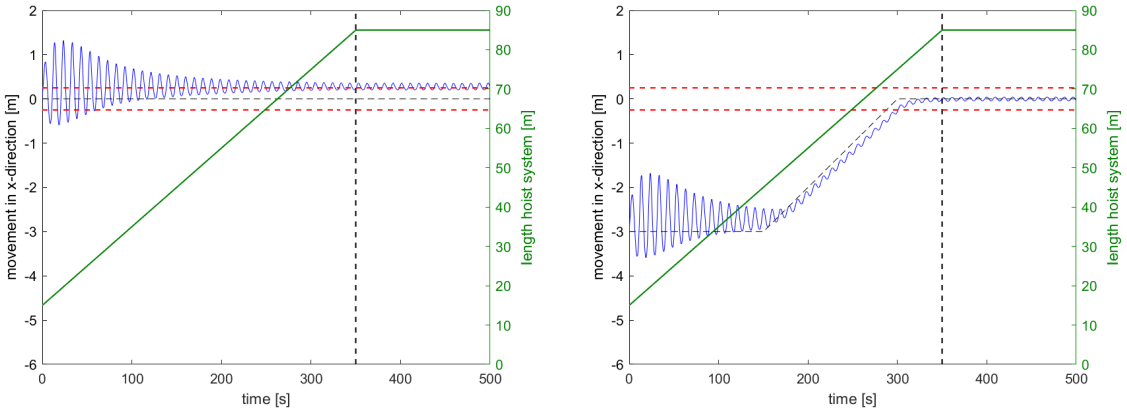

(a) PD controller result **(b)** LQR-FF controller result

Figure 4-10: Controller output

The last two performance indicators are illustrated by Figure 4-11. The maximum actuator force needed is 40 [t], with a maximum actuator power of 47 [kW]. The performance values are also shown in Table 4-2. It is important to note that actuator power is approximated using the power stroke, force times velocity, to compute the power as in Equation (4-11).

$$P = u\dot{x} \tag{4-11}$$

Depending on the actuator dynamics this might not be accurate. More on this will be discussed in Chapter 6.
In Figure 4-11a it is shown that a large force is needed to control the sway when the natural period of the hoist system is similar to the ship motion period, but the need decreases as the hoist system becomes longer. The transient of the feedforward gain is also cleary visible starting from t = 150 [s].

In Figure 4-11b it is shown that the required power is relatively similar during the connection process. First a large power is required to exert the large force, and later in the process a large power is needed because the movement of the lower block relative to the ship is large.

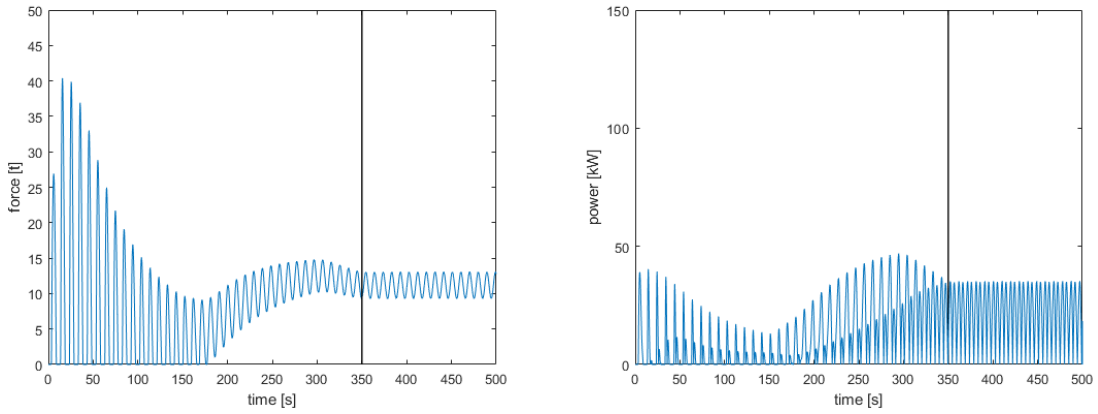

(a) Control input force **(b)** Control input power

Figure 4-11: Control input LQR controller

Finally the four performance indicators of the PD controller are compared to the indicators of the LQR-FF controller in Table 4-2. Both controllers have similar performance, but it is clear that the final sway is significantly reduced by using a feedforward gain to create an initial offset.

Table 4-2: LQR controller performance

Controller	max sway [m]	final sway [m]	max tension [t]	max power [kW]
PD	1.29	0.36	40	40
LQR-FF	1.29	0.045	40	47

4-3-2 Drift compensation

Now that the sway reducing algorithm has been developed, it will be tested with the approximated ship motion with drift, as shown in Figure 4-3. The effect of the slow ship motion is very apparent in the movement of the lower hoist block, as illustrated by Figure 4-12. This results in a large violation of the final amplitude goal. Which means that this control algorithm will not be able to compensate if the ship drifts from the jacket.

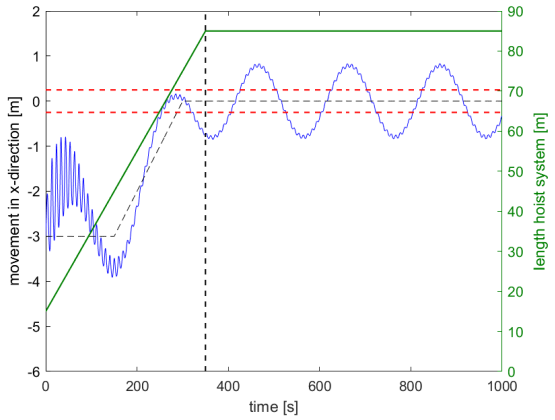

Figure 4-12: LQR-FF controller result with drift

The solution is quite simple. The ship motion can be measured. And if this measurement is low-pass filtered to reveal only the slow ship motion, it can be used to generate a reference signal to compensate the ship motion. The filtering does create a time delay, as seen in Figure 4-13, thus a compromise must be made between filtering low frequency dynamics, and creating extra delay.

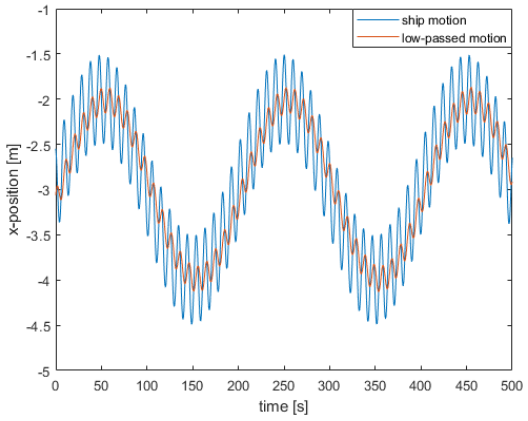

Figure 4-13: Filtered ship motion

This filter is also used in foresight of the additive noise which will be implemented in Chapter 5. If the ship motion was used un-filtered the feedforward gain would be very sensitive to noise.
The use of the feedforward gain will most likely create a steady-state offset, both in the initial reference and the drift compensation. To compensate for this offset an integrator will be used. The integral gain has the form of

$$u = K_I \int e(t)\, dt, \tag{4-12}$$

with K_I the integral gain, and the error $e = r - x$, with r the reference value and x the position of the lower block in x-direction.
An integral gain of $K_I = 1 \times 10^4$ was implemented, together with the LQR-FF control algorithm. This gain is not needed before the reference signal has reached zero, thus the integral gain is activated when $r(t) = 0$. The results are shown in Figure 4-14a. A large improvement can be seen in final amplitude. The slow motion is almost cancelled and the final amplitude is within the performance goals.

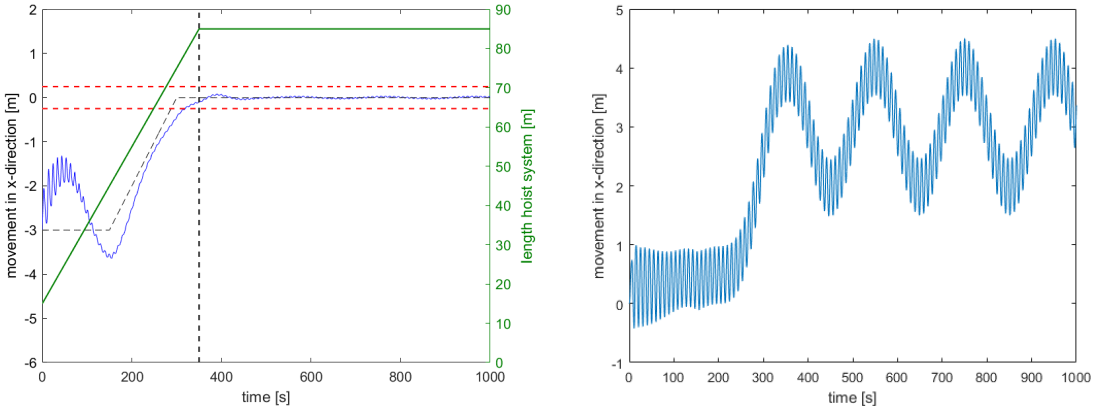

(a) LQRi FF controller result **(b)** Lower block motion relative to ship

Figure 4-14: Control output LQRi FF controller

The large movement between 0 and 200 seconds is not a problem, as the motion relative to the ship is kept small, as illustrated by Figure 4-14b. The maximum sway relative to the ship is actually very small, less than a metre as seen in Table 4-3. This improved performance is due to the more aggressive control settings used for the drift compensation. The maximum power output is therefore doubled. In the next section it will be discussed if the controller can be changed so that it is only aggressive when it needs to, making it more efficient.

4-3-3 Gain scheduling

As mentioned in the previous section, the maximum sway relative to the ship, when the hoist system is short, is overcompensated by the aggressiveness of the control algorithm. Which is not negative for the performance, but it creates unneeded power and force demands on the actuator, as illustrated by Figure 4-15. These peak power and force demands could be brought down by using smaller controller gains, in trade of a lower performance. Therefore a gain schedule is proposed based on the length of the hoist system.

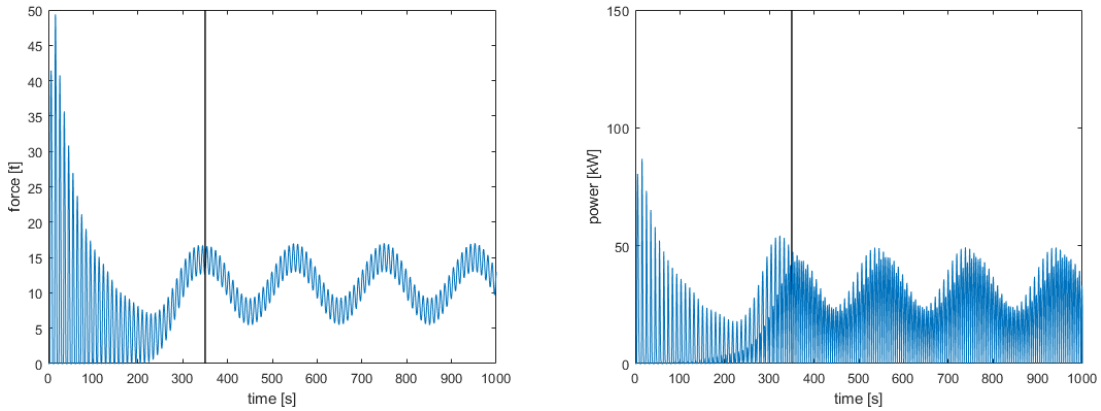

(a) Control input force **(b)** Control input power

Figure 4-15: Control input LQRi FF controller

With a gain schedule the controller can be made less aggressive when the hoist system is short, by using smaller gains at lower length values, as illustrated by Figure 4-16 where the derivative gain K_d is shown. These smaller gains can easily be calculated by increasing the weight on the input gain R, as mentioned in Section 4-3-1-2-2. To avoid a large spike in input gain, a transient is calculated between the low gain at lengths shorter than 30 metres, and the high gain needed at lengths longer than 70 metres. The location and slope of the ramp can be used as additional tuning parameters.

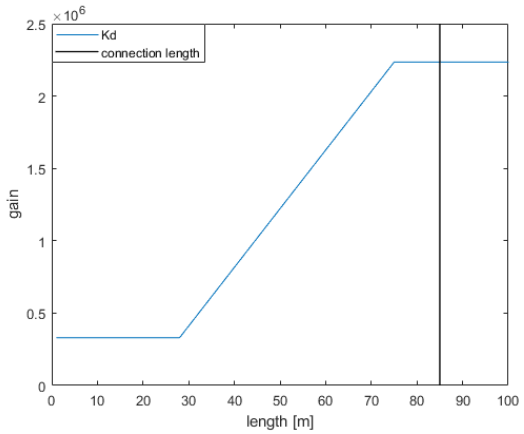

Figure 4-16: Gain schedule for derivative action

By implementing the gain schedule the performance is decreased as seen in Figure 4-17a. But the demands on the actuator are also decreased as illustrated by Figures 4-17b and 4-17c.

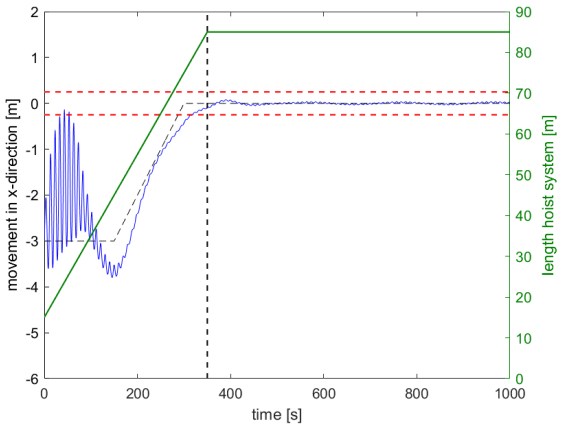

(a) sLQRi-FF results

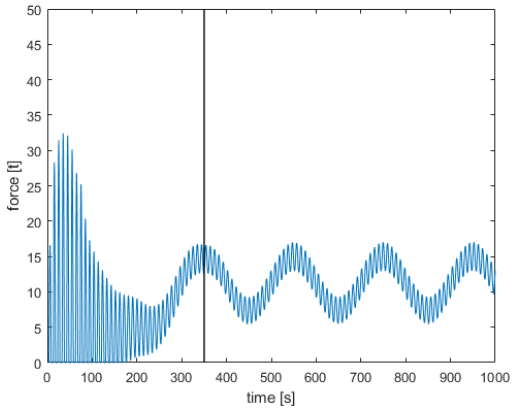

(b) Control input force

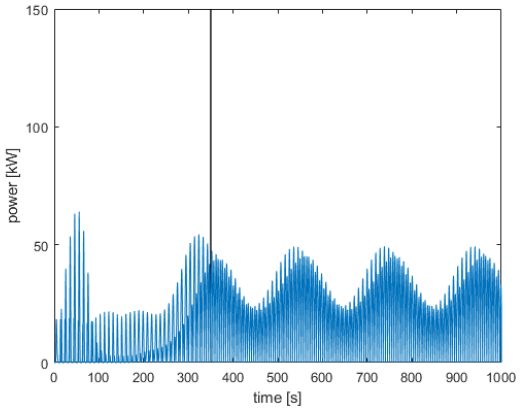

(c) Control input power

Figure 4-17: Control input and output for sLQRi FF controller

Table 4-3 shows the performance indicators for the LQR with integral and feedforward gain (LQRi-FF), and the gain scheduled LQR with integral and feedforward gain (sLQRi-FF). It is clear that the gain schedule decreased the peak performance needs on the actuator, in trade off an increased maximum sway.

Table 4-3: LQRi-FF controller performance

Controller	max sway [m]	final sway [m]	max tension [t]	max power [kW]
LQRi-FF	0.99	0.036	49	87
sLQRi-FF	1.92	0.036	32	64

4-4 Summary

In this chapter the problem analysis of the hoist system is converted into a clear control objective. This control objective is then fulfilled by implementing an LQR controller with

switching logic inspired by literature. This controller is then further enhanced with a feed-forward gain and integral gain, to compensate for ship drift during the connection process. Lastly a gain schedule is implemented on the LQR, to improve the efficiency of the controller.

4-5 Conclusion

Although the proposed actuator has a clear disadvantage, only being able to pull, this could partially be overcome by choosing an advantages equilibrium-point as reference. The simple controller could then easily reduce the sway amplitudes. With the oscillations reduced, the drift of the ship still had a large influence on the position of the lower hoist block. By incorporating the motion of the ship into the reference signal, the drift could be compensated. The motion of the ship still impacts the lower hoist block position, but the motion of the block is small enough to be able to connect to the jacket. In short, this controller design can fulfil the control objective set out in the beginning of this chapter.
These simulations are however performed on the single pendulum model the controller is developed on, with the assumption of full state information. Performance decreases are expected when it is implemented on the hoist system model with limited state information, and implementation of actuator dynamics, additive noise, and model uncertainty; which will be discussed in Chapter 5 and Chapter 6.

Chapter 5

Observer development

The sway reducing controller in Chapter 4 was developed assuming full state information was available, such as the position and velocity of the lower hoist block in world coordinates. In practise this is not the case. An observer was developed to obtain the needed state information for the controller. To provide input for this observer a new measurement system will be proposed which can be combined with sensors already present on *Pioneering Spirit* to measure the position of the lower hoist block. First the available measurements will be reviewed, then the observer structure will be discussed.

5-1 Measurement system

In this section a measurement system will be proposed to measure the position of the lower hoist block. This measurement system will measure the position relative to the ship. As the hoist system moves relative to the jacket due to the ship motion, the hoist system position relative to the jacket should also be measured. This can be done using sensors already present on *Pioneering spirit*.

5-1-1 Lower hoist block measurement

The proposed measurement system will be installed on the deck of the ship as illustrated by Figure 5-1. It will track the lower hoist block and measure the distance to the lower hoist block, which is depicted by L, using an optic or laser sensor. An angle decoder will measure the angle between the hoist block and the sensor, which is depicted in the figure by α. By combining these two measurements the distance d can be obtained. The position of the sensor relative to the hoist system will be known, therefore the distance d can be used to obtain the deflection of the lower hoist block in x-direction, X_r, which will be called the relative x-position of the lower hoist block. The relative x-position X_r will be one of the inputs for the observer.

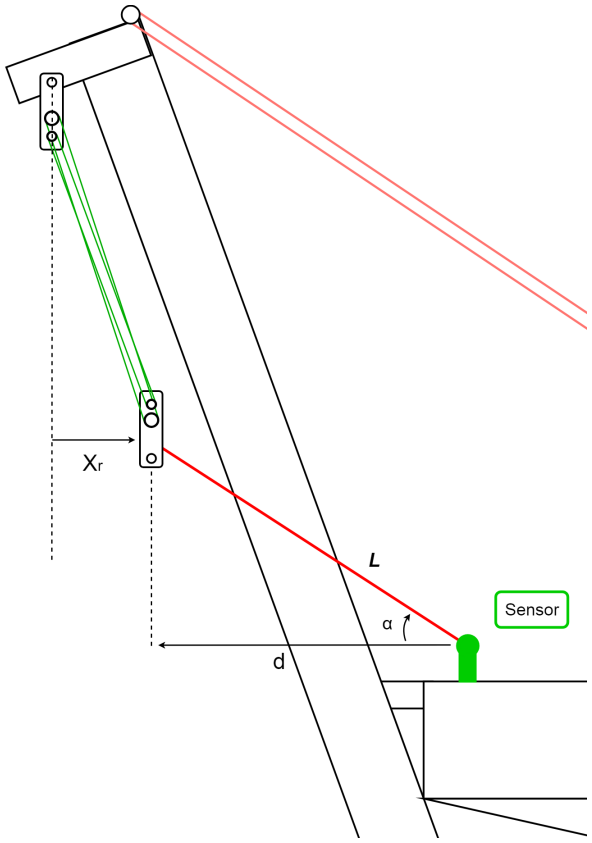

Figure 5-1: Block position measurement

5-1-2 Ship motion measurement

With the proposed measurement system X_r can be obtained, but the controller needs to know the position of the lower hoist block relative to the jacket, illustrated in Figure 5-2 as X_G. This is called the global x-coordinate, as the jacket is connected to the global coordinate system (the world).

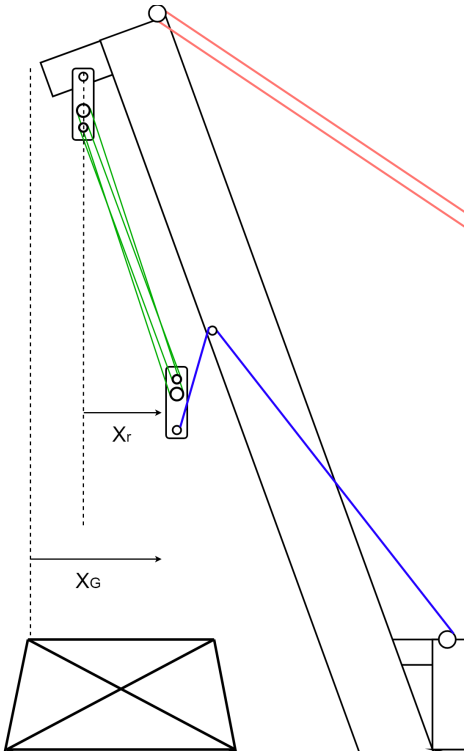

Figure 5-2: Global coordinate

To obtain X_G from X_r the ship motion in x-direction is needed. Fortunately sensors aboard the *Pioneering Spirit* already keep track of the motion of the ship using multiple Inertial Navigation Systems (INS). According to Tampere University of Technology [10]: "An inertial navigation system uses gyroscopes and accelerometers to maintain an estimate of the position, velocity, and attitude rates of the vehicle in or on which the INS is carried". The internal navigation systems also make use of information gathered by the Global Navigation Satellite System (GNSS) receivers aboard the ship. These internal navigation systems provide among other things the surge, sway and heave of the ship.

5-2 Observer structure

The observer consists of a simplified hoist system model which uses the state-information provided by the proposed measurement system as feedback. The Kalman optimal feedback gains are computed using a linearisation of this observer model.

5-2-1 Observer model

The pendulum model used for the development of the control algorithm in Chapter 4 proved to be not accurate enough to perform satisfactory state tracking. Therefore the observer model was made by simplifying the hoist system model. In the observer model the cables are replaced by linear spring-damper elements, as illustrated by Figure 5-3. By disregarding

the cable dynamics the model is much lighter, as there are no small very stiff elements which make computing hard. The neglected distributed mass of the cables is compensated by added equivalent mass in the lower hoist block.

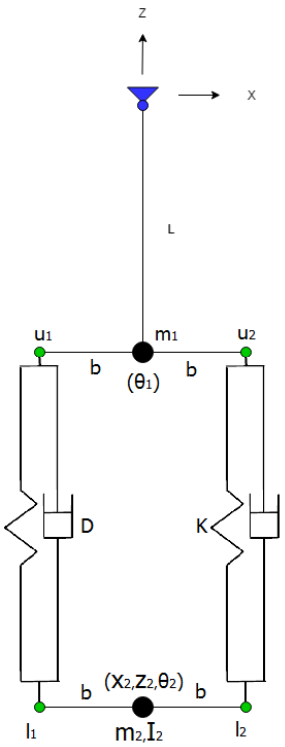

Figure 5-3: Observer model

The cable tension in the observer model will be modelled as a spring force, which makes the tension in the cable

$$T_1 = K(\sqrt{(u1_x - l1_x)^2 + (u1_z - l1_z)^2} - s_0) \tag{5-1}$$

$$T_2 = K(\sqrt{(u2_x - l2_x)^2 + (u2_z - l2_z)^2} - s_0) \tag{5-2}$$

The forces acting upon the cable attachments points u1, u2, l1, and l2 are

$$F_{u1,x} = T_1 \frac{(l1_x - u1_x)}{\sqrt{(u1_x - l1_x)^2 + (u1_z - l1_z)^2}} \qquad F_{u1,z} = T_1 \frac{(u1_z - l1_z)}{\sqrt{(l1_x - u1_x)^2 + (u1_z - l1_z)^2}} \tag{5-3}$$

$$F_{u2,x} = T_2 \frac{(l2_x - u2_x)}{\sqrt{(u2_x - l2_x)^2 + (u2_z - l2_z)^2}} \qquad F_{u2,z} = T_2 \frac{(l2_z - u2_z)}{\sqrt{(u2_x - l2_x)^2 + (u2_z - l2_z)^2}} \tag{5-4}$$

$$F_{l1,x} = T_1 \frac{(u1_x - l1_x)}{\sqrt{(u1_x - l1_x)^2 + (u1_z - l1_z)^2}} \qquad F_{l1,z} = T_1 \frac{(u1_z - l1_z)}{\sqrt{(u1_x - l1_x)^2 + (u1_z - l1_z)^2}} \tag{5-5}$$

$$F_{l2,x} = T_2 \frac{(u2_x - l2_x)}{\sqrt{(u2_x - l2_x)^2 + (u2_z - l2_z)^2}} \qquad F_{l2,z} = T_2 \frac{(u2_z - l2_z)}{\sqrt{(u2_x - l2_x)^2 + (u2_z - l2_z)^2}} \tag{5-6}$$

With these cable forces the equations of motion for the lower hoist block are

$$m_2\ddot{x}_2 = F_{l1,x} + F_{l2,x} \tag{5-7}$$
$$m_2\ddot{z}_2 = F_{l1,z} + F_{l2,z} \tag{5-8}$$
$$I_2\ddot{\theta}_2 = F_{l1,x}\frac{b}{2}\sin(\theta_2) - F_{l2,x}\frac{b}{2}\sin(\theta_2) + F_{l1,z}\frac{b}{2}\cos(\theta_2) - F_{l2,z}\frac{b}{2}\cos(\theta_2), \tag{5-9}$$

The equation of motion for the upper hoist block is

$$m_1L^2\ddot{\theta}_1 = -m_1gL\sin(\theta_1) - m_1L\cos(\theta_1)\ddot{X}_s(t) - m_1L\sin(\theta_1)\ddot{Z}_s(t) + M_1 + M_2, \tag{5-10}$$

The angular moments M_1 and M_2 are generated by the spring forces on the cables attachment points u1 and u2.

$$M_1 = F_{u1,x}\left(\frac{b}{2}\sin(\theta_{bu}) + L\cos(\theta_{bu})\right) + F_{u1,z}\left(-\frac{b}{2}\cos(\theta_{bu}) + L\sin(\theta_{bu})\right) \tag{5-11}$$
$$M_2 = F_{2,x}\left(-\frac{b}{2}\sin(\theta_{bu}) + L\cos(\theta_{bu})\right) + F_{u2,z}\left(\frac{b}{2}\cos(\theta_{bu}) + L\sin(\theta_{bu})\right). \tag{5-12}$$

5-2-2 Observer input

The inputs required by the model are the control input u, the length of the hoist cable L, and the motion of the ship in x- and z-direction, X_s and Z_s respectively. The accelerations of the ship at the hinge point $\ddot{X}_s$ and $\ddot{Z}_s$, depicted in Equation (5-10), are not used used as input of the observer model, as the measurements in the current setup are to susceptible too noise and did not contribute to the accuracy of the observer.

5-2-3 Observer feedback

The feedback of the observer is only based on the position of the lower hoist block, as there is no velocity measurement of the lower hoist block. The observer feedback is a combination of two measurement signals, X_r and the ship motion in x-direction X_s.

$$y(t) = X_G(t) = X_r(t) + X_s(t). \tag{5-13}$$

Thus the feedback signal is

$$y(t) - \hat{y}(t) = X_G(t) - x_2(t). \tag{5-14}$$

5-2-4 Observer gains

The feedback signal fed back into the observer model, $y(t) - \hat{y}(t)$, is amplified using a Kalman optimal observer gain. To compute the optimal observer gain, the observer model was linearised around the operating point $x_2 = 0$.

$$\dot{\hat{q}} = A\hat{q} + Bu \tag{5-15}$$
$$\hat{y} = C\hat{q}, \tag{5-16}$$

with the state vector $\hat{q} = [\hat{\theta}_1, \dot{\hat{\theta}}_1, \hat{x}_2, \dot{\hat{x}}_2, \hat{z}_2, \dot{\hat{z}}_2, \hat{\theta}_2, \dot{\hat{\theta}}_2]'$. The optimal observer gain L_{obs} was then computed, and the feedback loop was closed.

$$\dot{\hat{q}} = A\hat{q} + Bu + L_{obs}(y - \hat{y}) \tag{5-17}$$
$$\hat{y} = C\hat{q}, \tag{5-18}$$

5-3 Observer Performance

To test the performance of the observer two simulations were done. The first simulation implemented the controller on the hoist system model described in Chapter 2, with full state information. The observer was run along side the plant to regard the accuracy. The true position and observed position are plotted against the time in Figure 5-4a. They are almost indistinguishable therefore the error is plotted next to it in Figure 5-4b. The error consists of a couple of millimetres, which is more than adequate for this application

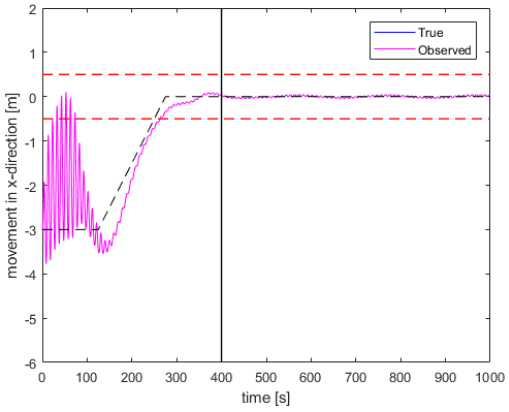

(a) Controlled hoist system model
. *Full state information*

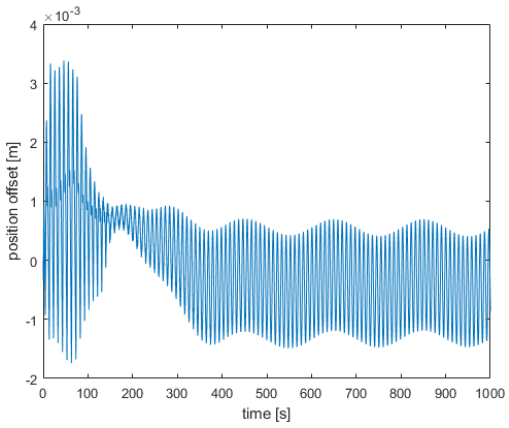

(b) Observer offset: position

Figure 5-4: Observer performance: position

As the controller has a derivative gain, the velocity estimation is also of importance. Figure 5-5b shows the velocity error of the observer. If the velocity error is compared with the movement in Figure 5-4a it shows that the relative error is larger when the movement is small. This is probably caused by un-modelled cable dynamics in the observer model. The effect is shown at steady state in Figure 5-5a, as a decreased velocity amplitude.

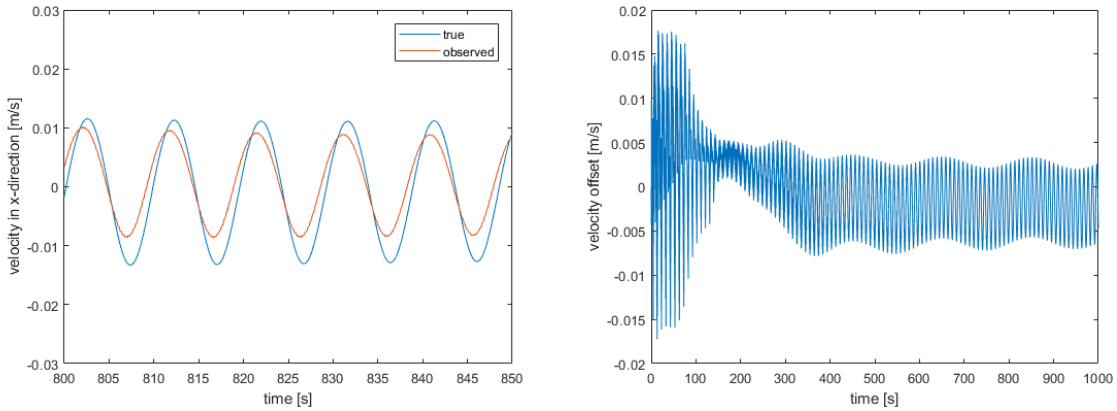

(a) Lower hoist block velocity **(b)** Observer offset: velocity

Figure 5-5: Observer performance: velocity

In the second simulation the controller was implemented using the state information from the observer. The performance of the controller was evaluated for full state information and observer state information. The simulation output illustrated by Figure 5-6 is very similar to Figure 5-4a. This is the result from proper state tracking by the observer.

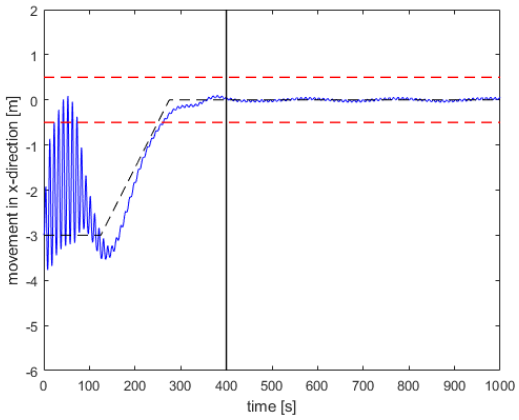

Figure 5-6: Controlled hoist system model
Observed state information

The performance indicators show a 17% increase in final sway amplitude. This is caused by the relatively high velocity error at steady state. Other performance indicators hardly changed.

Table 5-1: Controller performance Full state vs Observer

Controller	max sway [m]	final sway [m]	max tension [t]	max power [kW]
Full state	2.14	0.047	36	94
Observer	2.18	0.054	36	98

5-4 Conclusion

In this chapter a measurement system is proposed which can provide the state information needed for the observer, when used in combination with on-board measurement systems. Secondly the make up of the observer model is discussed. This observer model was linearised for the computation of the Kalman optimal feedback gains. Lastly the performance of the controller was tested for full state information and observed state information, to evaluate the performance of the observer.
It was shown that the state information provided by the proposed measurement system could be used in conjunction with an observer to adequately track the states; to control the hoist system with the developed controller.
The position tracking is very accurate, but the velocity estimation has a larger error. At low velocities the estimation error is relatively large, which reduces the performance of the controller to reduce the final amplitude.
The observer performance was evaluated without addition of noise or parameter uncertainties. This will be evaluated in the next chapter, and it is expected that the observer performance will go down.

Chapter 6

Performance analysis

In Chapter 4 the performance of the control algorithm was evaluated for the simple pendulum model. In this chapter the controller performance will be evaluated for the hoist system model described in Chapter 2. But first some additions should be made to the hoist system model which could degrade the controller performance. One of the additions was made in Chapter 5, namely the observer. This chapter will discuss the impact of the addition of actuator dynamics, real ship motions, model uncertainty, and sensors noise. But first the standard simulation case will be presented as reference.

6-1 Standard simulation case

The simulation results from the cases presented in this chapter are all variations on the standard simulation case. In this simulation case the gain scheduled LQR with integral and feedforward gain (sLQRi-FF) discussed in Chapter 4, was implemented on the hoist system model discussed in Chapter 2, together with the observer discussed in Chapter 5. The approximated ship motion with drift discussed in Section 4-1-2 was imposed on the hinge point of the hoist system. Additional graphs are shown in Appendix B-1.
At $t = 0$ $[s]$ the hoist system starts lowering the lower hoist block by increasing the length of the hoist cables, as illustrated in Figure 6-1 by the green line. The hoist system length starts at 15 metres, and stops at 85 metres at $t = 400[s]$ accentuated by the vertical black line.
The control system is started at $t = 0$ $[s]$, with low gains scheduled for short hoist system lengths, as discussed in Section 4-3-3. It is also illustrated by Appendix Figure B-3a. When the hoist system is 40 metres long, the feedforward gain is engaged, which occurs at $t = 126$ $[s]$. The reference signal for the feedforward gain also contains the drift compensation, as discussed in Section 4-3-2. This signal is increased in intensity from 0% at $L = 40$ $[m]$ to 100% at $L = 70[m]$. This is illustrated by Appendix Figure B-3b. This is done to avoid a sudden increase in cable tension. The integral gain is engaged when the hoist system is 80 metres long. This is illustrated by Appendix Figure B-3a. This is done to decrease the overshoot normally expected of a reference tracking integral action.

In Figure 6-1 it is illustrated that the lower hoist block is allowed to oscillated within the limits stated by the maximum sway amplitude to decrease the power needed from the winch. From $L = 40$ $[s]$ the motion of the lower hoist block is decreased gradually whilst pulling it closer to the ship, such that it is positioned at the target of $x = 0$ $[m]$ when it reaches $L = 85$ $[m]$. At this point the goal is to keep the amplitude, called the final amplitude, within 0.25 metres. This final amplitude goal is illustrated by the dashed red lines.
The cases presented in this chapter are identical to the standard simulation case, unless stated otherwise.

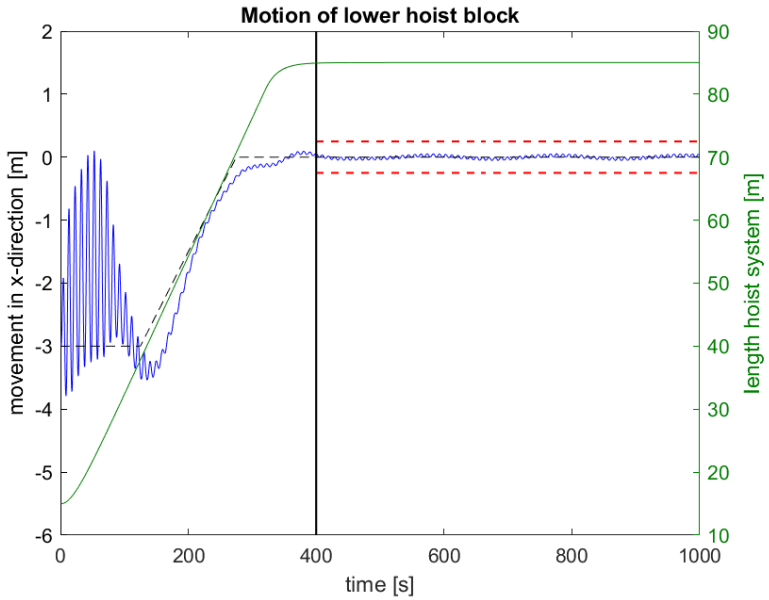

Figure 6-1: Hoist system length

6-2 Actuator Dynamics

In the standard simulation case the winch and tugline dynamics were neglected. To evaluate if the actuator dynamics will decrease controller performance, a simple model was created of the winch and tugline, according to advice of OrcaFlex [11]. The wire rope was modelled as a linear spring. This makes the tension T only dependent on rope stiffness K and rope strain ϵ

$$T = K\epsilon(t) = K\frac{l(t) - l_0(t)}{l_0(t)}, \tag{6-1}$$

with l_0 the paid out length and l the stretched length of the wire rope. The winch is modelled as a drum with inertia and damping. The acceleration of the drum is controlled by the wire rope tension T and the force applied by the winch motor f. The motor dynamics are neglected, and the motor force is assumed to be equal to the control input.

$$I\ddot{l_0} = (T - f)r - C_d\dot{l_0}, \tag{6-2}$$

with I the inertia of the drum, C_d a damping constant, and r the radius of the drum. To evaluate the impact of the actuator dynamics, first the standard simulation case was run, where the control input was directly used as the wire rope tension. The output of this simulation is shown in Figure 5-6. The tension in the wire rope is illustrated by Figure 6-2a.

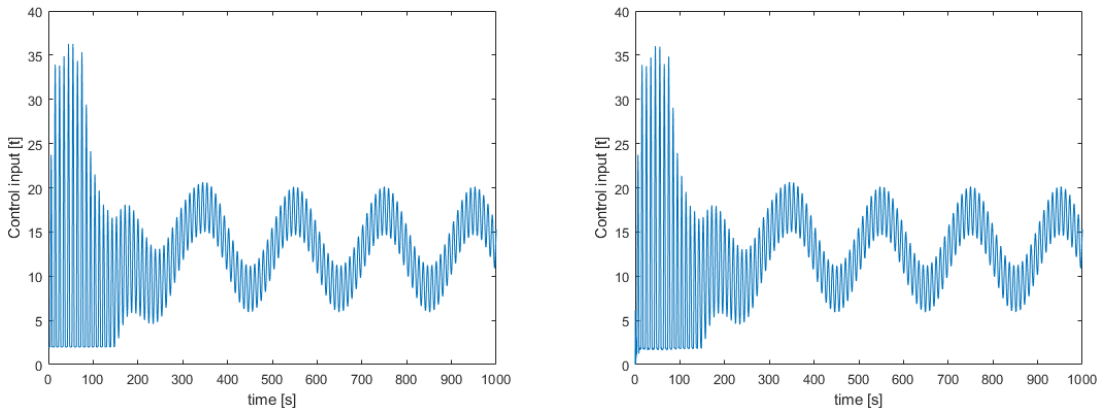

(a) Wire rope tension - standard simulation case **(b)** Wire rope tension - with added winch dynamics

Figure 6-2: Observer performance: position

The second simulation was run with the winch dynamics implemented as shown above, where the applied motor force f is replaced with control input u. The inertia of the drum was chosen to be $I = 94$ $[kgm^2]$, with a drum radius of $r = 0.25$ $[m]$ and a cross-sectional wire rope stiffness of $EA = 269$ $[MN]$. As seen in Figure 6-2b the winch dynamics hardly impact tension in the wire rope. To further support this statement the performance indicators are shown in Table 6-1. Other than small differences the performance is the same.

Table 6-1: Controller performance no dynamics vs actuator dynamics

Dynamics	max sway [m]	final sway [m]	max tension [t]	max power [kW]
no dynamics	2.18	0.054	36	98
actuator dynamics	2.15	0.055	36	95

Although the performance was not affected much by the chosen actuator parameters they do impact the behaviour of the controller. A lower wire rope stiffness means that the winch has to pay in more rope to reach a certain tension in the wire. Which means a rope which is less stiff will need a faster winch. Also the drum inertia will dictate what accelerations you can achieve. A heavier drum could decrease the controller performance. If a different winch or wire rope has to be selected a similar evaluation has to be performed to ensure the controller still performs as desired.
In Chapter 4 it was mentioned that the actuator power was approximated using the movement of the lower hoist block and the input force. It is however more accurate to approximate the actuator power using the speed of wire rope being paid out $\dot{l}_0$ and the line tension T, as in Equation (6-3). This way the approximated power is also dependent on wire rope stiffness as mentioned above. Using this new approximation an increase in maximum actuator power

is observed when comparing tables from Chapter 4, and Chapters 5 and 6. However the maximum power need in a specific simulation is not a safe way to determine the maximum power needed for the control system under all conditions. This will be discussed in Section 6-6-2.

$$P = T\dot{l}_0 \tag{6-3}$$

The simulation cases following after this section all have the actuator dynamics included.

6-3 Ship motion

The approximated ship motion determined in Chapter 4-1-2 is made up of two sinus signals with constant amplitudes, which have been determined by a motion report. The real ship motions are more erratic and have changing amplitudes, sometimes even larger than were used in the approximation. Thus it is expected that the controller performance will be lower when using real ship motions as input.

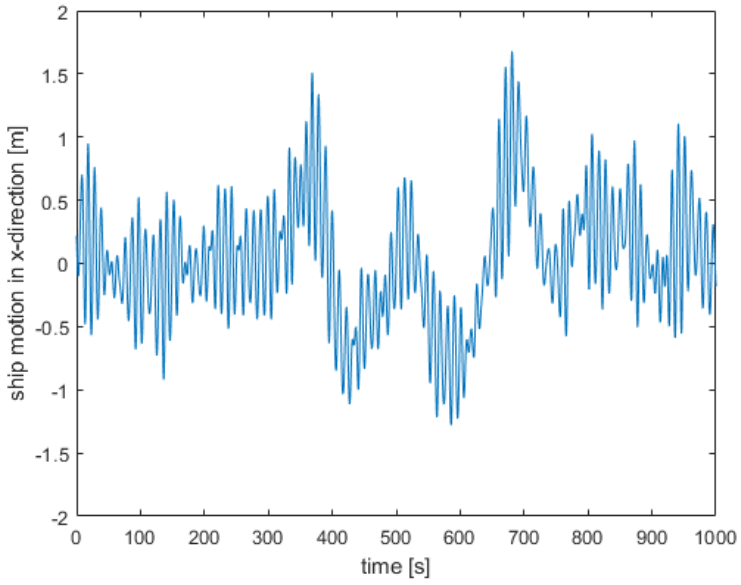

Figure 6-3: Ship motion in x-direction

Figure 6-3 shows a time trace of the ship motion in x-direction which has been chosen to evaluate the control system. The significant wave height during this time trace was 2.5 metres. Between zero and 50 seconds, where the natural period of the hoist system is similar to the period of the fast motion, the amplitude of the fast motion is large, which will give large excitations to the hoist system. This will test the ability of the controller to reduce the maximum sway amplitude. Then between 350 and 750 seconds a large amplitude of the slow motion can be seen. This will test the ability of the controller to track the reference when the ship periodically drifts off. Between 800 and 1000 seconds lay more peak amplitudes of

the fast motion. This will test the ability of the controller to reduce the final amplitude. This time-trace contains a variety of the harshest conditions the Jacket Lift System (JLS) will encounter during an operation at a sea state of 2.5 metres, and is therefore a good tool to evaluate the control system on real ship motions.

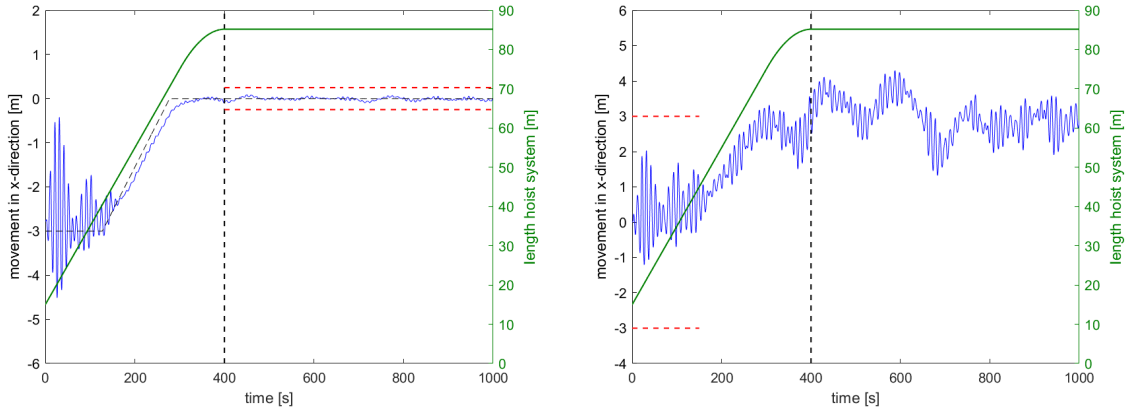

(a) Global position **(b)** Relative position

Figure 6-4: System output

The standard simulation case with added actuator dynamics, was run with the implementation of the ship motion shown in 6-3. Figure 6-4 illustrates that the controller still fulfils the objectives, which are represented by the red dashed lines. In Figure 6-4a can be seen that the lower hoist block follows the reference trajectory and the final amplitude is small enough to connect the hoist system to the jacket. Note the right y-axis depicts the length of the hoist system for the given time in seconds in green. Figure 6-4b illustrates that the maximum relative amplitude is bounded within 3 metres between zero and 150 seconds, to avoid any collision risks. The performance indicators are shown in Table 6-2. The final sway amplitude is increased with 80%, which is caused by the increase of the the maximum fast motion amplitude by using the real ship motions; which is also around 80%.

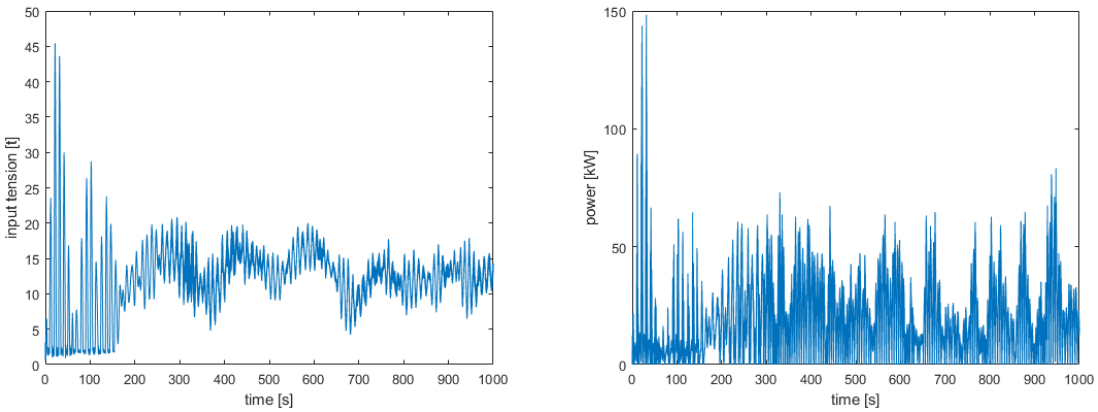

(a) Wire rope tension **(b)** Winch power output

Figure 6-5: System input

The larger fast amplitude in the real ship motion results in larger control inputs to reach the same performance goals, as illustrated by Figure 6-5. The maximum tension is increased with 25%, and the maximum power is increased by 57%. This increase in actuator input is largely caused by the increase in ship motion velocities, resulting from the increased fast amplitude. Larger velocities result in the need for a faster paying out speed for the winch, which in turn increase the needed winch motor power.

Table 6-2: Controller performance on real ship motion

	max sway [m]	final sway [m]	max tension [t]	max power [kW]
approximated ship motion	2.15	0.055	36	95
real ship motion	2.05	0.079	45	149

In addition to the gain scheduling discussed in Chapter 4 the maximum wire rope tension could be reduced using a control input limit, which could decrease the maximum power need, in trade for an increase in maximum sway amplitude. Another way is to limit the maximum pay in/out speed of the winch. Both these options do however have their limitations as having the limits too low will decrease controller performance significantly.
Another way to decrease actuator power is increasing the wire rope stiffness, which can result in lower pay in/out speeds. This however also has its limitations, as a stiffer rope is larger and heavier. A too stiff rope can also cause large snap loads.

6-4 Model uncertainty

During the development of the controller and observer it was assumed that the parameters of the hoist system were perfectly known. In reality the parameters can only be approximated with a finite precision. Unforeseen circumstances can also contribute to model uncertainty. For instance the hook might need to be replaced, but the replacement has a different mass and this change is not implemented in the control system. To test the robustness against such model uncertainties the plant parameters were varied up to 20%. The standard simulation case was used with the added actuator dynamics and the real ship motions were implemented.

6-4-1 Hoist block mass

The mass of the hoist blocks influence the weight and inertia of the system. By inserting an uncertainty in its value three parts of the control system are influenced, decreasing performance. The first is the observer. The uncertainty in mass creates an extra discrepancy between the plant and the observer model, decreasing prediction accuracy. But as the observer already uses measurements of the plant to compensate for model mismatch this effect is minor. The second system is the LQR. The optimal feedback gains are computed using the model parameters. If the parameters are not correct the computed gains are not optimal. This effect is also minor. The third system affected by the uncertainty is the feedforward gain. The uncertainty in mass creates a discrepancy between the real weight of the system, and the approximated weight used for the feedforward gain. Therefore the uncertainty will

create a steady state offset between the reference signal and the lower hoist block position. This can be seen in Figure 6-6a, where the observer mass was made 20% smaller, and Figure 6-6b, where the observer mass was made 20% larger. Between 300 and 400 seconds the offset created by the feedforward gain error is distinctly visible.

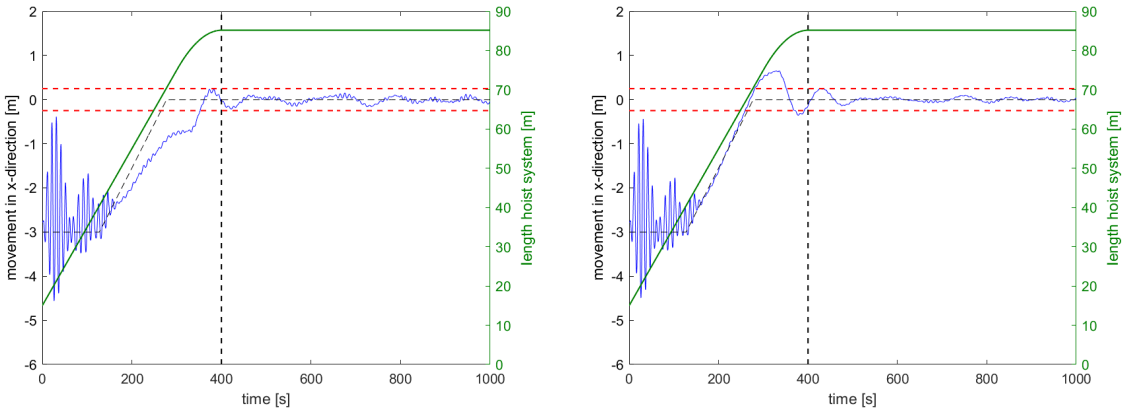

(a) +20% mass **(b)** -20% mass

Figure 6-6: Output with mass uncertainty

If the mass is underestimated the offset is negative, if the mass is overestimated the offset is positive. The offset is eventually compensated by the integrator gain which is activated at $t = 350$ $[s]$. In Table 6-3 can be seen that the mass uncertainty of 20% has increased the final sway amplitude up to 106%. The final sway amplitude can be reduced by increasing the integrator gain, but this will make the controller more susceptible to measurement noise.

Table 6-3: Controller performance with mass uncertainty

mass	max sway [m]	final sway [m]	max tension [t]	max power [kW]
accurate mass	2.05	0.079	45	149
+20%	2.06	0.163	45	206
-20%	2.02	0.097	46	173

6-4-2 Hoist system length

A large uncertainty in Hoist system length is not likely, as keeping track of the paid out hoist cable length can be done fairly accurately. Nonetheless it is important to test what would happen if a large uncertainty is introduced.
Inserting an uncertainty in the length of the hoist system has a similar effect as the mass, only reversed. For a shorter length a larger feedforward gain is needed to create a three meter offset from the equilibrium point. Therefore when the length is underestimated the gain is too large and an overshoot is observed, as illustrated by Figure 6-7a. When the length is overestimated the gain is too small and a negative offset from the reference is observed, as illustrated by Figure 6-7b. These offsets are again compensated by the integrator gain that is activated at $t = 350$ $[s]$.

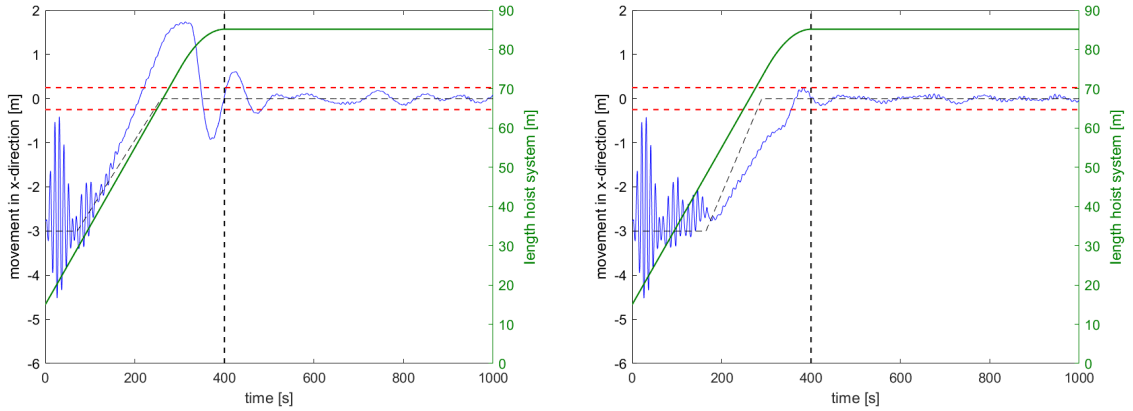

(a) +20% length **(b)** -20% length

Figure 6-7: Output with length uncertainty

As the feedforward gain is more strongly dependent on length the performance loss is greater. With an uncertainty of 20% the final sway amplitude is increased up to 137%, as can be seen in Table 6-4.

Table 6-4: Controller performance with length uncertainty

length	max sway [m]	final sway [m]	max tension [t]	max power [kW]
accurate length	2.05	0.079	45	149
+20%	2.10	0.187	46	152
-20%	2.03	0.127	45	149

The observer, and LQR are again also affected by the parameter uncertainty, but again the effect is minor in comparison with the feedforward error.

6-4-3 Cable stiffness

As cable stiffness is in reality non-linear, and can vary under different operating conditions, this parameter is most likely to be uncertain. But the effect of the uncertainty is negligible. Figure 6-8 shows the output of simulations done with a 20% overestimation (a), and 20% underestimation (b). And the performance indicators can be seen in Table 6-5, and are almost identical.

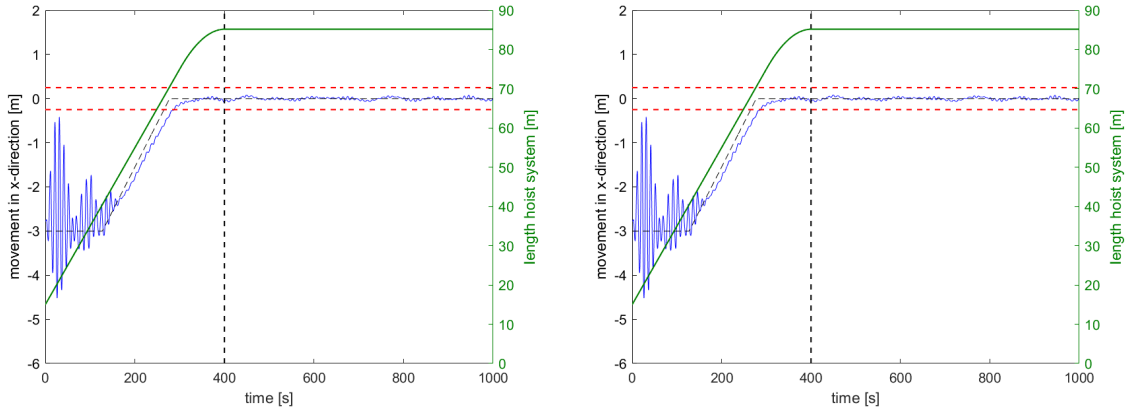

(a) +20% stiffness **(b)** -20% stiffness

Figure 6-8: Output with stiffness uncertainty

Table 6-5: Controller performance with stiffness uncertainty

stiffness	max sway [m]	final sway [m]	max tension [t]	max power [kW]
accurate stiffness	2.05	0.079	45	149
+20%	2.04	0.079	45	157
-20%	2.04	0.079	45	145

6-5 Measurement frequency and noise

The measurements which are used by the observer were assumed to be perfect, without any noise on the signals. In reality the accuracy of the measurements is finite, and noise is expected to be present. In this section is discussed what type of noise is expected, and what influence it will have on the controller performance.

6-5-1 Lower hoist block measurement

The accuracy of laser-based distance sensors is around 2 $[mm]$ at a distance of a hundred metres. As the noise level of the measurement system that would be used is not known; Gaussian white noise was used to simulate the noise on the output signal of the plant. To evaluate the robustness of the control system, the variance of the noise is tuned to represent an accuracy ranging from 2 $[mm]$ to 20 $[mm]$. This is accomplished by setting the standard deviation to be equal to a third of the accuracy, and thus the variance becomes,

$$\sigma^2 = \left(\frac{accuracy}{3}\right)^2 \tag{6-4}$$

The sample time of such a distance sensor can be expected to be around the 2 $[ms]$; and thus the noise $n_{ZOH}(t)$ is generated by using a random number generator with a sampling time equal to $T_s = 2$ $[ms]$ and a distribution as stated above. Figure 6-9 illustrates two time traces

of the simulated noise.

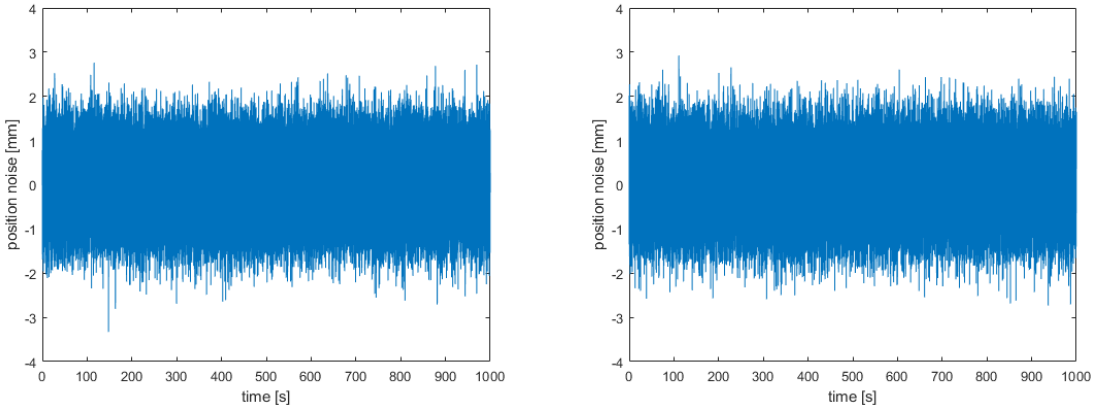

(a) Example 1 **(b)** Example 2

Figure 6-9: Noise on distance sensor for position lower hoist block

The output signal $y(t)$ will also be sampled using a zero order hold, with the same sampling time T_s, to create $y_{ZOH}(t)$,

$$y_{ZOH}(t) = \sum_{n=-\infty}^{\infty} y[n] \cdot \text{rect}\Big(\frac{t - T_s/2 - nT_s}{T_s}\Big) \tag{6-5}$$

The noise signal $n_{ZOH}(t)$ is added to this sampled output signal $y_{ZOH}(t)$.

$$\bar{y}(t) = y_{ZOH}(t) + n_{ZOH}(t) \tag{6-6}$$

6-5-2 Ship motion measurement

The ship motion measurements are a different story. As the inertial navigation system uses multiple internal and external sensors which are internally processed and filtered, the higher frequency measurement noises is already filtered out. But multiple processes can add noise to the output signals. As there is no information known about the noise levels, a multi frequency signal will be constructed with a standard deviation matching the specified accuracy of the inertial navigation system. The specified accuracy of the surge, sway, and heave from the inertial navigation system is 50 $[mm]$, thus a range is used between 50 $[mm]$ – 500 $[mm]$ to evaluate the robustness of the control system. The standard deviation is defined as,

$$\sigma = \frac{accuracy}{3} \tag{6-7}$$

Ten sinusoids with frequencies ranging between 0.001 $[rad/s]$ and 10 $[rad/s]$ are used to generate the signal, with amplitudes between 1 and 0.1. The amplitudes are then scaled to match the desired standard deviation.

$$\vec{\mathbf{A}} = \frac{\vec{\mathbf{A}}\sigma}{\sqrt{\vec{\mathbf{A}}^{\intercal}\vec{\mathbf{A}}}}, \tag{6-8}$$

with $\vec{A}$ a vector containing the amplitudes. The sinusoids are then added together to create the noise signal. Figure 6-10 illustrates two time traces of the simulated noise.

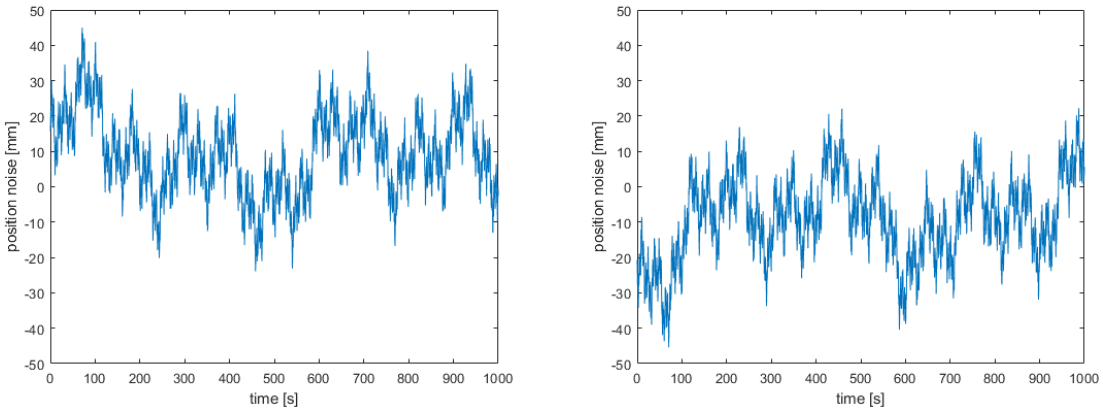

(a) Example 1 **(b)** Example 2

Figure 6-10: Noise on inertial navigation system surge,sway,heave

The inertial navigation system has a sampling time of 10 $[ms]$. Therefore after the ship measurements and the noise are added up, a zero order hold is performed.

$$\bar{X}(t) = \sum_{n=-\infty}^{\infty} \Big(X[n] + n[n]\Big) \cdot \text{rect}\Big(\frac{t - T_s/2 - nT_s}{T_s}\Big) \tag{6-9}$$

Equation (6-9) depicts the output of the surge measurement, this equation is similar for sway and heave.

6-5-3 Performance

To evaluate the robustness to noise, the noise on the lower hoist block measurement and the ship motion measurement are first introduced separately before being introduced together. This way the individual influence can be determined as well as their combined influence. The standard simulation case was used with the added actuator dynamics and the real ship motions were implemented.
First the noise on the lower hoist block measurement will be regarded. The Gaussian white noise is added to the measurement signal $y(t)$ and the signal is discretized using a zero order hold which results in $\bar{y}(t)$, as mentioned in Section 6-5-1. In the observer the $y(t)$ in Equation (5-17) is replaced with $\bar{y}(t)$. Figure 6-11 illustrated the output of the system for accuracies 2 $[mm]$ and 20 $[mm]$. The accuracy is related to the variance as stated in Equation (6-4). It is clear that the performance of the controller is not degraded by the added noise. The performance indicators shown in Table 6-6 support this. The Kalman based observer is well suited for filtering Gaussian white noise, which makes the control system robust against noise on the lower hoist block measurement.

If the noise level would be further increased, which would then be more than ten times the expected level, the velocity approximation would become noisy, which in turn makes the control input noisy through the application of the derivative gain; which would result in large motor reference speed fluctuations. As long as the motor could keep up, the controller performance would degrade very little with the added noise.

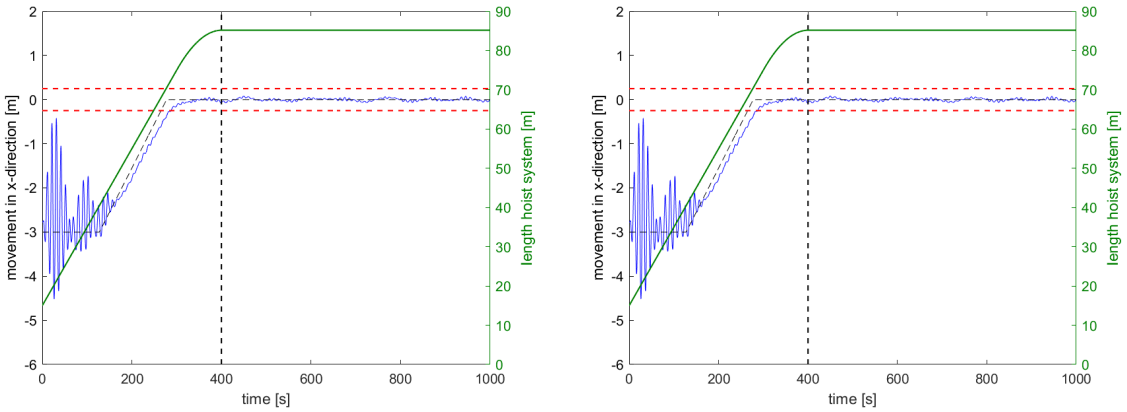

(a) Example 1: accuracy of 2 $[mm]$ **(b)** Example 2: accuracy of 20 $[mm]$

Figure 6-11: Noise on inertial navigation system surge,sway,heave

The noise on the ship motion measurement has a larger influence on the performance, as illustrated by Figure 6-12. With an accuracy of 50 $[mm]$ the performance is only degraded a little. The final sway amplitude is increased by 20%, which is still within acceptable levels. When the accuracy is decreased to 500 $[mm]$ however the final sway amplitude is increased by 400%, as shown in Table 6-6. This large influence is the cause of multiple factors. The first factor is that the ship motion measurement is used for multiple purposes. Firstly it is combined with the lower hoist block measurement as shown in Equation (5-13). And secondly it is used to predict the motion of the upper hoist block, as shown in Figure 5-3. The second factor is that the noise added to the ship motion measurement is not white, has low frequencies, and its equilibrium is locally not zero, as illustrated by Figure 6-10. These two factors combined cause the predicted and measured lower hoist block position to be off set from the real position. The integral gain will control the block, using this off set position, and give the wrong control input; creating an offset between the real position and the reference position. The LQR and feedforward control algorithms add to this effect but with smaller impact. Decreasing the integral gain would reduce this effect, but not by much.
As this noise level is ten times larger then expected this is not seen as a problem. But in the event that the accuracy of the ship motion measurements do create a large performance decrease in the control system, a more accurate measurement system will be needed to measure the position of the ship relative to the jacket.

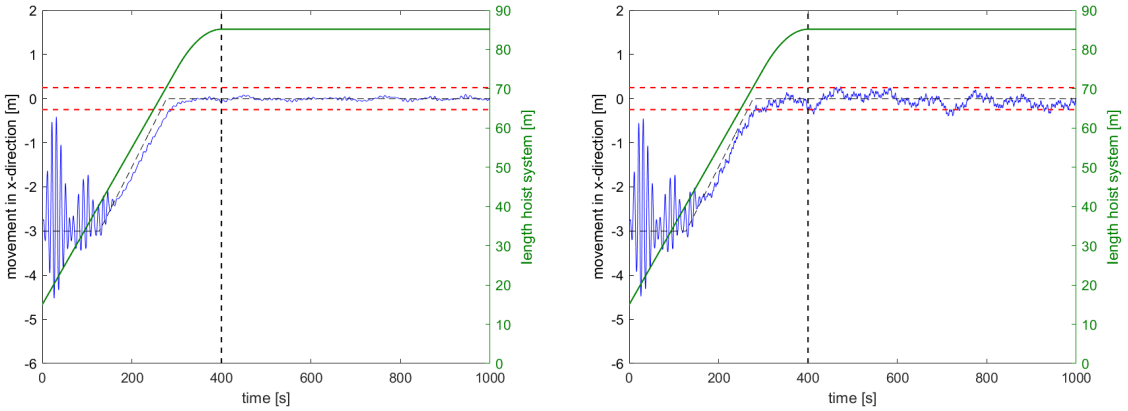

(a) Example 3: accuracy of 50 $[mm]$ **(b)** Example 4: accuracy of 500 $[mm]$

Figure 6-12: Noise on inertial navigation system surge,sway,heave

Lastly the performance is evaluated when the noise is implemented on both signals. As the noise on the lower hoist block measurement had such little influence, it is expected that the ship motion measurement noise will dictate the performance. In Example 5, illustrated by Figure 6-13a, the lower hoist block measurement accuracy is set at 2 $[mm]$, and the ship motion measurement accuracy is set at 50 $[mm]$. As expected the final sway amplitude is slightly increased, as also shown in Table 6-6. In Example 6, illustrated by Figure 6-13b, the lower hoist block measurement accuracy is set at 20 $[mm]$, and the ship motion measurement accuracy is set at 500 $[mm]$. And here also as expected the final sway amplitude is increased by 450%. The exact performance can vary from simulation to simulation as the noise seed is randomized, but it is clear that the performance degradation is almost completely caused by the noise on the ship motion measurement.

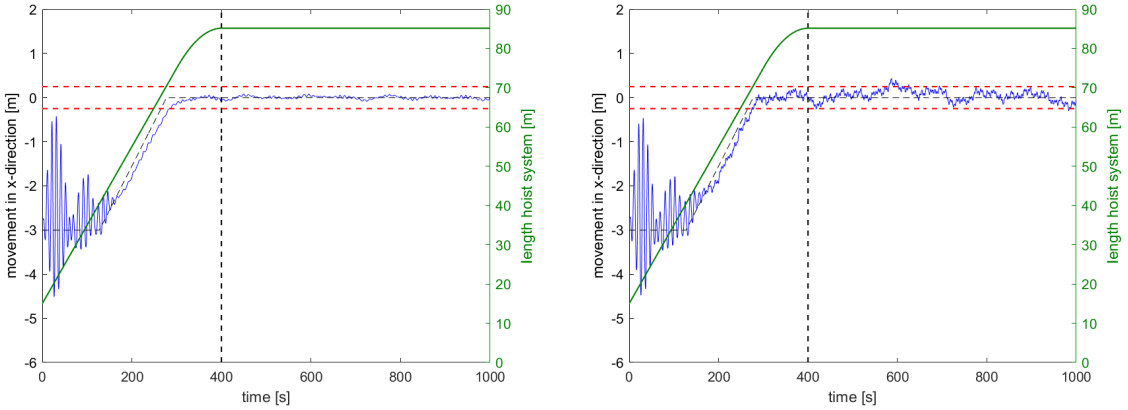

(a) Example 5 **(b)** Example 6

Figure 6-13: Noise on inertial navigation system surge,sway,heave

In Table 6-6 is shown that with the added noise the performance of the control system is still adequate, except for large noise levels on the ship motion measurement. As long as

the accuracy of the measurement systems are within specified values, the robustness against measurement noise is adequate. Note also that if the noise levels are high enough to degrade the performance, stability of the control system is still maintained.

Table 6-6: Controller performance with noise

noise on y & X_s	max sway [m]	final sway [m]	max tension [t]	max power [kW]
no noise	2.05	0.079	45	149
Example 1: 2 mm & 0 mm	2.03	0.079	46	169
Example 2: 20 mm & 0 mm	2.04	0.079	45	155
Example 3: 0 mm & 50 mm	2.04	0.097	46	194
Example 4: 0 mm & 500 mm	2.00	0.395	45	155
Example 5: 2 mm & 50 mm	2.03	0.085	45	156
Example 6: 20 mm & 500 mm	1.99	0.437	45	148

6-6 Actuator

The actuator proposed in Section 4-2 has a guidance sheave, which was proposed to have a height of 85 $[m]$. In this section will be discussed if this is indeed the optimal height. Secondly it will be discussed what maximum force and power will be required from the winch motor.

6-6-1 Actuator guidance sheave position

The sheave, or sheaves, that guide the tagline to the lower hoist block are assumed to be fixed in position during an operation. In Section 4-2 it was proposed to position the sheave at $z = 85$ metres, measured from the hinge point of the hoist system as illustrated by Figure 6-14. In this section it is discussed if a position closer to the hinge point would be beneficial to the controller performance.

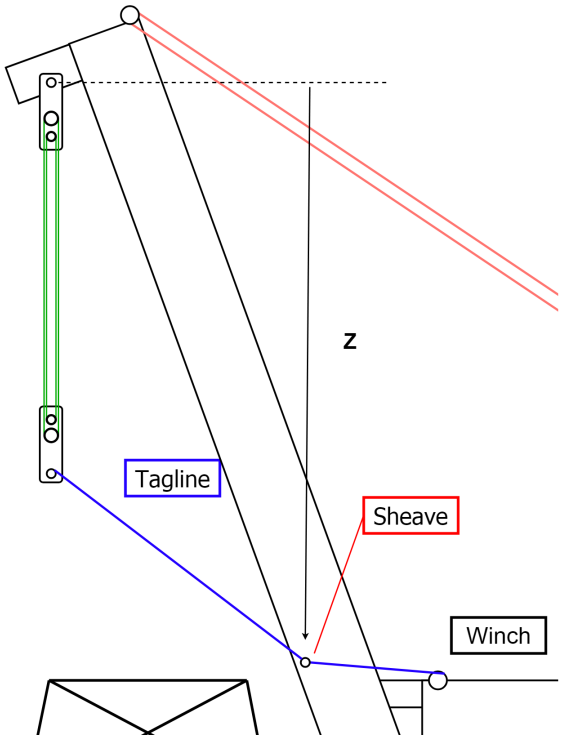

Figure 6-14: Actuator guidance sheave

When the guidance sheave is level with the lower hoist block the actuator can apply its force to the hoist block most efficient. Thus by changing the height of the guidance sheave the operating point where the actuator is most efficient also changes in height. It is expected that when the guidance sheave is closer to the hinge point the maximum sway amplitude is reduced, as it will increase controller performance when the hoist system is short. It will however decrease controller performance when the hoist system is long, and increase final sway amplitude. This expectation is supported by the performance indicators resulting from the simulations, seen in Table 6-7. With decreasing sheave height, measured from the hinge point down, the maximum sway amplitude decreases, and the final sway amplitude increases. At 25 $[m]$ the angle between the tagline and the horizontal plane of the hoist block is so large, at the connection phase, that the controller has a hard time reducing the final sway amplitude, resulting in loss in performance, and increase in actuator tension and power. Within limits the guidance sheave height is a trade off between maximum sway and final sway. In this situation the increase in maximum sway is not that influential, as long as it stays within limits. It is however preferable to keep the final sway as small as possible.

Table 6-7: Controller performance with varying sheave height

Sheave height [m]	max sway [m]	final sway [m]	max tension [t]	max power [kW]
85	2.03	0.095	45	151
65	2.00	0.112	44	133
45	1.94	0.169	65	235
25	1.83	0.329	152	700

Thus the conclusion is that the guidance sheave height should be at 85 $[m]$ for optimal actuator efficiency at the point of connection, to reduce the final sway amplitude as much as possible.

6-6-2 Actuator motor power

Two of the performance indicators are linked to the winch motor parameters. The maximum tension and maximum power. The maximum tension needed in the wire rope is assumed to be equal to the needed force the winch has to put out. The maximum tension required varies with different controller tunings and hoist system parameters. The simulations suggest that a winch motor with upwards of 46 $[t]$ of force is needed to control the sway in the hoist system. Determining the maximum power requirement is less straight forward.
The maximum power needed during a simulated lowering of the hoist block is approximated as discussed in Section 6-2, with the pay in/out speed of the winch multiplied with the current cable tension. As the peak tensions and peak pay in/out speed are not always at the same times, the maximum power parameter can vary significantly between simulations. It is therefore a safer option to determine the required maximum winch motor power in accordance to the maximum power multiplied with the maximum pay in/out speed. Figure 6-15 shows an example of a typical pay in speed graph. The positive speed means the wire rope is being paid out, the negative speed means the wire rope is being paid in. The maximum pay in/out speed shown is around 0.8 $[m/s]$. With a margin the required maximum pay in/out speed of the winch can be assumed to be 1 $[m/s]$. If the motor is required to handle this speed at the maximum required tension than the maximum required motor power is equal to

$$P = t\dot{l}_0 = 46 \cdot 9.813 \cdot 1 \approx 452 \ [kW]. \tag{6-10}$$

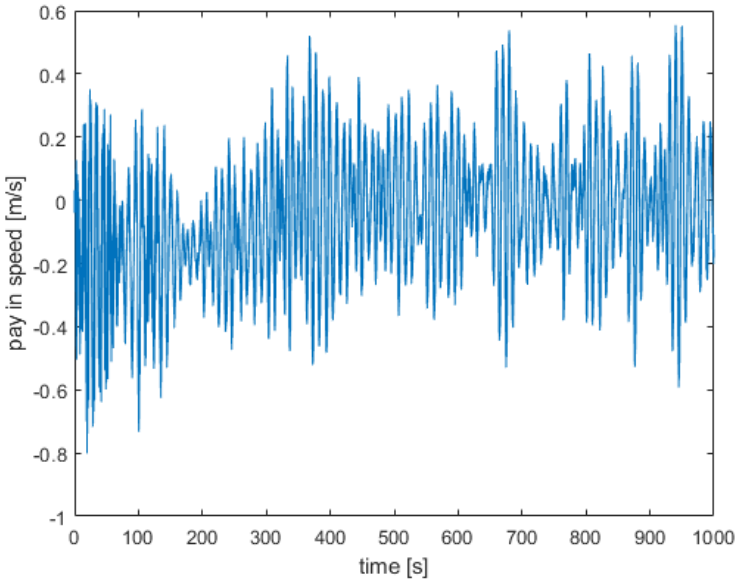

Figure 6-15: Pay in speed

This value is a lot higher than the maximum power performance indicator values seen throughout this section. In numerous situations this amount of peak power will not be needed, but for that one situation that the peak tension aligns with the peak pay in speed it is required to be able to handle this situation. If the motor is not able to pay in/out the cable, the winch can exceed its force limitations and has to be put on the breaks. This locks the ability of the winch to control the tension in the cable. If the winch can not control the tension, the hoist system can not be connected to the jacket and the operation would have to be suspended till the situation is resolved.

6-7 Summary

In this chapter was discussed how various factors influenced the performance of the control system. Actuator dynamics, real-life ship motions, model uncertainty, measurement noise, and sheave position were all regarded. Finally it was shortly discussed what this meant for the actuator winch motor requirements.
The implementation of the control algorithm on the full detail hoist system model, with addition of actuator dynamics and real ship motions, resulted in a small decrease in performance compared to the results from Chapter 4.
The model uncertainties that were implemented resulted in a further decrease in performance, and notable over- and undershoot of the feedforward gain. However there was no indication of instability of the controlled system.
The controlled system also remained stable with the addition of noise on the measured signals. It was notable that in particular the noise on the measured ship motion had a negative impact on the controller performance. If the noise levels would stay in the expected limits however, the decrease in performance was small.
In this section was also concluded that a height of 85 $[m]$ was the optimal height of the actuator guidance sheave.

6-8 Conclusion

This chapter discussed how various factors influenced the performance of the developed control system. The results of simulations show that the control system can still perform within the specified control objectives with noise levels ten times larger than expected, and model uncertainties of 20%, without becoming unstable. In good conditions, meaning minimal model uncertainties and noise levels as in Example 5 of Table 6-6, the control system is able to reduce the maximum sway to a little over 2 $[m]$. The final sway is reduced to 0.1 $[m]$. This can be achieved with a winch motor with approximately 46 $[t]$ of force, and 452 $[kW]$ of power. With this performance the hoist system can be safely lowered and connected to the jacket, proving that this control system concept can in theory solve the control problem stated in Section 4, and thus achieve the goals set out at the beginning of this thesis.

Chapter 7

Conclusion

The goal of this thesis was to develop a control system which could decrease the sway in the hoist system during the lowering of the lower hoist block, to increase safety of the hoist system, and enable the connection process between the lower hoist block and the jacket.
To achieve this goal, the hoist system was modelled using a lumped-mass cable model combined with a point mass and a pendulum. This hoist system model was used to analyse the dynamics of the hoist system, and determine the cause of the sway problem. After the cause of the problem was determined the control objective could be outlined. A control algorithm was developed based on a Proportional Derivative (PD) controller found in literature to achieve this objective. After it was proven that the control algorithm could fulfil the objective when implemented on a single pendulum model under optimal conditions, the control algorithm was implemented on the hoist system model. At this point, an observer was added to track the states of the plant, completing the control system.
To evaluate the performance and robustness of the control system, multiple factors were added to the hoist system model. Actuator dynamics were implemented, as well as ship motions recorded in real life situations. Lastly, model uncertainty, and additive noise on the measurement signals were introduced, to test the robustness of the system. The performance analysis showed that the control system could achieve the control objectives and is robust against model uncertainty and measurement noise, proving the concept control system. This does not conclude the research needed to implement such a system, but it is a good start. By proving the lower hoist block position can be controlled using actuators installed on the deck of the ship, a potential alternative can be offered to the existing concept of using a auxiliary fibre rope and installing sheaves on the jacket.
The use of the wire rope actuator was also evaluated in passive operating modes. It was found that the passive modes did not satisfy the objective.

7-1 Model

An obvious limitation of the hoist system model is the fact that it is a two dimensional model. In this thesis due to the dimensional limitations the sway problem could only be analysed in x- and z-direction, whilst in y-direction sway will also be present. The 2D control system developed during this thesis will not be sufficient to control the three dimensional hoist system. By proving the concept of the developed 2D control system however an important step is made towards a 3D control system. With the implementation of an additional winch actuator a multi-variable control system can be developed based on the 2D control system. To capture the dynamics of the hoist system in 3D and adapt the control system concept developed in this thesis, a 3D model should be developed in future research.
It was also observed that the bending stiffness included in the hoist system model did not have a significant influence on the dynamics of the model, and can be neglected in future research.
The hoist system model was partially validated using theoretical wire rope equations. It is recommended to build a full sized test setup of the hoist system in the future, to tune and validate the 3D hoist system model. This test setup can also be used for the evaluation of the controller.

7-2 Controller

The PD controller used by Ku [3] could reduce the sway amplitude of the hoist system, but the reference tracking was very limited. Also it could not compensate for drift. The PD type feedback controller was exchanged for a Linear-Quadratic Regulator (LQR) type feedback controller, to optimize the feedback gains. A feedforward and integral were added to improve trajectory tracking and disturbance rejection. Lastly a gain schedule was implemented for the feedback gains to enhance the efficiency of the control input. The resulting sLQRi-FF controller can limit the maximum sway amplitude to a little over 2 metres, and the final sway amplitude to around 10 centimetres at a significant wave height of 2.5 metres. It has also shown to be robust against model uncertainty and input measurement noise.
The performance of the controller can still be improved upon by tuning the gains to make the controller more aggressive. The maximum amplitude can be reduced by at least 50% by increasing the feedback gains. This, however, will increase the maximum force and power required from the winch. The feedback gains for the final amplitude could also be made more aggressive to increase performance. But making the controller more aggressive will also make it more susceptible to noise. This is especially noticeable at the final amplitude as the motion is already suppressed to small amplitudes.
If the future 3D hoist system model proves to be able to accurately predict the dynamics of the hoist system, the sLQRi-FF could be improved using Model Predictive Control (MPC). The gain scheduled LQR adapts its gains according to a fixed schedule using certain states of the system. In contrast, the MPC computes the optimal gains on-line according to the predicted future states. The use of a MPC could prove to enhance the performance of the controller, but could also increase sensitivity to model uncertainty.

7-3 Results

The results of the simulations showed that the sLQRi-FF controller could achieve the control objective under, even under adverse conditions such as 20% model uncertainty and measurement noise with a standard deviation of 167 $[mm]$, at a significant wave height of 2.5 metres. The winch actuator does need a powerful motor of approximately 50 tonnes of pulling force and 500 $[kW]$. This power requirement is mostly dictated by the weight of the hoist system and the velocities of the ship motion. This power estimate is however a conservative value. In simulations the maximum required power was only 200 $[kW]$. A positive note is that this is already a decrease in power compared to the winches needed for the other concept using the auxiliary tugline, which need to have at least 300 tonnes of pulling force.
It was observed that the control system is sensitive to inaccuracies of the ship motion measurements. If in future research this inaccuracy proves to cause significant performance losses, it is recommended to implement a more accurate measurement system to obtain the motion of the ship relative to the jacket. Such as an optical or laser-based distance sensor pointed towards the jacket.

7-4 Future work

As mentioned before, the control system has to be three dimensional before it can be used in practice. In this section it will be discussed how the work done in this thesis can be elevated to a three dimensional control system in future work.
One actuated wire rope attached to the lower hoist block allows a force to be applied in one direction. This will probably not be enough to regulate the position of the lower hoist block in x- and y-direction. To regulate the position in x- and y-direction two actuated wire ropes can be used if the direction of the wire ropes are chosen appropriately, meaning in such a way that the magnitude of the forces applied by the wire ropes is sufficient in both x- and y-direction. Best case scenario is when the two wire ropes describe a 90 degree angle in x-y plane. Similar to Section 4-3-1-2-3 an offset from the lower hoist block equilibrium can be created, such that a pushing force can be emulated by decreasing wire rope tension. In this way the wire ropes can control the force balance of the lower hoist block in x- and y-direction. To control this extended system, the control algorithm should be made multi-variable. The x- and y-coordinate of the lower hoist block can be used as the two inputs, and the tension values of the two wire ropes can be the two outputs. This is required as the tension of both wire ropes have to be controlled to obtain a motion in one direction. To control the position of the lower hoist block in x- and y-direction two decoupled algorithms can be used, such as the sLQRi-FF developed in this thesis, to calculate the control input forces separately for x- and y-direction. These forces in x- and y-direction should then be translated in tension values for the two wire ropes, which will depend on the angles between the coordinate system and the wire ropes.

Appendix A

Motion report

Motion Response Calculator - results form

Allseas

General		
Date	22-Sep-2017	
Project	JLS	
Specification	-	
Originator	Nma	
Revision	01	
Vessel	*Pieter Schelte*	[-]
Draft	*17.02*	[m]
AQWA *.lis file	*_WIDE_T=17M_WD=100M..*	[-]
Water depth	100	[m]
Operational / survival condition	Operational	[-]
Wave spectrum	Pierson Moskowitch	[-]
Wave directions	[0:15:345]	[deg]
Peakedness factor (γ)	1	[-]
Significant wave height	[2.5]	[m]
Wave period	[6]	[s]
Wave period type	Tz	[-]
Wave height reduction applied?	yes	[-]

Location of interest*	x-Coor [m]	y-Coor [m]	z-Coor [m]
JLS_T17_HOF_CL_GP	-6.93	0.00	31.04

Remarks

***Coordinate system**
- positive x-axis points from the APP towards the bow
- positive y-axis points from CL towards PS
- positive z-axis points from the keelline orthogonal upwards
- 0 degree wave direction coming form the stern, positive defined anti-clock wise.

3 hours maximum, single amplitude motions and corresponding environmental conditions

Position**		x	y	z	rx	ry	rz	Hs [m]	Tz [s]	γ [-]	Wave Dir. [deg]
Surge	[m]	**0.07**	0.00	0.59	0.00	0.21	0.00	2.5	6	0.0	0
Sway	[m]	0.02	**0.46**	0.62	0.58	0.28	0.11	2.5	6	0.0	75
Heave	[m]	0.03	0.36	**0.68**	0.59	0.26	0.12	2.5	6	0.0	105
Roll	[deg]	0.03	0.36	0.68	**0.59**	0.26	0.12	2.5	6	0.0	105
Pitch	[deg]	0.02	0.46	0.62	0.58	**0.28**	0.11	2.5	6	0.0	75
Yaw	[deg]	0.03	0.36	0.68	0.59	0.26	**0.12**	2.5	6	0.0	105

Velocity**		x	y	z	rx	ry	rz	Hs [m]	Tz [s]	γ [-]	Wave Dir. [deg]
Surge	[m/s]	**0.05**	0.00	0.40	0.00	0.14	0.00	2.5	6	0.0	0
Sway	[m/s]	0.01	**0.30**	0.39	0.32	0.18	0.08	2.5	6	0.0	75
Heave	[m/s]	0.02	0.26	**0.43**	0.33	0.17	0.09	2.5	6	0.0	105
Roll	[deg/s]	0.02	0.26	0.43	**0.33**	0.17	0.09	2.5	6	0.0	105
Pitch	[deg/s]	0.01	0.30	0.39	0.32	**0.18**	0.08	2.5	6	0.0	75
Yaw	[deg/s]	0.02	0.26	0.43	0.33	0.17	**0.09**	2.5	6	0.0	105

Acceleration**		x	y	z	rx	ry	rz	Hs [m]	Tz [s]	γ [-]	Wave Dir. [deg]
Surge	[m/s^2]	**0.07**	0.00	0.28	0.00	0.10	0.00	2.5	6	0.0	0
Sway	[m/s^2]	0.05	**0.27**	0.26	0.18	0.12	0.06	2.5	6	0.0	285
Heave	[m/s^2]	0.05	0.22	**0.28**	0.19	0.11	0.06	2.5	6	0.0	105
Roll	[deg/s^2]	0.05	0.22	0.28	**0.19**	0.11	0.06	2.5	6	0.0	105
Pitch	[deg/s^2]	0.05	0.27	0.26	0.18	**0.12**	0.06	2.5	6	0.0	75
Yaw	[deg/s^2]	0.05	0.22	0.28	0.19	0.11	**0.06**	2.5	6	0.0	105

****Remarks**
- listed values for motions,velocities and accelerations are single amplitudes
- all values are related to 3 hours maxima
- for a complete description of the model and calculation method see the motion report.
- the gravity contribution [g*sin(phi)] is incorporated in all affected values
- Motion analyzer rev. 11

Figure A-1: 3 hour maximum motion report - Pioneering spirit

Appendix B

Simulation cases

In this appendix extra visual information is given for the standard simulation case, and the final simulation case.

B-1 Standard simulation case

The following graphs contain extra visual information for the standard simulation case described in Section 6-1.

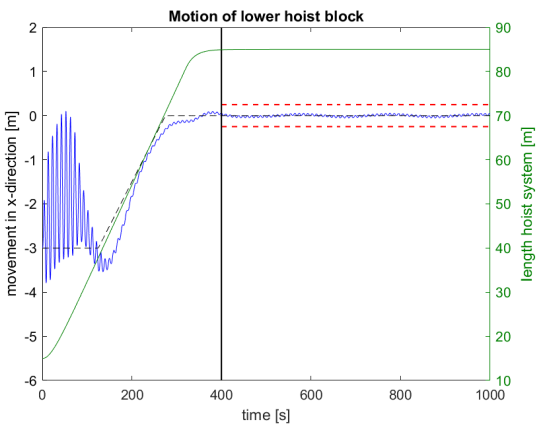

(a) Global motion of lower hoist block in x-direction

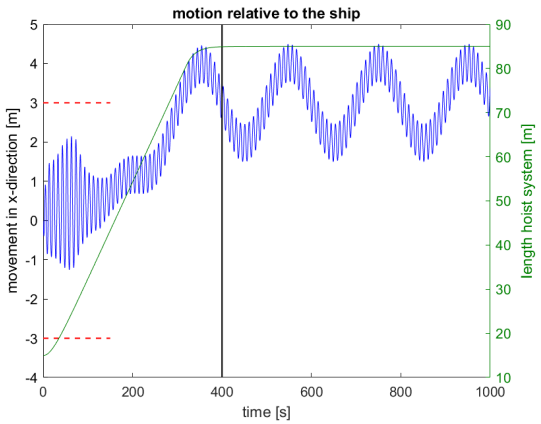

(b) Relative motion of lower hoist block in x-direction

Figure B-1: Standard simulation case - lower block motion

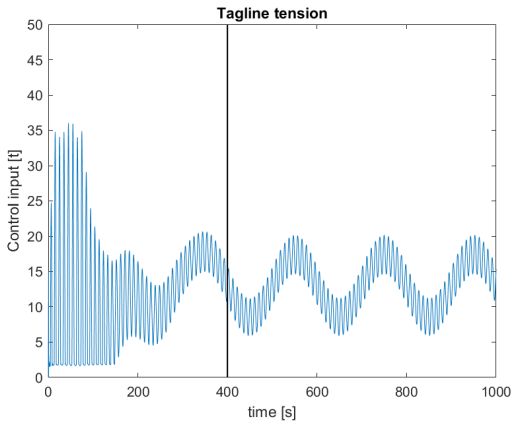

(a) Actuator wire rope tension

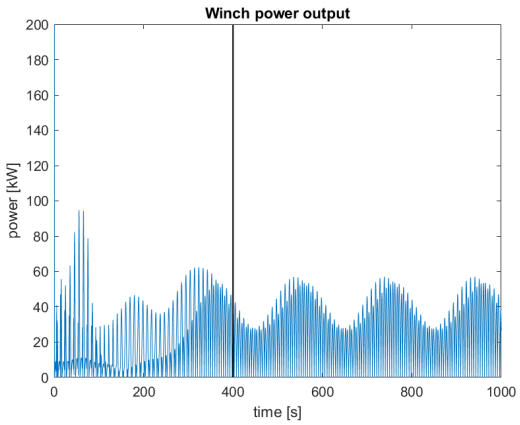

(b) Winch power output

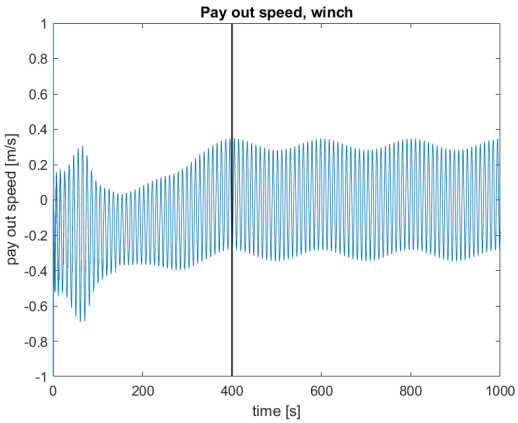

(c) Winch pay out speed (+ is pay out, - is pay in)

Figure B-2: Standard simulation case - Actuator states

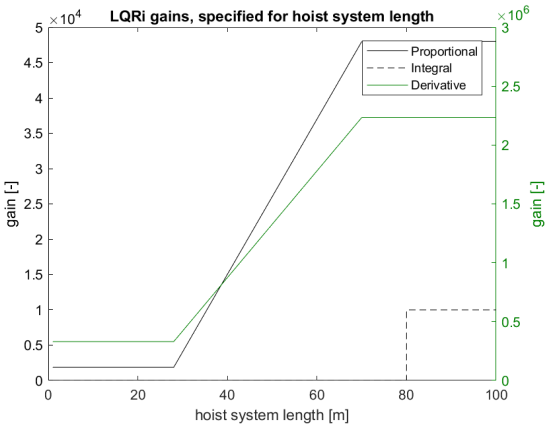

(a) LQRi gains

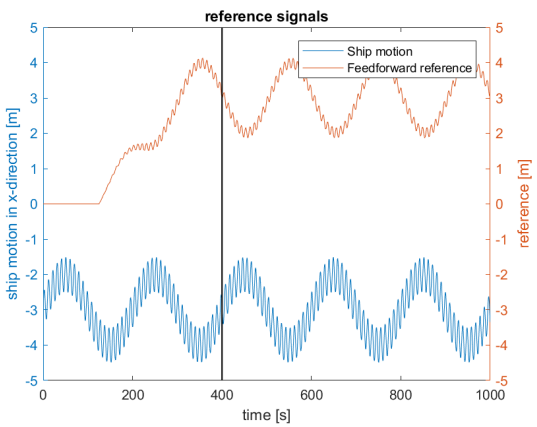

(b) Feedforward reference, and ship motion

Figure B-3: Standard simulation case - Controller gains and reference signal

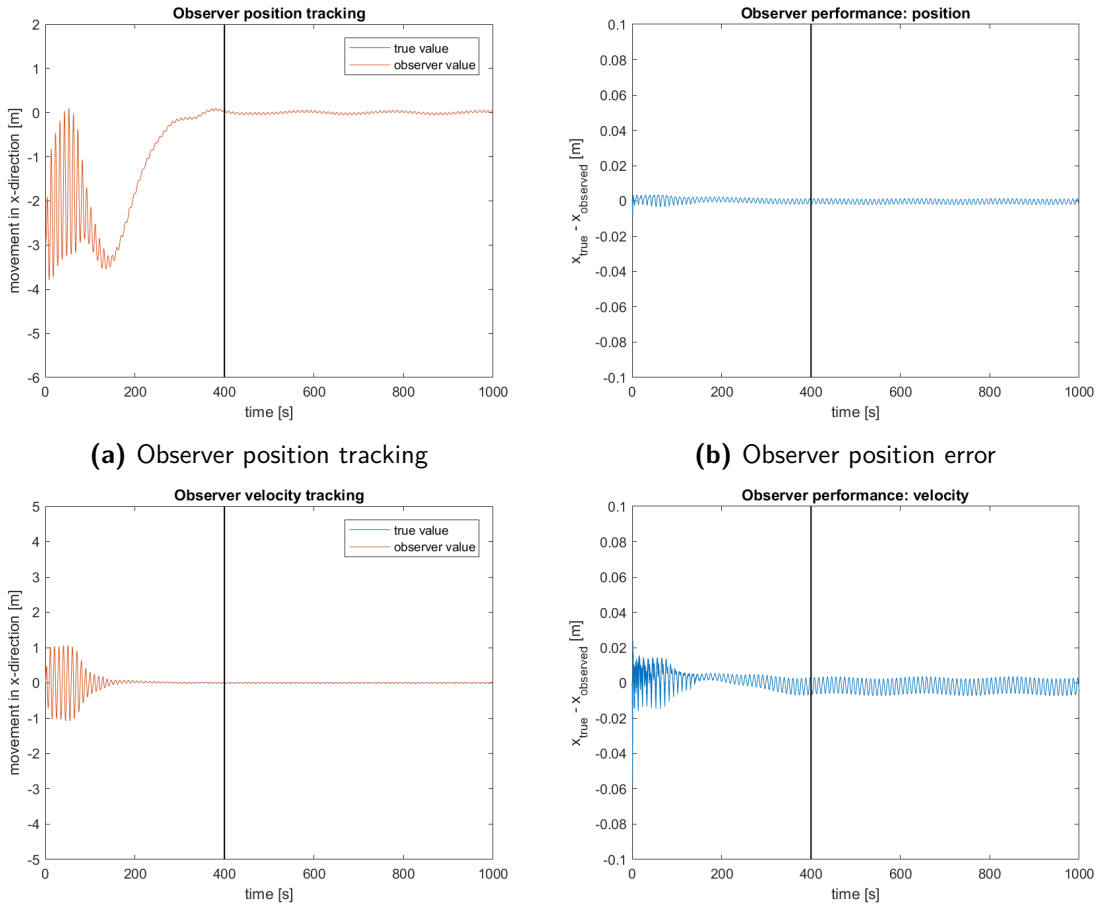

(a) Observer position tracking

(b) Observer position error

(c) Observer performance tracking

(d) Observer velocity error

Figure B-4: Standard simulation case - Observer performance

B-2 Final simulation case

The final simulation case is almost identical to the Example 5: 2 mm & 50 mm described in Section 6-5-3. It is the standard simulation case, with added actuator dynamics, implementation of real ship motion shown in Figure 6-3, and the addition of noise on the measurement signals as described in Section 6-5. For the lower hoist block measurement an accuracy of 2 mm is used, for the ship motion measurement an accuracy of 50 mm is used.
Where the final simulation case differs is the addition of a start-up period. In the graphs plotted below two vertical black dashed lines, and one vertical black solid line are visible. The simulation starts at $t = 0$ $[s]$ when the hoist system is 15 metres long, and the control system is disabled. The winch actuator is in constant tension mode trying to keep the tension a constant $T = 2$ $[t]$.
The first dashed line marks $t = 250$ $[s]$, at this time the controller is turned on. This results in a peak in wire rope tension as seen in Figure B-6a, and a peak in winch power as seen in Figure B-6b. In practise this could be resolved by a transition algorithm to ease the controller into full power, which prevents these peaks in force and power. Figure B-5b illustrates that

the controller reduces the maximum sway amplitude relative to the ship to a value within the objective goal of 3 metres, represented by the horizontal red dashed lines.
The second vertical black dashed line marks $t = 500$ $[s]$, at this time the lower hoist block will start lowering towards the length of 85 metres, which will be reached at $t = 900$ $[s]$ represented by the vertical solid black line. The length of the hoist system is illustrated by the green line. During the lowering process the natural period of the hoist system will cross the period of the ship motion. Because of this the ship motion inserts a lot of energy in the motion of the lower hoist block, as can be seen by the increased sway amplitude. The sway amplitude is however kept within the objective goal by the control system.
When the hoist system length reaches 40 metres the feedforward gain is enabled, which occurs at $t = 626$ $[s]$, as illustrated in Figure B-5a by the non-vertical black dashed line. At $t = 900$ $[s]$ the final amplitude is reached and the lower hoist block can be connected to the jacket.

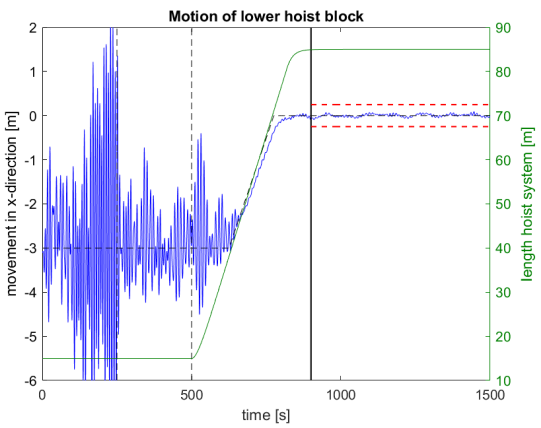

(a) Global motion of lower hoist block in x-direction

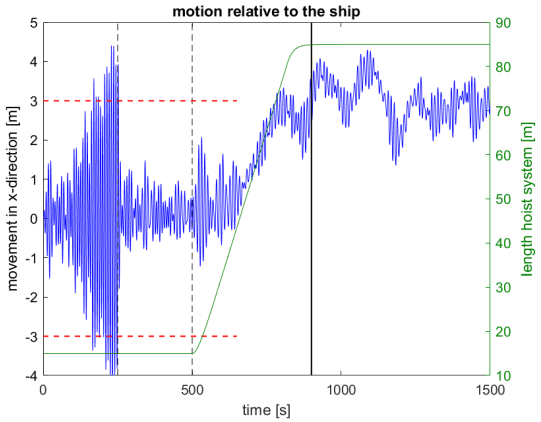

(b) Relative motion of lower hoist block in x-direction

Figure B-5: Final simulation case - lower block motion

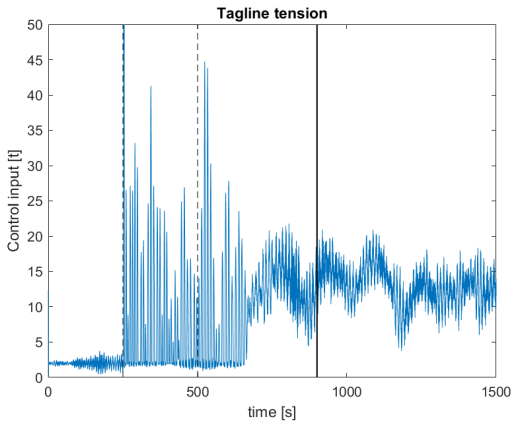

(a) Actuator wire rope tension

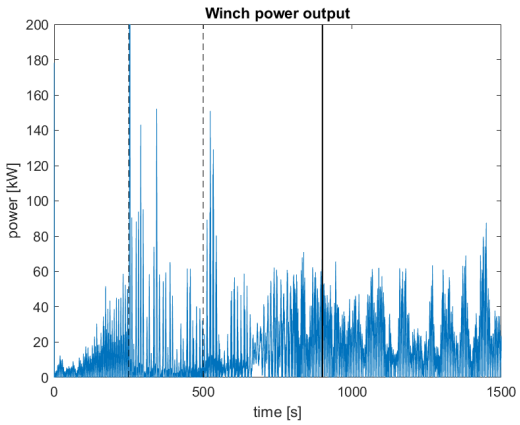

(b) Winch power output

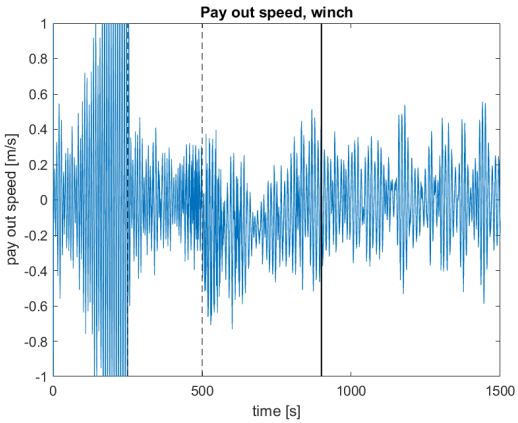

(c) Winch pay out speed (+ is pay out, - is pay in)

Figure B-6: Final simulation case - Actuator states

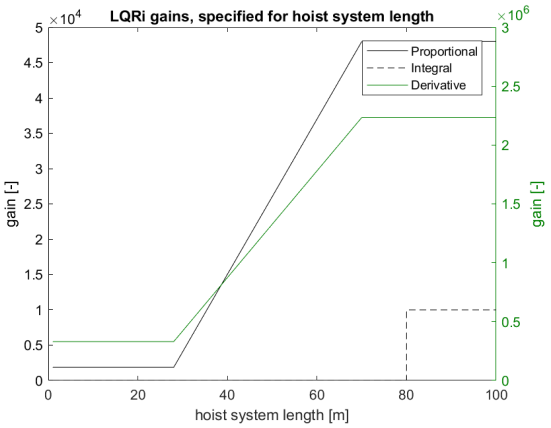

(a) LQRi gains

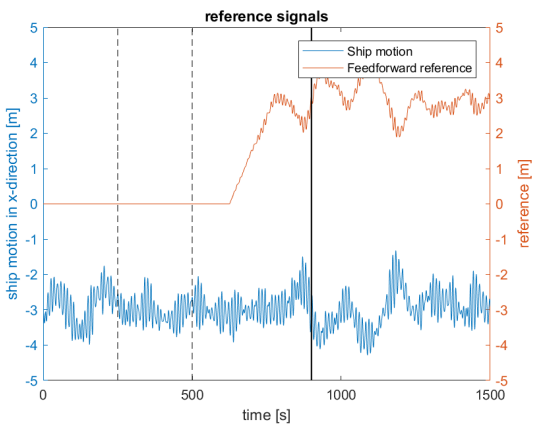

(b) Feedforward reference, and ship motion

Figure B-7: Final simulation case - Controller gains and reference signal

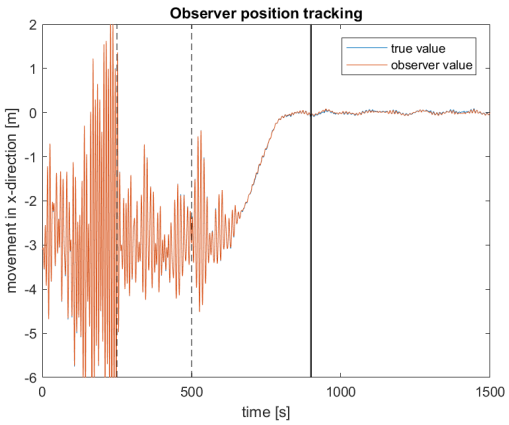

(a) Observer position tracking

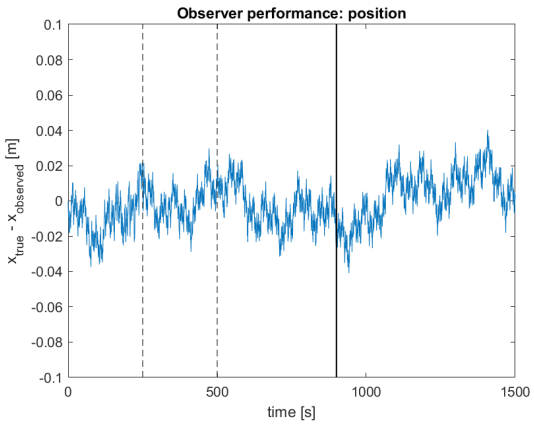

(b) Observer position error

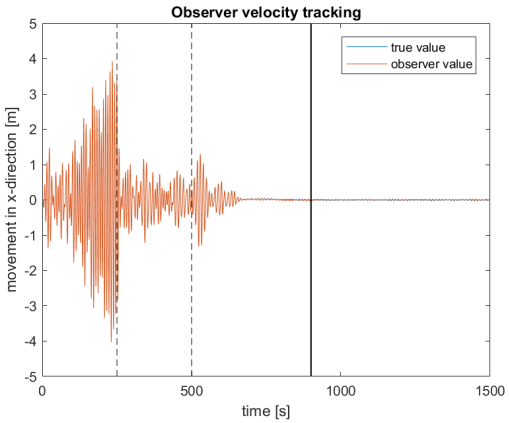

(c) Observer performance tracking

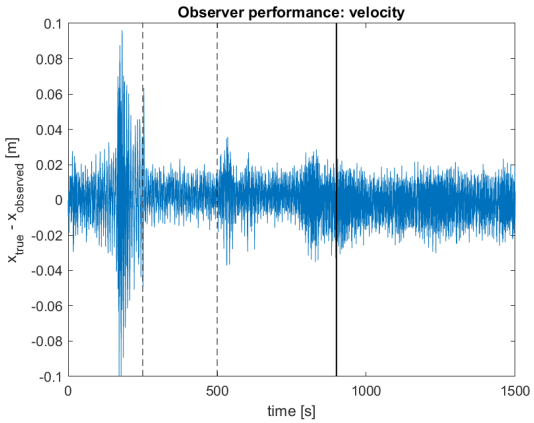

(d) Observer velocity error

Figure B-8: Final simulation case - Observer performance

Bibliography

[1] D. Mohammadshahi, "Dynamics and control of cables in cable-actuated systems," Master's thesis, McGill University, Montreal, 2013.

[2] K. O. Papailiou, *Bending of helically twisted cables under variable bending stiffness due to internal friction, tensile force and cable structure.* PhD thesis, EidgenÃűssische Technische Hochschule Zurich, 1995.

[3] N.-K. Ku, J.-H. Cha, M.-I. Roh, and K.-Y. Lee, "A tagline proportional-derivative control method for the anti-sway motion of heavy load suspended by floating crane in waves," *Journal of Engineering for the Maritime Environment*, vol. 227, no. 4, pp. 357–366, 2013.

[4] M. D. Todd, S. T. Vohra, and F. Leban, "Dynamical measurements of ship crane load pendulation," in *OCEANS'97. MTS/IEEE Conference Proceedings*, vol. 2, pp. 1230–1236, IEEE, 1997.

[5] Y. Chu, F. Sanfilippo, V. Æsøy, and H. Zhang, "An effective heave compensation and anti-sway control approach for offshore hydraulic crane operations," in *Mechatronics and Automation (ICMA), 2014 IEEE International Conference on*, pp. 1282–1287, IEEE, 2014.

[6] G. Parker, M. Graziano, F. Leban, J. Green, and J. D. Bird, "Reducing crane payload swing using a rider block tagline control system," in *OCEANS 2007-Europe*, pp. 1–5, IEEE, 2007.

[7] T. P. Dreyer and van Vuurenv J. H., "A comparison between continuous and discrete modelling of cables with bending stiffness," *Applied Mathematical Modelling*, vol. 23, no. 7, pp. 527–541, 1999.

[8] L. Meirovitch and R. Parker, "Fundamentals of vibrations," *Applied Mechanics Reviews*, vol. 54, p. B100, 2001.

[9] Y. Hsu and C. Pan, "The static wkb solution to catenary problems with large sag and bending stiffness," *Mathematical Problems in Engineering*, vol. 2014, 2014.

[10] Tampere University of Technology, "Basic principles of inertial navigatoin seminar on inertial navigation systems." http://www.aerostudents.com/courses/avionics/InertialNavigationSystems.pdf. page 5, Accessed: 04-07-2018.

[11] "OrcaFlex winch theory." https://www.orcina.com/SoftwareProducts/OrcaFlex/Documentation/Help/Content/html/WinchTheory.htm. Accessed: 16-01-2018.